



HAL
open science

Jurassic–Early Cretaceous tectonic evolution of the North China Craton and Yanshanian intracontinental orogeny in East Asia: New insights from a general review of stratigraphy, structures, and magmatism

Huabiao Qiu, Wei Lin, Yan Chen, Michel Faure

► **To cite this version:**

Huabiao Qiu, Wei Lin, Yan Chen, Michel Faure. Jurassic–Early Cretaceous tectonic evolution of the North China Craton and Yanshanian intracontinental orogeny in East Asia: New insights from a general review of stratigraphy, structures, and magmatism. *Earth-Science Reviews*, 2023, 237, pp.104320. 10.1016/j.earscirev.2023.104320 . insu-03959137

HAL Id: insu-03959137

<https://insu.hal.science/insu-03959137v1>

Submitted on 30 Jan 2023

HAL is a multi-disciplinary open access archive for the deposit and dissemination of scientific research documents, whether they are published or not. The documents may come from teaching and research institutions in France or abroad, or from public or private research centers.

L'archive ouverte pluridisciplinaire **HAL**, est destinée au dépôt et à la diffusion de documents scientifiques de niveau recherche, publiés ou non, émanant des établissements d'enseignement et de recherche français ou étrangers, des laboratoires publics ou privés.

1 **Jurassic–Early Cretaceous tectonic evolution of the North China Craton and Yanshanian**
2 **intracontinental orogeny in East Asia: new insights from a general review of stratigraphy, structures,**
3 **and magmatism**

4

5 **Huabiao Qiu^{1,2,3}, Wei Lin^{1*}, Yan Chen², Michel Faure²**

6 ¹State Key Laboratory of Lithospheric Evolution, Institute of Geology and Geophysics, Chinese
7 Academy of Sciences/Innovation Academy for Earth Science, Chinese Academy of Sciences,
8 Beijing100029, China

9 ²Univ. Orléans, CNRS, BRGM, ISTO, UMR 7327, F-45071, Orléans, France

10 ³Petroleum Exploration and Production Research Institute, SINOPEC, Beijing 100083, China

11 *Corresponding author: (linwei@mail.iggcas.ac.cn)

12 **Abstract**

13 The tectono-magmatic evolution of the North China Craton (NCC) plays a crucial role in
14 understanding the Jurassic–Early Cretaceous (Yanshanian) intracontinental orogeny in East Asia.
15 A holistic understanding of multi-phased deformation and magmatism in the NCC is greatly
16 complicated by the sporadically distributed Mesozoic strata with significantly different
17 stratigraphic associations in various zones. In this paper, we review the Jurassic–Early Cretaceous
18 litho-stratigraphy with emphasis on unconformities to define a coherent chronostratigraphic
19 framework of the entire NCC. Integrating available data concerning tectonic deformation, and
20 geochemistry and fabric of igneous rocks into the well-established coherent chronostratigraphic
21 framework, a four-stage tectonic evolutionary model of the NCC is proposed, providing new
22 insights into the dynamics of the Yanshanian intracontinental orogeny in East Asia. The first stage
23 concerns a N–S extension in the NCC during the Early–early Middle Jurassic (~200–170 Ma),
24 expressed by the E–W striking brittle normal faults developed in the Lower–lower Middle Jurassic
25 strata, and magmatism along the southern and northern margins of the NCC. It could be related to
26 the post-orogenic extension after the deep continental subduction of the South China Block
27 beneath the NCC. The second one is characterized by a N–S compression (i.e., Event A of the
28 Yanshanian orogeny) in the late Middle Jurassic (~170–160 Ma), evidenced by the unconformity
29 above the Lower–lower Middle Jurassic strata and the upper Middle Jurassic syn-tectonic
30 deposition. The associated N–S directed thrusts and fault-related folds were mainly localized in
31 the northern part of the NCC, possibly responding to the far-field compression related to the
32 closure of the Mongol–Okhotsk Ocean. The third stage corresponds to a NW–SE compression
33 (i.e., Event B of the Yanshanian orogeny) during the Late Jurassic–earliest Cretaceous (~160–135
34 Ma), illustrated by the NW–SE directed thrusts and the overprint of pre-existing N–S directed
35 thrusts by the latter NW–SE directed thrusts. It was well recorded by the Upper Jurassic–
36 lowermost Cretaceous syn-tectonic deposition and the unconformity above. This NW–SE
37 compression in response to the flat slab subduction of the Paleo-Pacific Plate had influenced the
38 entire NCC. However, the latest Middle–early Late Jurassic (~165–150 Ma) local NE–SW
39 extension, recorded by ductile and brittle normal faults, magnetic lineation in granitic plutons, and
40 magmatism that extended to Northeast China and its adjacent areas, also occurred in the
41 northeastern part of the NCC. This could be related to tectonic transition from the N–S closure of

42 the Mongol–Okhotsk Ocean to the NNW-directed subduction of the Paleo-Pacific Plate. In the
43 latest stage during the Early Cretaceous (~135–115 Ma), the large-scale crustal extension,
44 characterized by metamorphic core complexes, magmatism, graben or half-graben basins,
45 occurred in a vast area extending more than 4000 km, from Transbaikalia, through the NCC, to
46 the South China Block. It could be the consequence of the lithospheric thinning and the formation
47 of the wide rift due to the southeastward stress relaxation of the NW–SE convergent East Asian
48 continent as the slab rollback of the Paleo-Pacific Plate. These results provide a notable example
49 of polyphase intra-plate deformation and magmatism paradigm in response to intracontinental
50 orogeny with variable plate-boundary geodynamics.

51 Keywords: Jurassic-Early Cretaceous, Stratigraphic Framework, Tectono-magmatic Process,
52 North China Craton, Geodynamics of East Asia

53 **1. Introduction**

54 The NCC, one of the important continental blocks that form the East Asian continent (Davis
55 et al., 2001), is separated from the Siberia Craton by the Central Asian Orogenic Belt in the north
56 and from the South China Block (SCB) by the Qinling-Dabie-Sulu Orogenic belt in the south
57 (Fig.1). After the Paleoproterozoic cratonization, the tectonic evolution of the NCC is related to
58 two Phanerozoic orogenic cycles, including the Paleozoic–Triassic continental amalgamation with
59 the Mongolian arc terranes and the SCB at block boundaries (Mattauer et al., 1985; Hacker et al.,
60 2000; Windley et al. 2007; Xiao et al., 2003, 2015; Xu et al., 2013), and the Jurassic–Early
61 Cretaceous intracontinental orogeny, referred to as “Yanshanian Movement” since about one
62 century ago (Wong, 1927; Davis et al., 2001; Faure et al., 2012; Dong et al., 2015; Zhang et al.,
63 2022). The welded Mongolian arc terranes-NCC-SCB continent formed after the Paleozoic–
64 Triassic amalgamation in the periphery of the NCC (Fig.1). In the NCC, the Jurassic–Early
65 Cretaceous intracontinental deformation, mainly characterized by the E–W to NE–SW striking,
66 and some N–S striking fold-thrust belts, small-scale normal faults, and coeval magmatism, is
67 widely exposed in the Yinshan-Yanshan belt, the Taihangshan belt, and the Ordos basin and its
68 adjacent areas (Fig. 2; Davis et al., 2001, Faure et al., 2012; Dong et al., 2015; Zhang et al., 2022).

69 The “Yanshanian Movement”, an orogenic terminology that characteristically refers to the
70 Jurassic–Early Cretaceous intracontinental orogeny in the Chinese literature, was initially defined
71 in the Yanshan belt in the west of Beijing by Wong (1927, 1929). During the past decades,

72 considerable advances have been achieved in generating a wealth of data related to the stratigraphy,
73 tectonic deformation, and magmatism in the NCC, aiding in a better understanding of the
74 Yanshanian intracontinental orogeny. However, the stratigraphy and tectonic studies in different
75 zones of the NCC, together with studies on igneous rocks, have not been integrated into a
76 comprehensive study, resulting in a suite of incompatible models for individual zones or
77 disciplines. This hinders the holistic understanding of the plate-scale tectono-magmatic process
78 and the evaluation of geodynamic evolution models of the Yanshanian intracontinental orogeny.
79 This is mainly reflected in the following aspects:

80 (1) The Yanshanian tectonic events were initially defined by two major unconformities below
81 and above the volcanics of the Upper Jurassic Tiaojishan Formation (J_{3t}) resulting from
82 deformation episodes in the Yanshan belt, i.e., Events A and B of the Yanshanian orogeny (Wong,
83 1927, 1929; Fig. 3). Nevertheless, the process of multi-phased deformation and magmatism is
84 greatly complicated by the sporadically distributed Mesozoic strata with significantly different
85 stratigraphic associations in various zones of the NCC, for instance, the corresponding
86 contemporaneous volcanics are absent anywhere outside of the Yanshan belt (Fig. 3). The syn-
87 tectonic strata were often neglected to constrain the deformation episodes in the holistically
88 stratigraphic framework. A reliable chronostratigraphic framework in the Jurassic-Lower
89 Cretaceous interval was never presented in detail through the North China-wide stratigraphic
90 correlation (Fig. 2);

91 (2) The timing and kinematics of the widely distributed Jurassic–Early Cretaceous multi-
92 phased deformation were rarely constrained within a coherent chronostratigraphic framework. The
93 accurate deformation episodes were blurred by the incompatible isotopic geochronological results
94 from different zones, hindering the holistic understanding of the deformation process of the NCC;

95 (3) The age and geochemistry of igneous rocks, and the fabric of syn-kinematic plutons
96 provide key constraints on the Jurassic–Early Cretaceous tectonic setting and geodynamic
97 mechanism of the NCC. However, the geochemistry and fabric results on the Jurassic–Early
98 Cretaceous igneous rocks in the NCC have not been integrated into tectonic studies within the
99 reliable chronostratigraphic framework, resulting in incompatible geodynamic models that are
100 often restricted by a single discipline.

101 After its Paleozoic–Triassic amalgamation, the East Asian continent was bounded by the
102 Mongol–Okhotsk Ocean (MOO) in the north, the Bangong–Nujiang Ocean (BNO) in the
103 southwest, and the Paleo-Pacific Ocean (Izanagi) in the southeast. In the NCC, the Jurassic–Early
104 Cretaceous tectono-magmatic evolutionary process with unified North China-wide timing and
105 kinematic constraints in the various episodes is never established yet. The geodynamics of
106 intraplate deformation in the NCC at large distances, 1,000 km or more, from the related plate
107 boundaries remain enigmatic. Due to the different perspectives of models restricted by individual
108 zones or disciplines, the Jurassic–Early Cretaceous intracontinental orogeny in the NCC was
109 generally interpreted to be the consequence of: i) the north–south closure of the MOO (Yin and
110 Nie, 1996); ii) the northwestward subduction of the Paleo-Pacific Plate (PPP; e.g., Zhu et al., 2011b;
111 Wu et al., 2019; Hao et al., 2020); iii) the north–south interactions between the Eurasian intraplate
112 deformation and the northwestward subduction of the PPP (Davis et al., 2001); or iv)
113 multidirectional multi-plate convergence of the MOO, BNO, and PPP (e.g., Dong et al., 2015;
114 Zhang et al., 2022). The NCC offers an ideal natural laboratory for polyphase intra-plate
115 deformation and magmatism paradigm in response to the Jurassic–Early Cretaceous
116 intracontinental orogeny with variable plate-boundary geodynamics. Intracontinental orogeny is
117 usually sensitive to far-field stress reconfigurations at active plate boundaries (Silva et al., 2018).
118 To understand the geodynamics of the Yanshanian intracontinental orogeny under multi-plate
119 convergence in East Asia, it is necessary to have great insight of the tectono-magmatic process in
120 the various episodes with accurate timing and kinematic constraints.

121 In this paper, we review available published data concerning Jurassic–Early Cretaceous litho-
122 stratigraphy with emphasis on unconformities, tectonic deformation, and magmatism of the NCC.
123 We combine results from multidisciplinary studies to develop a Jurassic–Early Cretaceous
124 evolutionary model of the NCC that shed light on the geodynamics of the Yanshanian
125 intracontinental orogeny in East Asia, with the following steps: (1) define a coherent
126 chronostratigraphic framework of the entire NCC through a detailed North China-wide
127 stratigraphic correlation by integrating previous litho-stratigraphy information and available
128 isotopic geochronological data; (2) constrain the accurate deformation episodes within the
129 established coherent chronostratigraphic framework; (3) integrate the geochemistry and fabric
130 results on Jurassic–Early Cretaceous igneous rocks into the tectonic studies, presenting a clear
131 tectono-magmatic process for the entire NCC; and (4) link the tectono-magmatic process to the

132 East Asian active plate boundaries to develop a logical geodynamic model for the Yanshanian
133 intracontinental orogeny. This contribution provides a significant example of polyphase intra-plate
134 deformation and magmatism responding to intracontinental orogeny with variable plate-boundary
135 geodynamics.

136 **2. Tectonic setting**

137 After the cratonization through the Paleoproterozoic amalgamation of the Eastern,
138 Intermediate (or Fuping), and Western blocks (Zhao et al., 2001; Faure et al., 2007; Li et al., 2012;
139 Trap et al., 2012), the NCC was surrounded by the Paleo-Asian Ocean in the north (Windley et al.
140 2007; Xiao et al., 2003, 2015; Xu et al., 2013) and the eastern branches of the Paleo-Tethys Ocean
141 in the south (Mattauer et al., 1985; Xu et al., 1986; Hacker et al., 2000). In the north of the NCC,
142 the closure of the Paleo-Asian Ocean was characterized by the amalgamation of several
143 microcontinental blocks in the Central Asian Orogenic Belt (e.g., the Erguna, Xing'an, Songnen,
144 Jiamusi, and Khanka blocks; Liu et al., 2017; Zhou et al., 2018; Fig. 1), albeit the timing of the
145 final closure of the Paleo-Asian Ocean remains still debated, i.e., Late Devonian (Xu et al., 2013;
146 Zhao et al., 2013) or Late Permian–Early Triassic (Chen et al., 2000; Li, 2006; Jian et al., 2008;
147 Lin et al., 2008; Xiao et al., 2003, 2015). In the south, the final amalgamation between the NCC
148 and SCB occurred through multistage orogeny during the Paleozoic to Triassic, giving rise to a
149 Late Triassic Dabie-Sulu high-pressure and ultrahigh-pressure (HP–UHP) orogenic belt (Fig. 1;
150 e.g., Mattauer et al. 1985; Faure et al., 1999, 2003; Meng and Zhang, 1999; Hacker et al., 2000;
151 Ratschbacher et al., 2003; Lin et al., 2005, 2009; Li et al., 2017, 2018).

152 During the Jurassic–Cretaceous, the welded East Asian continent was surrounded by the
153 MOO, PPP, and BNO. The closure time of the MOO between the Siberian Craton and North
154 China–Mongolian arc terranes remains controversial, e.g., the Early–Middle Jurassic (Zorin, 1999;
155 Kravchinsky et al., 2002), the Late Jurassic–early Early Cretaceous (Cogné et al., 2005; Metelkin
156 et al., 2010), or the Early Cretaceous (Enkin et al., 1992). Generally, it is acknowledged that the
157 MOO closed progressively from west to east during the Jurassic–Early Cretaceous (Yin and Nie,
158 1996; Zorin, 1999; Kravchinsky et al., 2002; Metelkin et al., 2010; Dong et al., 2015). The suture
159 extends from central Mongolia to the Okhotsk Sea (Tomurtogoo et al., 2005; Fig. 1). The onset of
160 the PPP subduction in the southeast has been considered to occur in the Late Triassic (Sagong et
161 al., 2005; Kim et al., 2015), or the Early Jurassic (Wu et al., 2007; Guo et al., 2015; Wang et al.,

162 2019). It is well agreed that the influence of the Paleo-Pacific tectonic regime has extended to
163 North and Northeast China since the Jurassic (e.g., Wu et al., 2007; Li et al., 2007a; Wang et al.,
164 2019). The PPP subducted northwestward beneath the East Asian continent until the latest
165 Mesozoic when the Izanagi-Pacific Ridge subducted (Lapierre et al., 1997). The BNO, extending
166 for more than 2000 km from east to west in central Tibet, separates the Qiangtang terrane from the
167 Lhasa terrane during the Mesozoic (Kapp et al., 2007; Zhu et al., 2016). The initial subduction has
168 been considered to be either prior to the Early Jurassic (Guynn et al., 2006; Zhu et al., 2011a) or
169 in the Middle Jurassic (Zhang et al., 2012; Li et al., 2016d). It has been widely accepted that a
170 diachronous collision from east to west between the Qiangtang and Lhasa terranes occurred during
171 the Middle Jurassic to Early Cretaceous (Guynn et al., 2006; Kapp et al., 2007; Zhu et al., 2016;
172 Yan et al., 2016; Liu et al., 2018a). During the Cenozoic, the tectonic setting of the NCC was the
173 consequence of the intracontinental deformation of the Eurasian plate and the subduction of the
174 western Pacific plate.

175 **3. Stratigraphic framework and unconformities**

176 The Jurassic–Lower Cretaceous strata are well preserved in the Ordos basin and its adjacent
177 areas, and scattered in a few isolated basins in the Yinshan-Yanshan belt (Fig. 2). Some residual
178 Jurassic–Lower Cretaceous strata are concealed below the Cenozoic Bohai Bay and Hefei basins.
179 The Jurassic–Lower Cretaceous strata unconformably or disconformably overlie the Triassic or
180 older strata (Fig.3; Zhang et al., 2011, Meng et al., 2019). Integrating geochronological data, litho-
181 stratigraphy, and syn-tectonic growth strata, we have carried out a detailed North China-wide
182 stratigraphic correlation to develop a coherent chronostratigraphic framework for the Jurassic–
183 Lower Cretaceous interval. It contains five tectonostratigraphic sequences, which are separated by
184 two regional angular unconformities that are ascribed to Events A and B of the Yanshanian
185 orogeny, as below: i) the Lower–lower Middle Jurassic sequence, ii) the upper Middle Jurassic
186 sequence, iii) the lower Upper Jurassic volcanic sequence, iv) the Upper Jurassic–lowermost
187 Cretaceous sequence, and v) the Lower Cretaceous sequence.

188 **3.1 Lower–lower Middle Jurassic sequence**

189 In the eastern NCC, the Lower–lower Middle Jurassic sequence is mainly scattered in the
190 Yanshan belt (Fig. 2). The Xingshikou Formation, which was formerly considered to be of Early

191 Jurassic, has been recently assigned to Upper Triassic according to new geochronological and
192 paleontological results (Yang et al., 2006; Chen et al., 2015; Meng et al., 2019). Thus, the Lower
193 Jurassic strata consist of fluvial conglomerates and sandstones, and abundant volcanics (e.g., basalt,
194 andesite, dacites, pyroclastic rocks, and tuffaceous sedimentary rocks) in the Nandaling Formation
195 and its counterparts (Fig. 3, Tables 1 and S1). These strata are unconformable on the Triassic or
196 older strata in the Western Hill of Beijing, and the Xiahuayuan, Luanping, and Beipiao basins, and
197 absent in a vast area (Meng et al., 2019; Figs. 2 and 3). The volcanic rocks from the Nandaling
198 Formation (J_{1-2n}) in the Western Hill yield a zircon age of 177–167 Ma (Zhao et al., 2006; He et
199 al., 2017; Gao et al., 2018; Hao et al., 2019, 2020; Meng et al., 2019; Fig. 3, Tables 1 and S1). In
200 the Luanping basin, the biotite ⁴⁰Ar/³⁹Ar age of a tuff sample from the Nandaling Formation (J₁₋
201 2n) is dated at 180 ± 1.8 Ma (Davis et al., 2001; Fig. 3, Tables 1 and S1). The tuff samples in the
202 Xinglonggou Formation (J_{1x}) in the Beipiao basin are of Early Jurassic (188–176 Ma; Chen et al.,
203 1997; Yang and Li, 2008; Fig. 3, Tables 1 and S1). In the above areas, the Lower Jurassic strata
204 are conformably overlain by the lower Middle Jurassic coal-bearing unit, which mainly consists
205 of basal conglomerates, sandstones, siltstones, mudstones, and coal measures (Meng et al., 2019;
206 Fig. 3, Tables 1 and S1). It is characterized by fining- and deepening-upward depositional cycle
207 from the Lower Jurassic fluvial deposits intercalated with volcanic rocks to the lower Middle
208 Jurassic coal-bearing units in lacustrine and swamp facies (Fig. 3). In the Western Hill, the
209 youngest detrital zircon ages from sandstones in the coal-bearing Yaopo Formation (J_{2yp}) are
210 dated at ~175–174 Ma (Yang et al., 2006; Hao et al., 2019; Fig. 3, Tables 1 and S1). The youngest
211 detrital zircon ages obtained from the coal-bearing Xiahuayuan Formation (J_{2x}) in the Xiahuayuan
212 and Luanping basins are ~175–170 Ma (Li et al., 2016a; Lin et al., 2018; Hao et al., 2020). In the
213 Beipiao basin in Western Liaoning, the ages of the coal-bearing Beipiao Formation (J_{2b}) are ~175–
214 168 Ma (Meng et al., 2019; Fig. 3, Tables 1 and S1). The lower Middle Jurassic coal-bearing strata
215 extend outward to a larger area (e.g., the Xiabancheng and Niuyingzi basins) where the lower
216 Middle Jurassic Xiahuayuan (J_{2x}) or Guojiadian (J_{2g}) Formation overlies directly on the pre-
217 Jurassic strata (Li et al., 2016a; Meng et al., 2019; Zhang et al., 2019; Fig. 3). The youngest detrital
218 zircon ages obtained from the Guojiadian Formation (J_{2g}) are ~171–163 Ma (Cope, 2017; Zhang
219 et al., 2019; Wu et al., 2021; Fig. 3, Tables 1 and S1).

220 In the western NCC, the Lower–lower Middle Jurassic sequence is mainly distributed in
221 the Daqingshan in the Yinshan belt and the Ordos basin and its adjacent areas (Fig. 2). Similar to

222 the eastern NCC, the Lower Jurassic strata were deposited scatteredly in local sags formed on the
223 underlying unconformity (Yang et al., 2005). The Lower Jurassic strata mainly consist of alluvial
224 and fluvial conglomerates and sandstones, whereas the contemporaneous volcanics are absent
225 except for the Jiyuan region (Darby et al. 2001; Ritts et al. 2001; Gong et al., 2015; Li et al., 2015;
226 Wang et al., 2017; Meng et al., 2019; Zhang et al., 2020; Fig. 3, Tables 1 and S1). In the Shiguai
227 basin in Daqingshan, the Lower Jurassic Wudanggou Formation (J_{1w}), which changes into
228 marginal alluvial conglomerates, and sandstones and shales in the shallow lacustrine and deltaic
229 facies, is much thicker than its counterparts in the Ordos basin and adjacent area (Wang et al.,
230 2017; Fig. 3, Tables 1 and S1). The syn-tectonic growth strata in the lowest Jurassic were
231 developed in small-scaled grabens (Darby et al., 2001), where the ages of diverse palynoflora
232 obtained from the Wudanggou Formation (J_{1w}) are ~200–183 Ma (Ritts et al. 2001; Wang et al.,
233 2017; Fig. 3, Tables 1 and S1). The interbedded tuff layers in the Yongdingzhuan Formation (J_{1y})
234 in the Ningwu-Jingle and Yungang basins have zircon U-Pb ages of 179–171 Ma and 187.6 ± 2 Ma,
235 respectively (Li et al., 2014c; Zhang et al., 2020; Fig. 3, Tables 1 and S1). In the West Henan
236 region, the Lower Jurassic Anyao Formation (J_{1a}) in the Jiyuan region contains abundant basic
237 volcanic rocks, which are dated at 178.31 ± 3.77 Ma (Lu et al., 2004; Fig. 3, Tables 1 and S1).
238 Similarly, the lower Middle Jurassic strata, conformably overlying the Lower Jurassic strata,
239 change into conglomerates, sandstones, and mudstones intercalated with coal measures in fluvial,
240 lacustrine, and swamp facies in the fining- and deepening-upward depositional cycle (Yang et al.,
241 2005; Li et al., 2015; Wang et al., 2017; Meng et al., 2019; Fig. 3, Tables 1 and S1). This coal-
242 bearing unit extends significantly outward to a vast area in the periphery of the Ordos basin and
243 overlies directly on the underlying erosional surface (Yang et al., 2005; Meng et al., 2019; Fig. 3,
244 Tables 1 and S1). The lower Middle Jurassic coal-bearing units as marker beds can be comparable
245 from area to area in the NCC. The Zhaogou Formation (J_{2zg}) in the Shiguai basin has been dated
246 by a palynoflora of the early Middle Jurassic age (Ge et al., 2010). In summary, the Lower–lower
247 Middle Jurassic sequence (dated at ~200–170 Ma) is characterized by fining- and deepening-
248 upward depositional cycle from the Lower Jurassic alluvial and fluvial deposits intercalated with
249 volcanic rocks to the lower Middle Jurassic coal-bearing units in lacustrine and swamp facies. The
250 Upper Jurassic volcanic rocks are mainly distributed in the northern and southern margins of the
251 NCC (i.e., the Yanshan belt and the Jiyuan district).

252 3.2 Upper Middle Jurassic sequence

253 Event A of the Yanshanian orogeny, representing a regional contraction event, was initially
254 defined by the unconformity beneath the volcanics of the Tiaojishan Formation (J_{3t}) in the Western
255 Hill of Beijing (Figs. 2 and 3; Wong, 1929). Although the Tiaojishan Formation (J_{3t}) directly
256 overlies all older strata in the Western Hill, the Tiaojishan Formation (J_{3t}) is in conformable contact
257 with the underlying Longmen-Jiulongshan Formations (J_{2l} - J_{2j}) where the Longmen-Jiulongshan
258 Formations (J_{2l} - J_{2j}) exist locally (Fig. 3; Li et al., 2014a; Hao et al., 2019, 2020). Drilling and
259 exploratory trench data reveal that the conformable Longmen-Jiulongshan (J_{2l} - J_{2j}) and Tiaojishan
260 (J_{3t}) Formations pinch out upwards by onlap against the underlying unconformity (Li et al., 2014a).
261 However, the upper Middle Jurassic Longmen-Jiulongshan Formations (J_{2l} - J_{2j}) and their
262 counterparts are absent in a vast area of the Yanshan belt (e.g., the Chicheng, Chengde,
263 Xiabancheng, and Niuyingzi basins), where the Tiaojishan Formation (J_{3t}) overlies unconformably
264 on the lower Middle Jurassic coal-bearing strata or pre-Jurassic strata (Fig. 3). Therefore, the
265 unconformity representing Event A of the Yanshanian orogeny is located above the coal-bearing
266 strata and older strata (Fig. 3; Li et al., 2014a; Liu et al., 2018b; Hao et al., 2019, 2020; Wu et al.,
267 2021).

268 In the Yanshan belt, the upper Middle Jurassic Longmen-Jiulongshan Formations (J_{2l} - J_{2j})
269 and their counterparts (i.e., the Jiulongshan Formation in the Xiahuayuan and Luanping basins and
270 the Haifanggou Formation in the Beipiao basin) comprise fluvial to alluvial conglomerates, and
271 sandstones in the lower and deltaic to lacustrine sandstones and mudstones in the upper (Zhao et
272 al. 2002; Liu et al., 2004; Shao and Zhang, 2014; Meng et al., 2019; Hao et al., 2020; Fig. 3, Tables
273 1 and S1). In the Western Hill, the youngest detrital zircon ages from sandstones in the Longmen
274 Formation are focused on 168–164 Ma (Hao et al., 2019; Wu et al., 2021), whereas the sandstone
275 and tuff samples yield the age of 161–154 Ma (Yang et al., 2006; Li et al., 2014a; Hao et al., 2019;
276 Meng et al., 2019; Fig. 3, Tables 1 and S1). The ages of the Jiulongshan Formation (J_{2j}) in the
277 Xiahuayuan and Luanping basins are concentrated on 163–156 Ma by dating the tuff and the
278 youngest detrital zircons of sandstones (Chen et al., 2014; Lin et al., 2018; Meng et al., 2019; Hao
279 et al., 2020; Fig. 3, Tables 1 and S1). In the Haifanggou Formation (J_{2h}) in the Beipiao basin, the
280 tuff–interbed within the basal conglomerates is dated at 167–164 Ma, whereas the topmost
281 tuffaceous breccia yields the eruption ages of 161.7 ± 1.9 Ma (Zhang et al., 2005; Yang and Li,
282 2008; Chang et al., 2014; Huang, 2019; Hao et al., 2020; Fig. 3, Tables 1 and S1). The

283 conglomerate-dominated lithological characteristics in the Longmen and Jiulongshan Formations
284 (J_{2l}-J_{2j}) and their counterparts in the Yanshan belt, which have been considered as syn-tectonic
285 deposition (Zhao et al., 2002, 2004), should be in response to Event A of the Yanshanian orogeny.

286 In the Yinshan belt, and the Ordos basin and its adjacent areas, the upper Middle Jurassic
287 sequence, which mainly consists of fluvial to lacustrine conglomerates, sandstones, and mudstones,
288 is comparable with those in the Yanshan belt (Zhang et al., 2008b; Li et al., 2014b; Li et al., 2016c;
289 Wang et al., 2017; Fig. 3, Tables 1 and S1). This upper Middle Jurassic sequence unconformably
290 overlies the underlying coal-bearing strata in the Yinshan belt, whereas it is disconformable on the
291 latter ones in the Ordos basin and its adjacent areas (Yang et al., 2013; Wang et al., 2017; Li et al.,
292 2014b; Zhang et al., 2020). The Changhangou Formation (J_{2c}) in the Shiguai basin, exhibiting a
293 pronounced growth geometry, unconformably onlaps onto the underlying erosional surface in the
294 coal-bearing strata (Wang et al., 2017). The tuff sample yields an age of 163.7 ± 1.0 Ma (Wang et
295 al., 2017; Fig. 3, Tables 1 and S1). The upper Middle Jurassic Yungang Formation (J_{2yg}) in the
296 Ningwu-Jingle and Yungang basins, exhibiting a typical wedge-like growth strata geometry,
297 onlaps onto the limb of the fault-related folds (Chen et al., 2019; Zhang et al., 2020). The detrital
298 zircons from the lower Yungang Formation in the Yungang and Ningwu-Jingle basins yield ages
299 of 168–165 Ma (Chen et al., 2019; Zhang et al., 2020), and the age of the youngest detrital zircons
300 obtained from the top of the Yungang Formation (J_{2yg}) in the Ningwu-Jingle basin is 160.7 ± 0.65
301 Ma (Li et al., 2015; Fig. 3, Tables 1 and S1). Although there is no obvious angular unconformity
302 between the Yungang/Dongmengcun/Ma'ao Formations (J_{2yg}/J_{2dm}/J_{2m}) and the lower Middle
303 Jurassic coal-bearing strata in the West Henan region, abrupt changes in the heavy mineralogy and
304 sedimentary facies occurred in these strata (Fig.3; Li et al., 2014b; Zhang et al., 2020), probably
305 indicating the existence of disconformity within these strata. Therefore, the unconformity (or
306 disconformity) above the coal-bearing strata and the overlying upper Middle Jurassic syn-tectonic
307 sequence (dated at ~170–160 Ma) in the entire NCC should be the response to Event A of the
308 Yanshanian orogeny.

309 3.3 Upper Jurassic–lowermost Cretaceous sequence

310 3.3.1 Upper Jurassic volcanics

311 The upper Jurassic volcanics, assigned to the Tiaojishan (J_{3t}) or Lanqi (J_{3l}) Formation, are
312 only distributed in the Yanshan belt and its adjacent areas (Fig. 2). As mentioned above, the upper
313 Jurassic volcanics are in conformable contact with upper Middle Jurassic sequence, and
314 unconformably overlie all older strata where the upper Middle Jurassic sequence is absent (Zhao
315 et al., 2002; Liu et al., 2018b; Hao et al., 2019; Fig. 3, Tables 1 and S1). The volcanics in the
316 Tiaojishan (J_{3t}) or Lanqi (J_{3l}) Formation comprise intermediate andesitic lavas, volcanic breccia,
317 andesitic tuff, pyroclastics, and interbedded sedimentary rocks (Zhao et al., 2002; Hao et al., 2019;
318 Fig. 3, Tables 1 and S1). The ages of the Tiaojishan Formation (J_{3t}) in the Western Hill range from
319 161 to 146 Ma (Li et al., 2001; Zhao et al., 2004; Yang et al., 2006; Yu et al., 2016; Hao et al.,
320 2019; Fig. 3, Tables 1 and S1). The Tiaojishan Formation (J_{3t}) in the Hunyuan basin yields zircon
321 ages of 152.77±0.6 Ma (Li et al., 2015; Fig. 3, Tables 1 and S1). In the Xiahuayuan and Luanping
322 basins, the volcanics in the Tiaojishan Formation (J_{3t}) are dated at ~164–153 Ma (Davis et al.,
323 2001; Zhang et al., 2005, 2008a; Liu et al., 2006; Cope et al., 2007; Yu et al., 2016; Hao et al.,
324 2020; Fig. 3, Tables 1 and S1). In the Chicheng basin, the andesite interlayers in the Tiaojishan
325 Formation (J_{3t}) yield ages of 165–157 Ma, (Qi et al., 2015; Jiao et al., 2016; Lin et al., 2019; Fig.
326 3, Tables 1 and S1). In the Xiabancheng and Niuyingzi basins, the Tiaojishan Formation (J_{3t}) is
327 of 164–153 Ma and the Lanqi Formation (J_{3l}) is of 159–158 Ma in age (Davis et al., 2001; Zhao
328 et al., 2002, 2004; Cope et al., 2007; Liu et al., 2006; Li et al., 2016a; Wu et al., 2021; Fig. 3,
329 Tables 1 and S1). In the Beipiao basin, the intermediate volcanic rocks in the Lanqi Formation (J_{3l})
330 yield ages of 166–153 Ma (Yang and Li, 2008; Zhang et al., 2008a; Wang et al., 2013b; Hao et al.,
331 2020; Fig. 3, Tables 1 and S1). In summary, the volcanics in the Tiaojishan (J_{3t}) or Lanqi (J_{3l})
332 Formation in the Yanshan belt approximately range from 165 to 150 Ma in age.

333 3.3.2 Upper Jurassic–lowermost Cretaceous clastic rocks

334 In the Yanshan belt, the Upper Jurassic strata above the Tiaojishan Formation (J_{3t}) are
335 absent in the Western Hill (Figs. 2 and 3). The unconformity, representing Event B of the
336 Yanshanian orogeny, was initially defined above the volcanics of the Tiaojishan Formation (J_{3t})
337 in the Western Hill; Wong, 1929). As a matter of fact, the Tiaojishan Formation (J_{3t}) in the

338 Yanshan belt is conformably overlain by thick upper Jurassic–lowermost Cretaceous coarse clastic
339 rocks of the Tuchengzi/Houcheng Formation (J_3 - K_{1tch}/J_3 - K_{1h} ; Liu et al., 2018b; Fig. 3, Tables 1
340 and S1). Therefore, the unconformity representing Event B of the Yanshanian orogeny should be
341 located above the Tuchengzi/Houcheng Formation (J_3 - K_{1tch}/J_3 - K_{1h}) in the Yanshan belt. The
342 Tuchengzi/Houcheng Formation (J_3 - K_{1tch}/J_3 - K_{1h}), which consists of conglomerates, sandstones,
343 and mudstones in the fluvial, alluvial to lacustrine facies, shares a similar lithology in different
344 areas of the Yanshan belt (Fig. 3, Tables 1 and S1). The Upper Jurassic–lowermost Cretaceous
345 Tuchengzi/Houcheng Formation (J_3 - K_{1tch}/J_3 - K_{1h}) in the Yanshan belt was constrained between
346 155 and 135 Ma (Swisher et al., 2002; Shao et al., 2003; Cope et al., 2007; Zhang et al., 2005,
347 2008a, 2009; Xu et al., 2012; Wang et al., 2013c; Li et al., 2015; Qi et al., 2015; Li et al., 2016a;
348 Fu et al., 2018; Liu et al., 2018b; Lin et al., 2019; Fig. 3, Tables 1 and S1). The Tuchengzi
349 Formation (J_3 - K_{1tch}) contains several growth strata packages, onlapping or offlapping onto the
350 limb of the fold-and-thrust belts in the Xiahuayuan and Chicheng basins (Liu et al., 2018b; Lin et
351 al., 2019; Shi et al., 2019). Therefore, the syn-tectonic Tuchengzi/Houcheng Formation (J_3 -
352 K_{1tch}/J_3 - K_{1h}) and the unconformity above in the Yanshan belt are thought to be in response to
353 Event B of the Yanshanian orogeny (Zhao, 1990; Cope et al., 2007).

354 In the Yinshan belt, and the Ordos basin and its adjacent areas, the Upper Jurassic volcanics
355 corresponding to the Tiaojishan Formation (J_{3t}) are absent (Fig. 3). The Upper Jurassic–lowermost
356 Cretaceous clastic rocks share a similar lithology with the Yanshan belt. These Upper Jurassic–
357 lowermost Cretaceous strata, which consist of fluvial, alluvial to lacustrine conglomerates,
358 sandstones, and mudstones, are in unconformable contact with the underlying upper Middle
359 Jurassic sequence (Zhang et al., 2008b; Li et al., 2014b, 2015; Wang et al., 2017; Meng et al., 2019;
360 Zhang et al., 2020; Fig. 3, Tables 1 and S1). The Upper Jurassic Daqingshan Formation (J_{3d}) in
361 the Shiguai basin exhibits typical growth strata geometry in the footwall of thrusts (Wang et al.,
362 2017). In the Ordos basin, the Fenfanghe Formation (J_{3f}) also contains syn-tectonic growth strata
363 in the western Ordos thrust and fold belt (Zhang et al., 2008b). The Upper Jurassic strata in the
364 Yungang basin are absent (Li et al., 2014b, 2015; Zhang et al., 2020). In the Ningwu-Jingle basin,
365 the Tianchihe Formation (J_{3t}) exhibits a typical growth strata geometry in the piggy-back basin
366 (Chen et al., 2019). The tuffaceous micrite at the bottom of the Upper Jurassic Tianchihe Formation
367 (J_{3t}) yields zircon ages of 160.6 ± 0.55 Ma (Li et al., 2014b; Fig. 3, Tables 1 and S1). Therefore,

368 the Upper Jurassic-lowermost Cretaceous syn-tectonic sequence and the unconformity above in
369 the entire NCC should be the response to Event B of the Yanshanian orogeny.

370 **3.3 Lower Cretaceous sequence**

371 In the NCC, the Lower Cretaceous is separated from the underlying Upper Jurassic–
372 lowermost Cretaceous sequence by a regional angular unconformity representing Event B of the
373 Yanshanian orogeny (Fig. 3). In the Yanshan belt, the Lower Cretaceous Zhangjiakou Formation
374 (K_1zh) and the Donglingtai Formation (K_1d) comprise a series of siliceous volcanic rocks (e.g.,
375 rhyolitic tuff, rhyolite, andesite, quartz trachyte, and pyroclastics; Qi et al., 2015; Lin et al., 2018;
376 Su et al., 2021; Tables 1 and S1). The Guyang Group (K_1g) in the Yinshan belt consists of fluvial
377 to lacustrine conglomerates and sandstones with volcanic rocks (Gong et al., 2015; Tables 1 and
378 S1). In the Yinshan-Yanshan belt, the Lower Cretaceous sequence, which fills a large number of
379 normal or detachment fault-bounded grabens or half-grabens (Zhang et al., 2004a; Davis and
380 Darby, 2010; Lin and Wei, 2018), has a lower age limit of 136–127 Ma (Niu et al., 2003, 2004;
381 Zhao et al., 2004; Yuan et al., 2005; Zhang et al., 2005; Davis and Darby, 2010; Tables 1 and S1).
382 The Lower Cretaceous sequence in the Ordos basin and its adjacent areas (e.g., Zhidan Group
383 (K_1z), and the Zuoyun Formation (K_1zy) in the Ningwu-jingle and Yungang basins) changes into
384 the fluvial conglomerates to sandstones (Zhang et al., 2011; Li et al., 2014b, 2016c; Zhang et al.,
385 2020). In the Yungang basin, the andesite at the base of the Zuoyun Formation (K_1zy) yields a
386 zircon U–Pb age of 130.1 ± 0.8 Ma (Li et al., 2016c; Tables 1 and S1).

387 **4. Regional deformation**

388 In the NCC, the Jurassic–Early Cretaceous intracontinental deformation, mainly
389 characterized by the supracrustal non-metamorphic structures, such as brittle thrust and normal
390 faults, is well exposed in the Yanshan belt (including the northern Taihangshan belt), the Yinshan
391 belt, and the periphery of the Ordos basin (Fig. 2; Davis et al., 2001; Zhang et al., 2011; Dong et
392 al., 2015). The well-preserved Jurassic–Lower Cretaceous strata in the Yanshan belt, the Yinshan
393 belt, and the Ordos basin and its adjacent areas could provide age constraints on the Jurassic–Early
394 Cretaceous brittle deformation. In this paper, the regional deformation in the Yanshan belt, the
395 Yinshan belt, and the periphery of the Ordos basin is summarized within the chronostratigraphic
396 framework as below.

397 **4.1 Yanshan belt**

398 **4.1.1 Inherited fold-thrust structures**

399 In the NCC, the pre-Jurassic deformation is inferred to correlate the tectonic events at block
400 boundaries, i.e., the closure of the Paleo-Asian Ocean or the collision between the NCC and SCB.
401 The related deformation includes the Middle–Late Triassic E–W striking south-verging Shangyi-
402 Chicheng ductile shear zone, the Fengning-Longhua ductile shear zone, the Damiao-
403 Niangniangmiao ductile shear zone, the Malanyu anticline, and the Jixian thrust in the Yanshan
404 belt (Fig. 4; Wang et al., 2013a), and the Late Triassic south-verging fold-thrusts in the southern
405 West Qinling (Meng and Zhang, 1999; Meng et al., 2019). Several pre-Jurassic ENE striking brittle
406 fold-thrusts in the central Yanshan belt were reworked during the Jurassic–Early Cretaceous (e.g.,
407 the Mengjiazhuang thrust, the Jiyuqing thrust, the Liudaohe thrust in the south Chengde basin;
408 Table 2, Fig. 4). The footwalls of these ENE striking fold-thrusts contain the vertically stacked
409 Cambrian–Ordovician, Permian–Triassic, and Middle Jurassic strata, whereas these strata are
410 absent in the hanging walls (Fig. 4b; Li et al., 2016a). The preserved Middle Jurassic strata concern
411 the Xiahuayuan Formation (J_{2x}; Meng et al., 2019), suggesting the pre-J_{2x} activity of these thrusts.
412 In these thrusts, the Late Jurassic Tiaojishan Formation (J_{3t}), unconformably overlying on the
413 tightly folded underlying strata, is only involved in the eastward trending open folding. This
414 suggests that the southward thrusting and tight folding occurred during the period of post-J_{2x} to
415 pre-J_{3t} (Fig. 4b; Li et al., 2016a). The locally distributed Longmen-Jiulongshan Formations (J_{2l}-
416 J_{2j}) and their counterparts should be syn-tectonic deposits in the flexural basins and/or piggy-back
417 basins, in response to the thrusting related to Event A of the Yanshanian orogeny. The open
418 refolding occurred in the Tiaojishan Formation (J_{3t}) and Tuchengzi Formation (J₃-K_{1tch}). The
419 Early Cretaceous Zhangjiakou Formation (K_{1zh}), bounded by the Chengde normal fault, overlies
420 these refolded strata (Fig. 4b; Li et al., 2016a). Considering the syn-tectonic deposition of the
421 Tuchengzi Formation (J₃-K_{1tch}), this open refolded event should be in response to Event B of the
422 Yanshanian orogeny during the period of post-J_{3t} to pre-K_{1zh}.

423 **4.1.2 Event A of the Yanshanian orogeny-related deformation**

424 In the central Yanshan belt, the Mesoproterozoic strata in the hanging wall of the E-striking
425 Duanshuwa-Jianbaoshan thrust thrust southward onto the Middle Jurassic Xiahuayuan Formation

426 (J_{2x}) and the underlying Paleozoic or Proterozoic rocks (Table 2, Fig. 4; Li et al., 2016a). The
427 Duanshuwa-Jianbaoshan thrust and several neighboring E-striking thrusts (e.g., the Xinglong
428 thrust, the Qingshuihu fault, the Zhujiagou fault, and the Miyun-Xifengkou fault and its NE
429 striking branch faults) are unconformably overlain by the Late Jurassic Tiaojishan volcanic rocks
430 (J_{3t}) or intruded by the Siganding and Wangpingshi plutons, and mafic dykes at the ages of 162
431 and 157 Ma, respectively (Chen, 1998; Zeng et al., 2021). It suggests that these thrusts should be
432 the response to Event A of the Yanshanian orogeny during the period of post-J_{2x} to pre-J_{3t}. In the
433 eastern Yanshan belt, the Guojiadian Formation (J_{2g}) in the footwall is involved in the
434 southeastward thrusting Yangzhangzi-Wafangdian fault, which is intruded by the 160.2 Ma
435 rhyolitic porphyry (Zhang et al., 2002). This phenomenon suggests that this fault was active during
436 the period of post-J_{2g} to pre-J_{3l}, responding to Event A of the Yanshanian orogeny (Zhang et al.,
437 2002).

438 **4.1.3 Event B of the Yanshanian orogeny-related deformation**

439 In the central Yanshan belt, the Mesoproterozoic strata in the hanging walls of several E–
440 NE striking thrusts (e.g., the Dayingzi thrust, the Shanggu-Pingquan thrust, the Gubeikou-
441 Pingquan fault, and the Chengde thrust) thrust on the Tuchengzi Formation (J₃-K_{1tch}) (Table 2,
442 Fig. 4; Davis et al., 2001; Li et al., 2016a). These thrusts are unconformably overlain by the Early
443 Cretaceous Zhangjiakou Formation (K_{1zh}) or intruded by the Early Cretaceous plutons (i.e., 132
444 Ma Wulingshan pluton, 130 Ma Shouwangfe pluton, the 113 Ma Jiashan pluton, the 111 Ma
445 Guozhangzi pluton, and the 129 Ma Qiancengbei pluton; Table 2, Fig. 4; Davis et al., 2001; Li et
446 al., 2016a). Considering that the Tuchengzi/Houcheng Formation (J₃-K_{1tch}/J₃-K_{1h}) in the Yanshan
447 belt was of the syn-tectonic deposits with a growth strata geometry in the footwalls or hanging
448 walls of thrusts (Liu et al., 2018b; Lin et al., 2019; Shi et al., 2019), these structural relationships
449 suggest that these thrusts are related to Event B of the Yanshanian orogeny during the period of
450 post-J_{3t} to pre-K_{1zh} (the same below). Meanwhile, the Sihetang ductile shear zone was considered
451 to form in the north of the Yunmengshan pluton during this period, in view of the 145 Ma syn-
452 tectonic Yunmengshan pluton (Table 2, Fig. 4; Davis et al., 2001; Zhu et al., 2015).

453 The E-striking Gubeikou-Pingquan fault extends westward along the Shangyi-Chicheng
454 ductile shear zone in the western Yanshan belt (Fig. 4; Lin et al., 2020; Yang et al., 2021). Several
455 NE-striking thrusts are developed in the south of the Gubeikou-Pingquan fault (e.g., the

456 Qianjiadian thrust, the Shaliangzi thrust, and the Tanghekou thrust). The first two faults thrust
457 southeastward and the latter one thrusts northwestward (Table 2, Fig. 4; Lin et al., 2020). To the
458 south, a series of nearly NE-striking thrusts are developed in the Western Hill, the Xiahuayuan
459 basin, and the Shangyi basin (e.g., the Nandazhai-Babaoshan thrust, the Xiahuayuan thrust, and
460 the Banshen-Shuiquangou thrust; Table 2, Fig. 4). These faults thrust northwestward, indicated
461 by the NW–SE directional fault-slip data (Table 2, Fig. 4; Zhang et al., 2006; Lin et al., 2020;
462 Yang et al., 2021). All these NE-striking thrusts displace the Meso- and Neo-Proterozoic strata
463 southeastward or northwestward over the Tuchengzi Formation (J₃-K₁tch)/Houcheng Formation
464 (J₃-K₁h) or the Tiaojishan Formation (J₃t) where the J₃-K₁tch is absent in the Western Hill, and
465 unconformably overlain by the Early Cretaceous Zhangjiakou Formation/Donglingtai Formation
466 (K₁zh/K₁d; Zhang et al., 2006; Lin et al., 2020; Yang et al., 2021). It suggests that these NE
467 striking thrusts are related to Event B of the Yanshanian orogeny during the period of post-J₃t to
468 pre-K₁zh/K₁d. The E-striking Gubeikou-Pingquan fault and Miyun-Xifengkou fault are considered
469 to have experienced a dextral strike-slip displacement (Zhang et al., 2004a; Faure et al., 2012).
470 The E- and WNW-striking secondary faults of the Gubeikou-Pingquan fault have a dominant
471 strike-slip or transpressional displacement with dextral or dextral oblique thrusting striations (Lin
472 et al., 2020). The paleostress field was a NW–SE compression, inferred from the fault-slip data
473 (e.g., striations) from secondary faults and adjacent NE-striking thrusts (Lin et al., 2020; Yang et
474 al., 2021). The Upper Jurassic Houcheng Formation (J₃-K₁h) is involved in the dextral Gubeikou-
475 Pingquan fault, unconformably overlain by the Lower Cretaceous Zhangjiakou Formation (Lin et
476 al., 2020). It suggests that the Gubeikou-Pingquan fault experienced a dextral strike-slip or
477 transpressional reactivation related to Event B of the Yanshanian orogeny during the period of
478 post-J₃t and pre-K, which is coeval with the thrusts in the western Yanshan belt.

479 The eastern Yanshan belt is mainly characterized by NE-striking thrusts (e.g., the
480 Nangongyingzi-Beipiao fault) that displace the Mesoproterozoic–Neoproterozoic or Paleozoic
481 sediments in the hanging walls southeastward or northwestward over the Upper Jurassic Tuchengzi
482 Formation (J₃-K₁tch) of the footwalls (Table 2, Fig. 4; Zhang et al., 2002). Most of these thrusts
483 are unconformably overlain by the Lower Cretaceous Zhangjiakou Formation/Yixian Formation
484 (K₁zh/K₁y; Zhang et al., 2002). The structural relationship suggests that these thrusts were mainly
485 active during the period of post-J₃l and pre-K₁y (Event B of the Yanshanian orogeny). The NE-
486 striking Jianchang-Chaoyang fault (also namely Nantianmen fault) displaces the Archaean

487 crystalline basement over the Lower Cretaceous and underlying strata (Su et al., 2020). The
488 Tuchengzi Formation (J₃-K₁tch) and underlying strata below an angular unconformity are involved
489 in the relatively tight fault-related folds, while the overlying Lower Cretaceous strata are slightly
490 deformed. It suggests that this fault was active during the period of post-J₃l to pre-K₁y and then
491 reactivated post-K₁y. Fault-slip data show that this fault firstly thrusts southeastward under a NW–
492 SE compression and then is reactivated as a reverse sinistral fault accommodating with a NNW–
493 SSE compression (Su et al., 2020).

494 **4.1.4 Three-stage extensional deformation**

495 In the eastern NCC, the three-stage extensional deformation occurred within the Yanshan
496 belt during the Jurassic–Early Cretaceous. The first extensional episode was documented in the
497 Niuyingzi basin where the Zhuzhangzi fault was originally a normal fault bounding the Guojiadian
498 Formation (J₂g) during the early Middle Jurassic (Fig. 2; Davis et al., 2009). During the second
499 extensional episode, a detachment ductile shear zone with a top-to-the-NE shear sense was initially
500 formed during the ~156–150 Ma NE–SW extension before the nucleation of the Early Cretaceous
501 Kalaqin metamorphic core complex (MCC; Fig. 2; Lin et al., 2014). This early Late Jurassic
502 extension is also suggested by the brittle normal faults bounding the volcanics of the Tiaojishan
503 Formation (J₃t) in the Chengde basin and the Diao’e and Houcheng sub-basins of the Chicheng
504 basin (Figs. 2 and 4; Davis et al., 2001; Qi et al., 2015; Lin et al., 2018). The well-known third
505 NW-SE extensional episode was well recorded by the Early Cretaceous MCCs (e.g., the
506 Yiwulüshan, Kalaqin, and Yunmengshan MCCs within a time span of 131–114 Ma) and the graben
507 or half-graben basins (Fig. 4; Wang et al., 2001; Lin et al. 2013a, 2013b, 2014; Lin and Wei, 2018).

508 **4.2 Yinshan belt**

509 **4.2.1 Two-stage contractional deformation**

510 In the Yinshan belt, the E–W striking high-angle basement-involved thrusts are widely
511 distributed in western Daqingshan. Numerous E–W striking thrusts cut the Lower Jurassic
512 Wudanggou Formation (J₁w) and underlying Archean crystalline basement through Paleozoic
513 strata in the south of the Shiguai basin (Table 2, Fig. 5; Gong et al., 2015; Wang et al., 2017). The
514 Hetangou-Dongerba thrust, bounding the Shiguai basin, displaces the Permian and underlying
515 strata over the Jurassic coal-bearing Wudanggou (J₁w) and Zhaogou (J₂zg) Formations (Table 2,

516 [Fig. 5; Wang et al., 2017](#)). The syn-tectonic Changhangou (J_{2c}) growth strata with a clear onlap
517 geometry were deposited ahead of the front of this thrust. A cross-cutting relationship of
518 superimposed striations shows that the N–S striations were overprinted by the NW–SE ones,
519 documenting an early N–S compression and a later NW–SE compression. To the north, the
520 Beilinshan thrust cuts the Changhangou (J_{2c}) growth strata, presenting the NW–SE striations with
521 the absence of the N–S ones ([Table 2, Fig. 5; Wang et al., 2017](#)). The Daqingshan Formation (J_{3d}),
522 exhibiting a growth strata geometry, onlaps onto a north-verging blind thrust in its central segment
523 or directly onlaps onto the front of this thrust elsewhere ([Wang et al., 2017](#)). To the east, this thrust
524 is truncated by the detachment fault of the Hohhot MCC in Louhuashan ([Fig. 5](#)). All the structural
525 relationships suggest that most of the E-striking thrusts occurred during the period of post-J_{2zg} to
526 pre-J_{3d} under a N–S compression related to Event A of the Yanshanian orogeny. Afterward, these
527 E-striking thrusts were reactivated or nucleated during the period of post-J_{2c} to pre-K_{1g} under a
528 NW–SE compression related to Event B of the Yanshanian orogeny. In the north, two NW-striking
529 dextral strike-slip faults, which cut the Daqingshan Formation (J_{3d}) and truncated by the Early
530 Cretaceous Hohhot detachment fault, should be active during this NW–SE compression ([Fig. 5;](#)
531 [Gong et al., 2015](#)).

532 The high-angle thrusts in western Daqingshan gradually change eastward into a low-angle
533 and thin-skinned geometry ([Wang et al., 2017](#)). In eastern Daqingshan, the low-angle Daqingshan
534 thrust was exhumed by the Early Cretaceous Hohhot detachment fault ([Table 2, Fig. 5](#)). The
535 allochthonous Proterozoic strata have been thrust northwestward from the SE atop the
536 autochthonous conglomerates of the Daqingshan Formation (J_{3d}), illustrated by the S–C fabrics
537 defined by marble lenses and a shear foliation ([Gong et al., 2015](#)). It suggests that the low-angle
538 thrusts in eastern Daqingshan nucleated during the period of post-J_{2c} to pre-K_{1g} under a NW–SE
539 compression.

540 Besides, in Langshan, a steeply dipping NE-striking thrust fault juxtaposes the Archean
541 crystalline basement against a variety of footwall units, most of which are Lower Cretaceous and
542 undifferentiated Jurassic strata ([Fig. 2; Darby and Ritts, 2007](#)). The Lower Cretaceous strata are in
543 unconformable contact with the Jurassic ones. The striations on thrust fault planes and axial planes
544 of related folds suggest that a Late Jurassic to Early Cretaceous NNW–SSE compression occurred
545 in Langshan ([Darby and Ritts, 2007](#)).

546 **4.2.2 Two-stage extensional deformation**

547 In the Yinshan belt, a series of small-scale normal faults, bounding syn-tectonic growth
548 strata in small-scale grabens, cut the Wudangou Formation (J_{1w}) and the unconformity below or
549 develop in the weakly folded Zhaogou Formation (J_{2zg}) in the Shiguai basin (Fig. 5; Darby et al.
550 2001; Ritts et al. 2001; Wang et al. 2017). The fault-slip data suggest that these normal faults
551 nucleated during the Early–early Middle Jurassic N–S extension. Stratigraphic and
552 sedimentological analyses also suggested that the Shiguai basin was an E–W striking Early–early
553 Middle Jurassic half-graben, which is inverted during the later contraction (Darby et al. 2001). The
554 Early Cretaceous extensional deformation in the Yinshan belt mainly includes the Hohhot MCC
555 and related detachment faults (Fig. 5; Davis and Darby, 2010). The south-dipping Hohhot
556 detachment fault shows the top-to-the-SE shearing under the NW–SE extension during 127–119
557 Ma. In addition, the Early Cretaceous extension, presented by brittle normal faults, also occurred
558 in Langshan (Fig. 2; Darby and Ritts, 2007).

559 **4.3 Periphery of the Ordos Basin**

560 **4.3.1 Event B of the Yanshanian orogeny-dominated deformation**

561 The intracratonic Ordos basin is surrounded by the Cenozoic Hetao and Fenwei Grabens
562 in the north and south, respectively (Fig. 2). The Jurassic–Early Cretaceous deformation is well
563 documented in the western and eastern margins. In the Western Ordos fold-thrust belt, the Jurassic
564 and underlying strata are involved in a series of eastward thrusting faults and unconformably
565 overlain by the Cretaceous strata, revealed by seismic reflection data (Figs. 2 and 6, Table 2).
566 Northward, a nearly N-striking fold-thrust belt in Zhuozishan juxtaposes the Lower Paleozoic and
567 underlying strata against a vertical to overturned Upper Jurassic Fenfanghe Formation (J_{3f}) in the
568 east (Figs. 7a and 7b, Table 2; Darby and Ritts, 2002; Li et al., 2022). A large number of striations
569 on the fault plane are oriented in the NW–SE direction (Li et al., 2022). These folded strata
570 involved in the west-dipping thrust faults are unconformably overlain by the Cretaceous strata in
571 the east of Zhuozishan (Fig. 7a). Considering the syn-tectonic growth strata of the Fenfanghe
572 Formation (J_{3f}) in the east of Zhuozishan (Zhang et al., 2008b), the fold-thrust belt in the western
573 Ordos margin should be active during the period of post- J_{2a} to pre- K_{1z} under the NW–SE
574 compression related to Event B of the Yanshanian orogeny.

575 Further west, a series of thrusts and folds in the northern Helanshan fold-thrust belt (e.g.,
576 the Chaqigou-Tatagou and Dashiugoumen-Dawukou faults) displace northwestward the
577 Carboniferous–Permian strata over the Triassic strata in the east (Table 2, Fig. 7c; Darby and Ritts,
578 2002; Huang, et al., 2015; Yang and Dong, 2018; Li et al., 2022). In the west, the Lower Paleozoic
579 strata thrust southeastward onto the Middle Jurassic Anding Formation (J_{2a}) in the hanging wall
580 of the Xiaosongshan fault. In the southern Helanshan fold-thrust belt, the Devonian strata thrust
581 southeastward onto the tightly folded Jurassic Fenfanghe Formation (J_{3f}) and underlying strata
582 along the Dazhanchang fault (Fig. 7d, Table 2; Yang and Dong, 2020). The Dazhanchang fault
583 and related folds are unconformably overlain in the thrust front by the Lower Cretaceous. All fault-
584 slip vectors of these thrusts and folds are consistent in the NW–SE direction (Huang, et al., 2015;
585 Yang and Dong, 2018, 2020; Li et al., 2022), indicating that a NW–SE compression related to
586 Event B of the Yanshanian orogeny occurred in the Helanshan fold-thrust belt during the period
587 of post-J_{2a} to pre-K_{1z}. Besides, the syn-tectonic growth strata in the Middle Jurassic Zhiluo
588 Formation (J_{2z}) and Anding Formation (J_{2a}) have been identified in the east of the Dazhanchang
589 fault (Fig. 7e; Cheng et al., 2022). A reversal of paleocurrent directions from west-directed to east-
590 directed occurred in the Zhuozi Shan during the Early–Middle Jurassic (Darby and Ritts, 2002).
591 Despite the lack of discovery of syn-sedimentary structures, these phenomena should be the
592 response to Event A of the Yanshanian orogeny during the late Middle Jurassic.

593 In the east of the Ordos basin, the Ningwu-Jingle basin is a NE-striking synclinal basin,
594 locally confined by the NE-striking thrust faults (e.g., the Chunjing thrust, the Mafangzhen thrust,
595 and the Dujiacun thrust; Table 2, Fig. 8a; Chen et al., 2019). The Lower–Middle Jurassic
596 Yongdingzhuang (J_{1y}) and Datong (J_{2d}) Formations and underlying strata are involved in the NE-
597 striking fold deformation. Two sets of vertically stacked growth strata (i.e., the Yungang
598 Formation (J_{2yg}) and the Tianchihe Formation (J_{3tc})) were deposited in the synclinal core (Fig. 8;
599 Chen et al., 2019). The NE-striking Yungang basin is bounded by the SE-dipping thrust faults in
600 the southeast (e.g., the northwestward thrusting Kouquan thrust and Emaokou fault). The syn-
601 tectonic growth strata in the Yungang Formation (J_{2yg}) were deposited in the thrust front and
602 unconformably overlain by the Lower Cretaceous strata in the north (Zhang et al., 2020). The fault-
603 slip vectors in the Yungang basin are consistent in the NW–SE direction, suggesting that these
604 NE-striking thrusts were active under a NW–SE compression (Zhang et al., 2020). Considering
605 the simultaneity with the Fenfanghe Formation (J_{3f}) in the Ordos basin and the Daqingshan

606 Formation (J_{3d}) in the Yinshan belt, the growth strata in the Tianchihe Formation (J_{3tc}) should be
607 deposited during the Late Jurassic–earliest Cretaceous NW–SE compression related to Event B of
608 the Yanshanian orogeny. The growth strata in the Yungang (J_{2yg}), coeval with the Zhiluo (J_{2z})
609 and Anding (J_{2a}) Formations in the Ordos basin and the Changhangou Formation (J_{2c}) in the
610 Yinshan belt, should be in response to the late Middle Jurassic N–S compression related to Event
611 A of the Yanshanian orogeny.

612 **4.3.2 Two-stage extensional deformation**

613 The Early–early Middle Jurassic extensional normal faults were widely distributed in the
614 Ordos basin and its adjacent areas (Fig. 2). In the central and northeastern Ordos basin, the NNE–
615 SSW or nearly N–S extensional normal faults, indicated by the NNE–SSW fault-slip vectors, were
616 identified in the Upper Triassic–Lower Jurassic strata (Zhang et al., 2011). In the Yungang and
617 neighboring Guangling basins, the normal faults, which cut the basal conglomerates in the lower
618 Lower Jurassic, are covered by the upper Lower Jurassic strata (Li et al., 2015). In the Qingshuihe
619 basin, east of the southern Ordos basin, the E–W to WNW–ESE-striking normal faults cut the
620 Paleozoic to Middle Jurassic strata (Zhang et al., 2011). In the southern NCC, the syn-sedimentary
621 normal faults and soft-sediment deformation also occurred in the Lower Jurassic Anyao Formation
622 (Meng et al., 2019). The Early–early Middle Jurassic extensional deformation is characterized by
623 the small-scale N–S extensional brittle normal faults. Besides, the Early Cretaceous NW–SE
624 extension is widely identified in the Ordos basin and its adjacent areas, mainly expressed by small-
625 scale brittle normal faults (Zhang et al., 2011).

626 **5. Magmatism**

627 **5.1 Petrological and geochemical characteristics of magmatic rocks**

628 The Jurassic magmatism that occurred in the eastern NCC can be divided into two stages (Fig.
629 9), i.e., Early–early Middle Jurassic (191–167 Ma), and Late Jurassic (~166–142 Ma with a peak
630 at 164–152 Ma). The Early Cretaceous (135–115 Ma) magmatism is distributed throughout the
631 NCC (Fig. 9). The Early–early Middle Jurassic (191–170 Ma) intrusive rocks, composed of granite,
632 monzogranites, monzonite, and syenite, are mainly distributed in the Yanshan belt, the southern
633 Yanbian area, the Liaodong peninsula, and sporadically in western Shandong as well as northern
634 Jiangsu (e.g., Zhang et al., 2014; Wu et al., 2019; and references therein; Fig. 2). These granitoids,

635 belonging to metaluminous, high-K calc-alkaline or shoshonitic, and I-type granites, are mainly
636 distributed in the southern and northern margins of the eastern NCC (Fig. 2). The Early–early
637 Middle Jurassic intrusive rocks (191–170 Ma) show typical characteristics of adakite-like primary
638 magmas derived from partial melting of the ancient lower crust. The $\epsilon\text{Nd}(t)$ and $\epsilon\text{Hf}(t)$ values,
639 from low negative to low positive, suggest the interaction of various lower to upper crust,
640 lithospheric mantle, and asthenospheric mantle sources (Lan et al., 2012; Zhang et al., 2014). In
641 the Western Hill, the Nandaling basalts, basaltic andesites, and dacites (188–176 Ma) present low
642 initial $^{87}\text{Sr}/^{86}\text{Sr}$ ratios and variable negative $\epsilon\text{Nd}(t)$ values, originating from upwelling of
643 asthenosphere and decompressional melting of the early subduction-metasomatized continental
644 lithospheric mantle (Guo et al., 2007; Wang et al., 2007; Fig. 2). The Xinglonggou andesites and
645 dacites in Western Liaoning (177–167 Ma) are high-Mg# adakites with arc-like isotopic
646 compositions, deriving from a subducted-oceanic slab (Yang and Li, 2008; Fig. 2).

647 The Late Jurassic (164–152 Ma) intrusive rocks, including granitoids and gabbro-pyroxenite
648 complexes, are mainly distributed in the eastern NCC, e.g., the Yanshan belt, the northern
649 Taihangshan, the southern Yanbian area, the Liaodong peninsula, the Jiaodong peninsula, and the
650 Bengbu area (Fig. 2; e.g., Zhang, 2007; Zhang et al., 2014; Wu et al., 2019; and references therein).
651 The granitoids, consisting of granite, monzodiorite, syenite, diorite, and monzonite, are mainly calc-
652 alkaline and I-type with minor A-type and S-type granites. These rocks have adakite-like
653 geochemical signatures and ancient crust-derived isotopic characteristics. The intermediate–mafic
654 intrusive complexes, possessing slightly to moderately enriched isotopic compositions, were
655 derived from the partial melting of subcontinental lithospheric mantle metasomatized by earlier
656 subduction slab-derived fluids (Zhang et al., 2004b; Zhang, 2007; Zhang et al., 2010). The
657 contemporaneous Tiaojishan volcanic rocks and their counterparts (i.e., Lanqi Formation and
658 Houcheng Formation) are mainly distributed in the Yanshan belt and its adjacent areas. The
659 eruption ages are variable from Western Liaoning (166–153 Ma), through Chengde-Luanping
660 (162–153 Ma) and Western Hill-Xuanhua-Yuxian (158–142 Ma; Guo et al., 2022). They are
661 andesite, dacite, trachyandesite, and volumetrically minor basalt and rhyolite (Zhang et al., 2014).
662 Late Jurassic volcanic rocks, mainly calc-alkaline and intermediate-felsic, share highly coherent
663 petrological, geochemical and unradiogenic Hf isotope features similar to those of volcanic rocks
664 from modern continental arcs in a subduction-related setting (Wu et al., 2005, 2008; Guo et al.,

665 2022). These volcanic rocks are mainly derived from the partial melting of the lower crust through
666 magma underplating at the crust-mantle boundary (Yang and Li, 2008).

667 The Early Cretaceous (135–115 Ma) magmatism, representing a giant igneous event (Wu et
668 al., 2005), is extensively distributed in the northern and southern margins of the NCC as well as
669 the interior of the eastern NCC (Zhang et al., 2004b; Zhang et al., 2014; Wu et al., 2019). The
670 Early Cretaceous intrusive rocks include dolerite, gabbro, diorite, granodiorite, I- and A-type
671 granite, and syenite, whereas the volcanic rocks are mainly basalt, rhyolite, rhyolitic tuff, trachyte,
672 and trachyandesite. Unlike Jurassic granitoids, these Early Cretaceous granitoids are not adakitic
673 but commonly alkaline (Zhang et al., 2014; Wu et al., 2019). The temporal and spatial distribution
674 of mafic magmatism suggests that the variably enriched Mesozoic lithospheric mantle existed
675 beneath the NCC during the Early Cretaceous (Zhang, 2007; Zhang et al., 2010). The Early
676 Cretaceous igneous rocks are derived from multiple sources, i.e., depleted mantle, enriched
677 lithospheric mantle, ancient lower crust, and juvenile crust, suggesting the intensive mantle-crust
678 interaction in the NCC during the Early Cretaceous time (Yang et al. 2004; Zhang et al., 2014; Wu
679 et al., 2019).

680 5.2 Fabrics of granitic plutons

681 The fabrics of granitic plutons have been used for their potential to record the tectonic regime
682 (i.e., compressional, extensional, and strike-slip) coeval with granite emplacement (e.g., Paterson
683 et al., 1989; Bouchez and Gleizes, 1995). The study of anisotropy of magnetic susceptibility (AMS)
684 is an effective and practical way to reveal the structural elements of apparently isotropic to weakly
685 deformed granitic plutons (e.g., Archanjo et al., 1994; Bouchez et al., 1997). In the NCC, numerous
686 granitic plutons have been targeted to understand the Jurassic–Early Cretaceous tectonic regime
687 through the AMS study.

688 5.2.1 New fabric data of Jurassic plutons

689 In the NCC, fabric studies have been rarely performed on the Jurassic granitic plutons in the
690 Yanshan belt. In this study, we selected the granitic Jianchang-Jiumen plutons in the eastern
691 Yanshan belt to provide Jurassic regional tectonic information through an AMS study (Fig. 4). The
692 Jianchang-Jiumen plutons, extending ~50 km along a NE–SW long axis (Fig. 10), are the
693 representative Jurassic plutons in North China. Both the Jiumen and Jianchang plutons appear

694 isotropic without observable planar and linear fabrics at outcrops. They consist of an Early Jurassic
695 pale-red monzogranite (194–176 Ma) in the Jiumen pluton and a Late Jurassic light gray
696 monzogranite (161–153 Ma) in the Jianchang one (Wu et al., 2006; Cui, 2015). New SIMS zircon
697 U-Pb dating of four samples (JJ39 in the Jiumen pluton, and JJ24, JJ30, and JJ42 in the Jianchang
698 one) yields the ages of 189.9 ± 2.7 Ma, 158.6 ± 2.5 Ma, 157.4 ± 2.3 Ma, 157.4 ± 2.3 Ma, respectively
699 (cf. Text S1 in supplementary materials for details; Figs. 10 and 11).

700 The Jianchang-Jiumen plutons intrude into the undeformed Archaean granite and
701 unmetamorphosed Neoproterozoic–Paleozoic sedimentary rocks (Fig. 10). To the north, these
702 Neoproterozoic–Paleozoic sedimentary strata are folded prior to pluton emplacement, as suggested
703 by the undeformed Late Triassic granitic stock intruded into the core of the Yangjiazhangzi
704 syncline (Fig. 10). The outward dipping bedding in the country rocks is subparallel to the pluton
705 border (Fig. 10). It suggests that the Jianchang-Jiumen plutons intruded into the pre-existing
706 anticline and were constructed by magma inflation and pushing aside the country rocks (cf. Text
707 S2 in supplementary materials for details). Microscopically, quartz grains are anhedral and
708 undeformed without signs of undulose extinction or weak dynamic recrystallization with some
709 small subgrains at the border of coarse grains with undulose extinction. The other rock-forming
710 minerals are all euhedral without any deformation. Thus, the fabrics in the Jianchang-Jiumen
711 plutons are magmatic or submagmatic, acquired during, or just after, the crystallization of the
712 magma without significant solid-state deformation (cf. Text S2 in supplementary materials for
713 details). Magnetic mineralogy investigations suggest that the magnetic fabrics of the Jianchang-
714 Jiumen plutons are dominated by pseudo-single domain magnetite, implying that the principal axis
715 of the magnetic fabrics can be correlated to the petro-fabrics of studied samples (e.g., Hargraves
716 et al., 1991; Tarling and Hrouda, 1993; cf. Text S3 in supplementary materials for details). At the
717 map scale, both magnetic foliation and lineation in the Early Jurassic Jiumen pluton are highly
718 scattered with variable dips (Fig. 12). This may be due to an overprint by the intrusion of the Late
719 Jurassic Jianchang pluton near its bottom where the remnant of the Jiumen pluton are scattered
720 within the Jianchang pluton (Fig. 10). Nevertheless, in the Jianchang pluton, the margin-parallel
721 magnetic foliations mainly present moderately to highly outward dipping around its northwestern
722 part and subparallel striking to the southeastern margin of the pluton (Fig. 12a). The margin-
723 parallel outward dipping magnetic foliations around the northwest define a dome-like roof beneath
724 the Jiumen pluton (Fig. 12a). The magnetic lineations display gentle to moderate NE–SW plunging

725 throughout the pluton (mean at $60^\circ/20^\circ$; Fig. 12b). Without any regional strain, the magmatic
726 lineation that reflects the magma flow within the pluton would have variable orientations and
727 plunges depending on magma convection (e.g., Paterson, 1989). These NE–SW plunging magnetic
728 lineations may provide a record of the early Late Jurassic NE–SW regional extension.

729 **5.2.2 Fabrics of Jurassic granitic plutons**

730 The Early Jurassic regional tectonic information is still not available from the fabrics of the
731 granitic plutons due to overprinting of the fabrics in the Jiumen pluton by the later intrusion of the
732 Jianchang pluton. Nevertheless, considerable effort has been devoted to the fabric study on
733 numerous Late Jurassic plutons in the Yanshan belt and Jiaodong peninsula (Table 3; Lin et al.,
734 2021). Similar to the Jianchang pluton, several contemporaneous granitic plutons are mainly
735 composed of isotropic granite without observable planar and linear fabrics at outcrops (e.g.,
736 Siganding pluton, Luanjiahe pluton, and Wendeng pluton; Table 3). Several Late Jurassic plutons
737 have been greatly overprinted by the NW–SE directed detachment faulting of the Early Cretaceous
738 MCCs (e.g., the Yiwulüshan, Linglong, and Queshan plutons; Wang, 2013; Lin et al., 2013a,
739 2013b; Meng and Lin, 2021; Lin et al., 2021). The syn-tectonic Kuyushan pluton exhibits the
740 margin-parallel gneissic to mylonitic foliation with a locally NE–SW subhorizontal mineral and
741 stretching lineation in its northern margin (Meng and Lin, 2021). The AMS measurement suggests
742 that the syn-emplacement fabrics of these Late Jurassic plutons possess mainly margin-parallel or
743 concentric magnetic foliation patterns, exhibiting a dome-like geometry (Lin et al., 2021; Table
744 3). The lineations in the plutons exhibit variable orientations and plunges without any correlation
745 with the regional strain (e.g., Paterson, 1989). Together with NE–SW striking mineral and
746 stretching lineations in the ductile shear zone in the northern margin of the Kuyushan pluton, the
747 consistent NE–SW magnetic lineations in several plutons (e.g., the Jianchang, Siganding,
748 Kuyushan, Luanjiahe, and Wendeng plutons) were considered to have recorded the early Late
749 Jurassic NE–SW regional extension in the northeastern part of the NCC (Lin et al., 2021; Table
750 3).

751 **5.2.3 Fabrics of the Early Cretaceous granitic plutons**

752 During the Early Cretaceous, MCCs are well developed in the NCC (Lin and Wei, 2018 and
753 references therein). Within the Yunmengshan MCC, the fabrics of the Early Cretaceous

754 Yunmengshan pluton were overprinted by the NW–SE directed Shuiyu detachment faulting
755 (Wang, 2013). The syn-tectonic Gudaoling, Yinmawanshan, Congjia, and Guojialing plutons
756 emplaced into the core of the South Liaoning and Linglong MCCs in the Liaodong and Jiaodong
757 Peninsulas (Charles et al., 2011; 2012). The fabrics of these Early Cretaceous plutons within the
758 core of the MCCs are consistent with the mylonitic ones in the ductile shear zones. The magnetic,
759 mineral and stretching lineations record the Early Cretaceous NW–SE regional extension (Lin et
760 al., 2021; Table 3). Besides, numerous Early Cretaceous granitic plutons without observable planar
761 and linear fabrics at outcrops are distributed in the NCC. The AMS measurement suggests that
762 these isotropic granitic plutons present almost margin-parallel or concentric magnetic foliation
763 patterns with a dome-like geometry (Lin et al., 2021; Table 3). Most of these isotropic plutons,
764 exhibiting highly scattered magnetic lineations, were not influenced by the regional strain.
765 However, the consistency of the NW–SE magnetic lineations in the Wang’anzhen and Aishan
766 plutons suggests that they record the Early Cretaceous NW–SE regional extension (Lin et al., 2021;
767 Table 3).

768 **6. Discussion**

769 A general review and synthesis of available data concerning strata and unconformities,
770 tectonic deformation, and magmatism enable us to establish a detailed Jurassic–Early Cretaceous
771 tectonostratigraphic framework of the NCC (Fig. 13). Integrating all structural elements with
772 associated kinematics, and geochemistry and fabric data of igneous rocks into a coherent
773 tectonostratigraphic framework, we propose a four-stage tectonic evolutionary model to delineate
774 the process of Jurassic–Early Cretaceous (Yanshanian) intracontinental orogeny in the NCC (Figs.
775 14–16). Accordingly, the geodynamic relationships of the episodic intracontinental deformation
776 with variable plate subduction/collision settings at different active boundaries in East Asia are
777 discussed. The results provide a significant example of polyphase intra-plate deformation and
778 magmatism paradigm in response to intracontinental orogeny with variable plate-boundary
779 dynamics.

780 **6.1 The Early–early Middle Jurassic (~200-170 Ma): N-S extension related to the post-**
781 **orogenic extension between the North China Craton and the South China Block**

782 In the NCC, an ongoing debate concerns the Early–early Middle Jurassic tectonic setting. The
783 Late Triassic–Early Jurassic compressional setting has been proposed to account for the
784 unconformity between the Triassic and Lower Jurassic strata. The Xingshikou conglomerate was
785 considered to represent the Lower Jurassic syn-tectonic molasse in a flexural basin (Zhao, 1990;
786 Liu et al., 2007; Liu et al., 2012; Li et al., 2016a). However, the Xingshikou Formation, which has
787 been assigned to Upper Triassic, is in disconformable contact with the overlying Lower Jurassic
788 strata (Yang et al., 2006; Meng et al., 2014, 2019). Sedimentary studies argue that the NCC was
789 under a Late Triassic–early Middle Jurassic extensional tectonic setting, in view of the fining- and
790 deepening-upward depositional associations containing abundant volcanic rocks (Meng et al.,
791 2014, 2019). The Lower–lower Middle Jurassic coal-bearing strata (~200–170 Ma) contain
792 abundant mafic volcanic rocks in the Nandaling and Xinglonggou Formations (J_{1-2n}/J_{1x}) in the
793 Yanshan belt and the Anyao Formation (J_{1a}) in the Jiyuan region (Fig. 13). Moreover, numerous
794 E–W striking brittle normal faults with N–S oriented striations on the fault plane in the Yinshan
795 belt as well as the Ordos basin and its adjacent areas (Fig. 14a; Darby et al., 2001; Ritts et al.,
796 2001; Li et al., 2004, 2015; Zhang et al., 2011). Therefore, it is reasonable to infer that the NCC
797 was under a N–S regional extension during the period of the Early–early Middle Jurassic (~200–
798 170 Ma), giving rise to rift basins that are filled with coal-bearing strata containing mafic volcanic
799 rocks.

800 To the north of the NCC, the closure of the Paleo-Asian Ocean occurred in the late Devonian
801 (Xu et al., 2013; Zhao et al., 2013) or the late Permian to Early Triassic (Chen et al., 2000; Jan et
802 al., 2008; Li, 2006; Lin et al., 2008; Xiao et al., 2003, 2015). In the south, the deep continental
803 subduction between the NCC and SCB occurred during the Triassic, giving rise to the Late Triassic
804 Dabie-Sulu HP–UHP orogenic belt (e.g., Mattauer et al. 1985; Faure et al., 1999, 2003; Hacker et
805 al., 2000; Ratschbacher et al., 2003; Lin et al., 2005, 2009; Li et al., 2017; Fig. 1). The onset of
806 subduction of the PPP was considered to occur in the Early Jurassic at least, as evidenced by the
807 occurrence of the Early Jurassic calc-alkaline igneous rocks and accretionary complexes in the
808 East Asian continental margin (e.g., in Northeast China and Korean Peninsula; Wu et al., 2007;
809 Guo et al., 2015; Tang et al., 2018; Wang et al., 2019; Li et al., 2020). It was proposed that the
810 NCC was under an Early Jurassic WNW-directed initial PPP subduction-related or back-arc

811 extensional setting, generating the Early Jurassic adakite-like igneous rocks (Wu et al. 2005, 2019;
812 Zhu et al., 2018; Hao et al., 2020). However, the E–W striking bimodal volcanic zone (~250 km
813 long and ~40 km wide, ages at ~190–165 Ma) with voluminous rhyolitic and basaltic rocks is only
814 distributed in the Nanling Range of the SCB interior (He et al., 2010; Yu et al., 2010; Fig. 15a).
815 The basalt–gabbro–syenite–granite rock suite, not metasomatized by the subduction-related fluids,
816 was considered to occur in a post-orogenic extensional setting in the SCB interior (Li et al., 2007b;
817 Li et al., 2021). Furthermore, both the Early–early Middle Jurassic volcanics and granitoids are
818 mainly distributed in the southern and northern margins of the NCC (Zhang, 2007; Fig. 14a).
819 Together with the widely distributed N–S extensional normal faults, we suggest that the N–S
820 extension in the NCC is more likely to be related to the post-orogenic extension after the deep
821 continental subduction of the SCB beneath the NCC (Fig. 15a). The initial high-angle subduction
822 of the PPP, if there was, could not influence the NCC interior. The Early Jurassic adakite-like
823 rocks were likely related to the pre-existing subducted paleo-oceanic slab (Guo et al., 2007; Wang
824 et al., 2007; Yang and Li, 2008).

825 **6.2 The late Middle Jurassic–earliest Cretaceous (~170–135 Ma): two-stage compression** 826 **with a latest Middle–early Late Jurassic (~165–150 Ma) local extension**

827 Albeit a consensus suggests that the NCC experienced a compression-dominated episode
828 during the Middle Jurassic–earliest Cretaceous (Davis et al., 2001; Zhang et al., 2014; Dong et al.,
829 2015; Li et al., 2016), a clear tectonic process has not been established yet. One group of
830 researchers considers that the NCC underwent a tectonic process characterized by alternating
831 contractional and extensional deformation during the Middle Jurassic–earliest Cretaceous (e.g.,
832 Davis et al., 2001, 2009; Zhang et al., 2011; Faure et al., 2012; Wang et al., 2017). Alternatively,
833 another group proposes that the NCC experienced multi-directed compressions under the East
834 Asian multi-plate convergent tectonic system during this Middle Jurassic–earliest Cretaceous
835 period (e.g., Dong et al., 2015; Zhang et al., 2022). The extensional episode has been not
836 considered by the latter. Integrating all structural elements and associated kinematics into a well-
837 established tectonostratigraphic framework, we present a clear tectono-magmatic process during
838 the late Middle Jurassic–earliest Cretaceous (~170–135 Ma), characterized by a two-stage
839 compression with the latest Middle–early Late Jurassic (~165–150 Ma) local extension, and related
840 dynamic origins.

841 **6.2.1. The late Middle Jurassic (~170–160 Ma): N–S compression in response to the far-field**
842 **compression related to the closure of the Mongol–Okhotsk Ocean**

843 The late Middle Jurassic N–S compressional event (i.e., Event A of Yanshanian orogeny) is
844 well recorded by the unconformity above the coal-bearing strata and the upper Middle Jurassic
845 syn-tectonic conglomerates and sandstones (Fig. 13). The N–S directed fold-thrusts were mainly
846 localized in the northern NCC (Fig. 14b), e.g., the E–ENE striking fold-thrust belts in the Yinshan–
847 Yanshan belt. The syn-tectonic Longmen and Jiulongshan Formations (J₂l–J₂j) and their
848 counterparts could locally fill into the flexural basins and/or piggy-back basins in the front or back
849 of the fold-thrusts (Figs. 4–8). The duration of Event A of Yanshanian orogeny has been
850 constrained to the period of post-Yaopo Formation (J₂yp) and its counterparts, to the depositional
851 period of the syn-tectonic Longmen and Jiulongshan Formations (J₂l–J₂j) and their counterparts,
852 i.e., ~170–160 Ma (Fig. 13). In the SCB, the contemporaneous late Middle Jurassic compressional
853 deformation was absent, presenting that the Middle to Late Triassic NW- or NWW- striking
854 intracontinental compressional deformation was overprinted by the Late Jurassic NE- striking
855 thrusts and fault-related folds (Chu et al., 2012a, 2012b, 2018, 2019; Li et al., 2016b, 2021). To
856 the north of the NCC, it is generally accepted that the MOO closed progressively from west to east
857 during the Jurassic–Early Cretaceous (Zorin, 1999; Kravchinsky et al., 2002; Metelkin et al., 2010).
858 Although the WNW-directed subduction of the PPP has been considered to be responsible for
859 Event A of the Yanshanian orogeny (e.g., Zhu et al., 2018; Hao et al., 2020), it is incompatible
860 with the N–S directed fold-thrusts developed in the northern NCC. Therefore, the far-field
861 compression related to the closure of the MOO can be considered as the best explanation for this
862 N–S compression during Event A of the Yanshanian orogeny in the northern NCC (Fig. 15b).

863 **6.2.2. The Late Jurassic–earliest Cretaceous (~160–135 Ma): large-scale NW–SE**
864 **compression in response to the flat slab subduction of the Paleo-Pacific Plate**

865 The Late Jurassic–earliest Cretaceous mainly NW–SE compressional event (i.e., Event B of
866 the Yanshanian orogeny) is well illustrated by the syn-tectonic deposition (the Tuchengzi
867 Formation and its counterparts) and the unconformity above them (Fig. 13). The NW–SE directed
868 fold-thrust belts are developed throughout the NCC (Fig. 14d). In the Yanshan belt, numerous NE-
869 to NNE- striking faults and fault-related folds have formed to accommodate a NW–SE shortening
870 (Davis et al., 2001; Zhang et al., 2002; Li et al., 2016a; Liu et al., 2020; Su et al., 2020). The pre-

871 existing E-striking late Middle Jurassic Gubeikou-Pingquan fault and Miyun-Xifengkou fault in
872 the Yanshan belt are considered to have experienced dextral strike-slip displacement due to this
873 oblique NW–SE compression (Faure et al., 2012; Lin et al., 2019). In western Daqingshan, and
874 the Ningwu-Jingle and Yungang basins, the late Middle Jurassic high-angle N–S directed thrusts
875 were overprinted by the younger NW–SE directed thrusts indicated by the superimposed N–S and
876 NW–SE trending striations, and the vertically superimposed syn-tectonic conglomerates (e.g., the
877 Changhangou (J_{2c}) and Daqingshan (J_{3d}) Formations, and the Yungang (J_{2yg}) and Tianchihe
878 Formations (J_{3tc}); Wang et al., 2017; Chen et al., 2019; Figs. 13 and 14d). Large-scale low-angle
879 thin-skinned thrusts recorded a NW–SE compression in eastern Daqingshan (Gong et al., 2015;
880 Fig.14d). Furthermore, the contemporaneous NW–SE directed thrusts were widely developed in
881 western Ordos, Helanshan, Zhuozishan, and Langshan (Darby and Ritts, 2002; Huang, et al., 2015;
882 Yang and Dong, 2018; Li et al., 2022). The NW–SE compression had influenced the western
883 margin of the NCC, indicated by the NW–SE striking fault-slip vectors in Helanshan (Huang, et
884 al., 2015; Yang and Dong, 2018, 2020; Li et al., 2022). In the front or back of these fold-thrusts,
885 the syn-tectonic Tuchengzi Formation (J₃-K_{1tch}) and its counterparts could fill into the flexural
886 basins and/or piggy-back basins (Figs. 4–8). The duration of Event B of the Yanshanian orogeny
887 has also been well constrained to the period of the depositional period of the syn-tectonic
888 Tuchengzi Formation (J₃-K_{1tch}) and its counterparts, to pre-Zhangjiakou Formation (K_{1zh}) and its
889 counterparts (Fig. 13; ~160–135 Ma in the western NCC and ~155–135 Ma in the eastern NCC).
890 Besides, as a Late Triassic syn-orogenic transform fault, the Tan-Lu fault reactivated as a
891 thoroughgoing sinistral strike-slip fault and offset the NCC during the earliest Cretaceous (143–
892 137 Ma; Zhu et al., 2018). The Late Triassic Xingcheng-Taili ductile shear zone adjacent to the
893 Tan-Lu fault reactivated during the Late Jurassic–earliest Cretaceous (~152–139 Ma; Liang et al.,
894 2015, 2022). During the Late Jurassic, the NNW-directed low-angle flat slab subduction of the
895 PPP occurred in the eastern margin of the NCC (Wu et al., 2019). Considering the widely
896 distributed NE striking thrusts and fault-related folds in the SCB under this Late Jurassic–earliest
897 Cretaceous NW–SE compression (Lin et al., 2000, 2008; Li et al., 2016b; Li et al., 2021), this
898 large-scale NW–SE compression in the NCC could be a consequence of the flat slab subduction
899 of the PPP beneath the East Asian continent (Fig. 15d). Due to the contemporaneous south-directed
900 Sihetang ductile zone locally developed in the Yanshan belt (Davis et al., 2001; Zhu et al., 2015),
901 it was also proposed that the united action, imposed by far-field compression related to the closure

902 of the MOO and the PPP subduction, controlled Event B of the Yanshanian orogeny (Zhu et al.,
903 2018). We suggest that the large-scale NW–SE compression dominated by the flat slab subduction
904 of the PPP had significantly influenced the entire NCC, according to the widely developed NW–
905 SE directed fold-thrust belts throughout the NCC (Fig. 15d).

906 **6.2.3. The latest Middle–early Late Jurassic (~165–150 Ma): local NE–SW extension related** 907 **to tectonic transition from the N–S closure of the Mongol–Okhotsk Ocean to the NNW–** 908 **directed subduction of Paleo-Pacific Plate**

909 Generally, in the western NCC, the late Middle Jurassic (~170–160 Ma) N–S compression
910 related to the closure of the MOO was immediately followed by the Late Jurassic–earliest
911 Cretaceous (~160–135 Ma) NW–SE compression in response to the subduction of the PPP (Figs.
912 13 and 15). It is characterized by two sequences of superimposed syn-tectonic conglomerates (e.g.,
913 the Changhangou (J_{2c}) and Daqingshan (J_{3d}) Formations, and the Yungang (J_{2yg}) and Tianchihe
914 Formations (J_{3tc}); Figs. 3 and 13). However, in the eastern NCC, the early Late Jurassic (~164–
915 152 Ma) volcanic and pyroclastic rocks (Tiaojishan/Lanqi Formation (J_{3t}/J_{3l}) and coeval intrusive
916 rocks are distributed in the northern Taihangshan, the Yanshan belt, the southern Yanbian area,
917 the Liaodong peninsula, the Jiaodong peninsula, and the Bengbu area (Figs. 2 and 14c). These
918 rocks are mainly adakites derived from partial melting of the low crust and the subcontinental
919 lithospheric mantle metasomatized by earlier subduction slab-derived fluids (Zhang et al., 2004b;
920 Zhang, 2007; Zhang et al., 2010). The brittle normal faults are widely distributed in the volcanic
921 strata in the Yanshan belt where part of these normal faults bound the small-scale rift basin (Davis
922 et al., 2001, 2009; Qi et al., 2015; Lin et al., 2018; Fig. 14c). A top-to-the-NE detachment ductile
923 shear zone was initially formed during Late Jurassic (~156–150 Ma) NE–SW extension before the
924 nucleation of the Early Cretaceous Kalaqin MCC (Lin et al., 2014; Fig. 14c). By the fabric studies
925 of granitic plutons, the consistent NE–SW trending magnetic lineations also recorded the early
926 Late Jurassic NE–SW extension in the northeast part of the NCC (e.g., the Jianchang, Siganding,
927 Kuyushan, Luanjiahe, and Wendeng plutons; Table 3, Fig. 14c). However, the latest Middle–early
928 Late Jurassic (~165–150 Ma) NE–SW extension and magmatism only occurred in the northeastern
929 part of the NCC. The contemporaneous magmatism extended from the northeastern part of the
930 NCC to Northeast China and its adjacent areas. A suite of Late Jurassic igneous rocks (~161–156
931 Ma) was also developed in the Erguna and Great Xing’an Ranges far away from the continental

932 margins, e.g., eastern NE China, Russian Far East, Japan, and Korea Peninsula (Zhang et al., 2022;
933 Fig. 15c). The Late Jurassic extension and magmatism mainly occurred in the transition zone
934 between the Paleo-Pacific domain and the Mongol–Okhotsk domain. In the SCB, Late Jurassic
935 roughly N–S extension, and contemporaneous granites and bimodal volcanic rocks only
936 distributed in the Nanling tectonic belt and its adjacent areas were considered to be related to slab
937 tearing of the NNW-directed subducted PPP (Shu et al., 2007; Li et al., 2021; Fig. 15c). The NNW-
938 directed low-angle flat slab subduction of the PPP could have gradually influenced the NCC
939 interior during the latest Middle–early Late Jurassic. It has been proposed that the NCC was in a
940 back-arc extensional setting related to the PPP subduction during the Late Jurassic (Zhu et al.,
941 2018). Given the widely large-scale NW–SE compression in the western NCC, we suggest that
942 this latest Middle–early Late Jurassic local NE–SW extension in the northeast part of the NCC,
943 probably extending to Northeast China, should be related to the tectonic transition from the closure
944 of the MOO to the PPP subduction (Fig. 15c).

945 **6.3 The Early Cretaceous (135–115 Ma): large-scale NW–SE extension related to the slab** 946 **rollback of the Paleo-Pacific Plate**

947 The Early Cretaceous large-scale crustal extension is one of the most pronounced
948 characteristics in East Asia, expressed by MCCs, magmatism, graben or half-graben basins in a
949 vast area extending more than 4000 km, from Transbaikalia, through the NCC, to the SCB (Wang
950 et al., 2011; Li et al., 2014b; Zhang et al., 2014, Wang et al., 2011; Lin and Wei, 2018; Fig.16).
951 The MCCs and syn-tectonic magmatic domes in East Asia with consistent NW–SE extensional
952 direction occurred during a relatively narrow time span (131–118 Ma), e.g., the Hohhot,
953 Yunmengshan, Kalaqin, Yiwulüshan, Xiuyan, South Liaoning, Linglong, Queshan, Jiaonan and
954 Xiaoqinling MCCs in the NCC (e.g., Wang et al., 2011; Lin and Wei, 2018; Fig. 16). Coeval with
955 the MCCs and extensional basins, a vast plutonic-volcanic flare-up occurred (e.g., Zhang et al.,
956 2014; Wu et al., 2019; Fig. 16). The Early Cretaceous magmatic rocks, ranging in age from 135 to
957 115 Ma with a peak at ca. 132–125 Ma, were derived from multiple sources, e.g., depleted mantle,
958 enriched lithospheric mantle, ancient lower crust, and juvenile crust (Yang et al. 2004; Wu et al.,
959 2019). The consistent NW–SE trending magnetic lineations in numerous granitic plutons also
960 recorded the Early Cretaceous NW–SE extension (Table 3). Multi-plate convergence (i.e., the
961 closure of the MOO, the subduction of the PPP, and the closure of the BNO) occurred in the East

962 Asia continent during the Jurassic to the Early Cretaceous (Dong et al., 2015; Fig. 16). The large-
963 scale NW–SE compression related to the NNW-directed flat slab subduction of the PPP had
964 influenced the north of the NCC during the earliest Cretaceous (Fig. 15d). In the southeast, as the
965 slab rollback of the PPP during the Early Cretaceous, it triggered lithospheric removal or
966 delamination, and thinning of the NCC (Liu et al., 2016; Lin and Wei, 2018; Wu et al., 2019).
967 Meanwhile, the wide rift could have occurred due to the southeastward stress relaxation of the
968 NW–SE convergent East Asian continent (Fig. 16). It resulted in the formation of the MCCs and
969 graben or half-graben basins (Wang et al., 2011; Lin and Wei, 2018), extensive magmatism with
970 extremely variable rock types and chemical compositions (Wu et al., 2005), and replacement of
971 the thick (~200 km) Archean lithospheric mantle beneath the eastern NCC to a thin (< 80 km)
972 juvenile one (Wu et al., 2019).

973 **7 Conclusions**

974 Synthesizing available data concerning strata and unconformities, tectonic deformation, and
975 magmatism, a clear four-stage tectonic evolution of the NCC during the Jurassic–Early Cretaceous
976 is proposed, providing new insights into the Yanshanian intracontinental orogeny in East Asia,
977 from which we draw four main conclusions.

978 1. The N–S extension related to the post-orogenic extension after the deep continent
979 subduction of the SCB beneath the NCC, characterized by the E–W striking brittle normal faults
980 in the Lower–lower Middle Jurassic strata, and the magmatism along the southern and northern
981 margins of the NCC, occurred during the Early–early Middle Jurassic (~200–170 Ma);

982 2. Two-stage compression, corresponding to Events A and B of the Yanshanian orogeny, was
983 well evidenced by the unconformity above the Lower–lower Middle Jurassic strata and the upper
984 Middle Jurassic syn-tectonic deposition, and the Upper Jurassic–lowermost Cretaceous syn-
985 tectonic deposition and the unconformity above, respectively. These syn-tectonic deposits could
986 be deposited in the flexural basins and/or piggy-back basins in the front or back of the fold-thrusts.
987 The late Middle Jurassic (~170–160 Ma) N–S compression (i.e., Event A of the Yanshanian
988 orogeny) occurred in the northern NCC in response to the far-field compression related to the
989 closure of the MOO. The Late Jurassic–earliest Cretaceous (~160–135 Ma) NW–SE compression
990 (i.e., Event B of the Yanshanian orogeny) in response to the flat slab subduction of the PPP had
991 affected the entire NCC;

992 3. The latest Middle–early Late Jurassic (~165–150 Ma) local NE–SW extension,
993 characterized by ductile and brittle normal faults and magnetic lineations in granitic plutons, and
994 magmatism that extended to Northeast China and its adjacent areas, occurred in the northeastern
995 part of the NCC. It could be related to the tectonic transition from the N–S closure of the MOO to
996 the NNW-directed PPP subduction;

997 4. The Early Cretaceous (~135–115 Ma) large-scale NW–SE crustal extension in East Asia
998 should be a consequence of the lithospheric removal or delamination and thinning, and the
999 formation of the wide rift due to the southeastward stress relaxation of the NW–SE convergent
1000 East Asian continent as the slab rollback of the PPP.

1001 Our study shows a new example of polyphase intra-plate deformation and magmatism
1002 paradigm in response to intracontinental orogeny with variable plate-boundary dynamics.

1003 **Acknowledgments**

1004 This work has been financially supported by the National Natural Science Foundation of China
1005 (91855212, 91755205, and 41472193). Dr. Zhiheng Ren, Dr. Lingtong Meng, and Dr. Jipei Zeng
1006 are acknowledged for their help in the field work. Prof. Franz Neubauer and two anonymous
1007 reviewers together with the editor Tim Kusky are thanked very much for their constructive
1008 comments and suggestions, which lead to a significant improvement of our manuscript.

1009 **References**

1010 Archanjo, C. J., Launeau, P., Bouchez, J. L., 1994. Magnetic fabrics vs. magnetite and biotite shape
1011 fabrics of the magnetite-bearing granite pluton of Gameleiras (Northeast Brazil). *Physics of the*
1012 *Earth and Planetary Interiors* 89(1–2), 63–75. [https://doi.org/10.1016/0031-9201\(94\)02997-P](https://doi.org/10.1016/0031-9201(94)02997-P)

1013 BGMNM (Bureau of Geology and Mineral Resources of the Nei Mongol Autonomous Region),
1014 1983. Geological map of the Nei Mongol Autonomous Region, People’s Republic of China
1015 (Tumute Youqi sheet): Nei Mongol Geological Bureau, scale 1:200 000.

1016 BGMH (Bureau of Geology and Mineral Resources of Hebei Province BGMH), 1989. Regional
1017 geology of Hebei Province. In: Beijing Municipality and Tianjin Municipality (in Chinese).
1018 Geological Publishing House, Beijing.

1019 BGML (Bureau of Geology and Mineral Resources of Liaoning Province BGML), 1989. The
1020 Geological Report of the People's Republic of China Ministry of Geology and Mineral Resources,
1021 Part One, Regional Geology, No. Fourteenth, Regional Geology of Liaoning Province (in
1022 Chinese). Geological Publishing House, Beijing.

1023 Bouchez, J.L., Gleizes, G., 1995. Two-stage deformation of the Mount-Louis-Andorra granite
1024 pluton (Variscan Pyrenees) inferred from magnetic susceptibility anisotropy. *Journal of the*
1025 *Geological Society* 152 (4), 669–679. <https://doi.org/10.1144/gsjgs.152.4.0669>

1026 Bouchez, J.L., Hutton, D., Stephens, W.E., 1997. Granite is Never Isotropic: An Introduction to
1027 AMS Studies of Granitic Rocks. *Granite: From Segregation of Melt to Emplacement Fabrics*, pp.
1028 95–112. Paris: Springer Science and Business Media. [https://doi.org/10.1007/978-94-017-1717-](https://doi.org/10.1007/978-94-017-1717-5_6)
1029 [5_6](https://doi.org/10.1007/978-94-017-1717-5_6)

1030 Chang, S.C., Zhang, H., Hemming, S.R., Mesko, G.T., Fang, Y., 2014. $^{40}\text{Ar}/^{39}\text{Ar}$ age constraints
1031 on the Haifanggou and Lanqi Formations: When did the first flowers bloom, in Jourdan, F., Mark,
1032 D.F., and Verati, C., eds., *Advances in $^{40}\text{Ar}/^{39}\text{Ar}$ Dating: From Archaeology to Planetary Sciences:*
1033 *Geological Society of London, Special Publications* 378, 277–284, [https://doi](https://doi.org/10.1144/SP378.1)
1034 [.org/10.1144/SP378.1](https://doi.org/10.1144/SP378.1)

1035 Charles, N., Gumiaux, C., Augier, R., Chen, Y., Zhu, R.X., Lin, W., 2011. Metamorphic core
1036 complexes vs. synkinematic plutons in continental extension setting: Insights from key structures
1037 (Shandong Province, eastern China). *Journal of Asian Earth Science* 40, 261–278.

1038 Charles, N., Gumiaux, C., Augier, R., Chen, Y., Faure, M., Lin, W., Zhu, R.X., 2012. Metamorphic
1039 core complex dynamics and structural development: Field evidences from the Liaodong Peninsula
1040 (China, East Asia). *Tectonophysics* 560-561, 22–50

1041 Chen, A., 1998. Geometric and kinematic evolution of basement-cored structures: intraplate
1042 orogenesis within the Yanshan orogen, northern China. *Tectonophysics* 292(1), 17-42.
1043 [https://doi.org/10.1016/S0040-1951\(98\)00062-6](https://doi.org/10.1016/S0040-1951(98)00062-6)

1044 Chen, B., Jahn, B. M., Wilde, S., Xu, B., 2000. Two contrasting Paleozoic magmatic belts in
1045 northern Inner Mongolia, China: Petrogenesis and tectonic implications. *Tectonophysics* 328(1),
1046 157–182. [https://doi.org/10.1016/S0040-1951\(00\)00182-7](https://doi.org/10.1016/S0040-1951(00)00182-7)

1047 Chen, H.Y., Zhang, Y.Q., Zhang, J.D., Fan, Y.G., Peng, Q.P., Lian, Q., Sun, L.P., Yu, L., 2014.
1048 LA-ICP-MS zircon U-Pb age and geochemical characteristics of tuff of Jiulongshan Formation
1049 from Chengde Basin, northern Hebei (in Chinese with English abstract). *Geological Bulletin of*
1050 *China* 33, 7, 966–973.

1051 Chen, H.Y., Zhang, Y.Q., Liu, B.B., Peng, Q.P., 2015. Sedimentary characteristics and
1052 stratigraphic age of Xingshikou Formation in Chengde Basin of Northern Hebei (in Chinese with
1053 English Abstract). *Geological Survey of China* 2, 31–34.

1054 Chen, X., Jiangyu, L.I., Dong, S., Shi, W., Bai, Y., Zhang, Y., Ding, W., 2019. Tectonic
1055 deformation of Jurassic Ningwu-Jingle basin and its implication for the beginning of Yanshanian
1056 orogeny in central North China Craton. *Geotectonica et Metallogenia* 43(3), 389-408.

1057 Chen, Y.X., Chen, W.J., Zhou, X.H., Li, Z.J., Liang, H.D., Li, Q., Xu, K., Fan, Q.C., Zhang, G.H.,
1058 Wang, F., Wang, Y., Zhou, S.Q., Chen, S.H., Hu, B., Wang, Q.J., 1997. *Liaoxi and Adjacent*
1059 *Mesozoic Volcanic Rocks: Chronology, Geochemistry and Tectonic Settings* (in Chinese with
1060 English abstract): Beijing, China, The Seismological Press.

1061 Cheng, Y., Gao, R., Lu, Z., Li, W., Su, H., Han, R., Chen, H., 2022. Meso-Cenozoic Tectonic
1062 Evolution of the Kexueshan Basin, Northwestern Ordos, China: Evidence from Paleo-Tectonic
1063 Stress Fields Analyses. *Frontiers in Earth Science* 10, 1-19.

1064 Chu, Y., Faure, M., Lin, W., Wang, Q., 2012a. Early Mesozoic tectonics of the South China block:
1065 Insights from the Xuefengshan intracontinental orogen. *Journal of Asian Earth Sciences* 61, 199–
1066 220.

1067 Chu, Y., Faure, M., Lin, W., Wang, Q., Ji, W., 2012b. Tectonics of the Middle Triassic
1068 intracontinental Xuefengshan Belt, South China: New insights from structural and chronological
1069 constraints on the basal décollement zone. *International Journal of Earth Sciences* 101(8), 2125–
1070 2150.

1071 Chu, Y., Lin, W., 2018. Strain analysis of the Xuefengshan Belt, South China: From internal strain
1072 variation to formation of the orogenic curvature. *Journal of Structural Geology* 116, 131–145.

1073 Chu, Y., Lin, W., Faure, M., Xue, Z., Ji, W., Feng, Z., 2019. Cretaceous episodic extension in the
1074 South China Block, East Asia: Evidence from the Yuechengling Massif of central South China.
1075 *Tectonics* 38. <https://doi.org/10.1029/2019TC005516>

1076 Cogné, J.P., Kravchinsky, V.A., Halim, N., Hankard, F., 2005. Late Jurassic–Early Cretaceous
1077 closure of the Mongol–Okhotsk Ocean demonstrated by new Mesozoic palaeomagnetic results
1078 from the Trans-Baikal area (SE Siberia). *Geophysical Journal International* 163, 813–832.

1079 Cope, T.D., 2003. Sedimentary Evolution of the Yanshan Fold-Thrust Belt, Northeast China. Ph.
1080 D Dissertation, Stanford University, pp. 1–230.

1081 Cope, T., 2017. Phanerozoic magmatic tempos of North China. *Earth and Planetary Science*
1082 *Letters* 468, 1–10.

1083 Cope, T.D., Shultz, M.R., Graham, S.A., 2007. Detrital record of Mesozoic shortening in the
1084 Yanshan belt, NE China: testing structural interpretations with basin analysis. *Basin Research*
1085 19(2), 253-272.

1086 Cui, F. H., 2015. Petrogenesis of Mesozoic granitoids and crustal evolution in Xingcheng area,
1087 western Liaoning Province. Ph. D Thesis, Jilin University, pp. 1-152.

1088 Darby, B.J., Davis, G.A., Zheng, Y.D., 2001. Structural evolution of the southwestern Daqing
1089 Shan, Yinshan belt, Inner Mongolia, China, in Hendrix, M.S., & Davis, G.A., eds., *Paleozoic and*
1090 *Mesozoic tectonic evolution of central Asia: From continental assembly to intracontinental*
1091 *deformation*, Boulder, Colorado. Geological Society of America Memoir 194, 199–214.

1092 Darby, B. J., Ritts, B. D., 2002. Mesozoic contractional deformation in the middle of the Asian
1093 tectonic collage: the intraplate Western Ordos fold–thrust belt, China. *Earth and Planetary Science*
1094 *Letters* 205(1-2), 13–24. [https://doi.org/10.1016/s0012-821x\(02\)01026-9](https://doi.org/10.1016/s0012-821x(02)01026-9)

1095 Darby, B. J., Ritts, B. D., 2007. Mesozoic structural architecture of the Lang Shan, North-Central
1096 China: Intraplate contraction, extension, and synorogenic sedimentation. *Journal of Structural*
1097 *Geology* 29(12), 2006–2016. <https://doi.org/10.1016/j.jsg.2007.06.011>

1098 Davis, G.A., Darby, B.J., 2010. Early Cretaceous overprinting of the Mesozoic Daqing Shan fold-
1099 and-thrust belt by the Hohhot metamorphic core complex, Inner Mongolia, China. *Geoscience*
1100 *Frontiers* 1(1), 1-20.

1101 Davis, G. A., Meng, J. F., Cao, W. R., 2009. Triassic and Jurassic tectonics in the eastern Yanshan
1102 belt, North China: insights from the controversial Dengzhangzi Formation and its neighboring
1103 units. *Earth Science Frontiers* 16 (3), 69–86. [https://doi.org/10.1016/S1872-5791\(08\)60090-1](https://doi.org/10.1016/S1872-5791(08)60090-1)

1104 Davis, G. A., Zheng, Y. D., Wang, C., 2001. Mesozoic tectonic evolution of the Yanshan fold and
1105 thrust belt, with emphasis on Hebei and Liaoning provinces, northern China. In: Hendrix, M.S.,
1106 Davis, G.A. (Eds.), Paleozoic and Mesozoic tectonic evolution of central Asia: From continental
1107 assembly to intracontinental deformation, Boulder, Colorado. Geological Society of America
1108 Memoir 194, 171–197.

1109 Dong, S., Zhang, Y., Zhang, F., Cui, J., Chen, X., Zhang, S., Miao, L., Li, J., Shi, W., Li, Z.,
1110 Huang, S., Li, H., 2015. Late Jurassic–Early Cretaceous continental convergence and
1111 intracontinental orogenesis in East Asia: a synthesis of the Yanshan revolution. *Journal of Asian*
1112 *Earth Sciences* 114, 750–770. <https://doi.org/10.1016/j.jseaes.2015.08.011>

1113 Enkin, R.J., Yang, Z., Chen, Y., Courtillot, V., 1992. Paleomagnetic constraints on the geodynamic
1114 history of the major blocks of China from the Permian to the present. *Journal of Geophysical*
1115 *Research Solid Earth* 97(B10), 13953–13989.

1116 Faure, M., Lin, W., Chen, Y., 2012. Is the Jurassic (Yanshanian) intraplate tectonics of North
1117 China due to westward indentation of the NCC? *Terra Nova* 24 (6), 456–466.
1118 <https://doi.org/10.1111/ter.12002>

1119 Faure, M., Lin, W., Scharer, U., Shu, L., Sun, Y., Arnaud, N., 2003. Continental subduction and
1120 exhumation of UHP rocks. Structural and geochronological insights from the Dabieshan (East
1121 China). *Lithos* 70(3), 213–241.

1122 Faure, M., Lin, W., Shu, L., Sun, Y., Scharer, U., 1999. Tectonics of the Dabieshan (eastern China)
1123 and possible exhumation mechanism of ultra high-pressure rocks. *Terra Nova* 11(6), 251–258.

1124 Faure, M., Trap, P., Lin, W., Monié, P., Bruguier, O., 2007. Polyorogenic evolution of the
1125 Paleoproterozoic Trans-North China Belt, new insights from the in Lüliangshan-Hengshan-
1126 Wutaishan and Fuping massifs. *Episodes Journal of International Geoscience*, Seoul National
1127 University 30 (2), 95–106.

1128 Feng, Q., 2021. Structural characteristics and evolution, and hydrocarbon occurrence of the south-
1129 central segment of the western Ordos Basin (in Chinese with English abstract). Dissertation for
1130 Master Degree. Xi'an: Northwest University. 1–87.

1131 Fu, Z. B., Zhao, Y., Liu, J. L., Zhang, S. H., Gao, H. L., 2018. Revisiting of the Yanshanian basins
1132 in western and northern Beijing, North China. *Journal of Asian Earth Sciences* 163, 90–107.
1133 <https://doi.org/10.1016/j.jseaes.2018.05.016>

1134 Gao, H-L., Zhao, Y., Ye, H., Zhang, S-H., Liu, J., Wang, G-C., 2018. Dating Jurassic volcanic
1135 rocks in the Western Hills of Beijing, North China: implications for the initiation of the Yanshanian
1136 tectonism and subsequent thermal events. *Journal of Asian Earth Sciences* 161, 164-177.
1137 <https://doi.org/10.1016/j.jseaes.2018.05.008>

1138 Ge, Y.H., Sun, C.L., Wang, Y.F., 2010. The flora from Zhaogou Formation in Shiguai basin, Inner
1139 Mongolia and the geological age (in Chinese with English abstract). *Global Geology* 29, 175–182.

1140 Gong, W., Hu, J., Chen, H., Li, Z., Qu, H., Yang, Y., 2015. Late Mesozoic tectonic evolution and
1141 kinematic mechanisms in the Daqing shan at the northern margin of the North China Craton.
1142 *Journal of Asian Earth Sciences* 114, 103-114. <http://dx.doi.org/10.1016/j.jseaes.2015.07.016>

1143 Guo, F., Li, H.X., Fan, W.M., Li, J.Y., Zhao, L., Huang, M.W., Xu W.L., 2015. Early Jurassic
1144 subduction of the Paleo-Pacific Ocean in NE China: Petrologic and geochemical evidence from
1145 the Tumen mafic intrusive complex. *Lithos* 244–245, 46–60.

1146 Guo, F., Fan, W.M., Li, X.Y., Li, C.W., 2007. Geochemistry of Mesozoic mafic volcanic rocks
1147 from the Yanshan belt in the northern margin of North China Block: relations with post-collisional
1148 lithospheric extension. In: Zhai, M., Windley, B.F., Kusky, T.M., Meng, Q. (Eds.), *Mesozoic Sub-*
1149 *continental Lithospheric Thinning Under Eastern Asia*. Geological Society, London, Special
1150 Publications 280, pp. 101–130.

1151 Guo, J.F., Ma, Q., Xu, Y.G., Zheng, J.P., Zhou, Z.Y., Ma, L., Bai, X.J., 2022. Migration of Middle-
1152 Late Jurassic volcanism across the northern North China Craton in response to subduction of
1153 Paleo-Pacific Plate. *Tectonophysics* 833, 229338. <https://doi.org/10.1016/j.tecto.2022.229338>

1154 Guynn, J.H., Kapp, P., Pullen, A., Gehrels, G., Heizler, M., Ding, L., 2006. Tibetan basement
1155 rocks near Amdo reveal “missing” Mesozoic tectonism along the Bangong suture, central Tibet.
1156 *Geology* 34, 505–508.

1157 Hacker, B.R., Ratschbacher, L., Webb, L., McWilliams, M.O., Ireland, T., Calvert, A., Dong, S.,
1158 Wenk, H., Chateigner, D., 2000. Exhumation of ultrahigh-pressure continental crust in east central

1159 China: Late Triassic-Early Jurassic tectonic unroofing. *Journal of Geophysical Research: Solid*
1160 *Earth* 105 (B6), 13339–13364. <https://doi.org/10.1029/2000JB900039>

1161 Hao, W., Zhu, G., Zhu, R., 2019. Timing of the Yanshan Movement: evidence from the Jingxi
1162 Basin in the Yanshan fold-and-thrust belt, eastern China. *International Journal of Earth Sciences*
1163 108(6), 1961-1978.

1164 Hao, W., Zhu, R., Zhu, G., 2020. Jurassic tectonics of the eastern North China Craton: Response
1165 to initial subduction of the Paleo-Pacific Plate. *Geological Society of America Bulletin* 133(1-2),
1166 19-36.

1167 Hargraves, R. B., Johnson, D., Chan, C. Y., 1991. Distribution anisotropy: the cause of AMS in
1168 igneous rocks? *Geophysical Research Letters* 18(12), 2193–2196.
1169 <https://doi.org/10.1029/91GL01777>

1170 He, Z.Y., Xu, X.S., Niu, Y.L., 2010. Petrogenesis and tectonic significance of a Mesozoic granite–
1171 syenite–gabbro association from inland South China. *Lithos* 119, 621–641.

1172 He, X.F., Santosh, M., Ganguly, S., 2017. Mesozoic felsic volcanic rocks from the North China
1173 craton: Intraplate magmatism associated with craton destruction: *Geological Society of America*
1174 *Bulletin*, 129(7–8), 947–969. <https://doi.org/10.1130/B31607.1>

1175 Huang, D.Y., 2019. Jurassic integrative stratigraphy and timescale of China. *Science China Earth*
1176 *Sciences* 62, 01, 227–259. <https://doi.org/10.1007/s11430-017-9268-7>

1177 Huang, X., Shi, W., Chen, P., Li, H., 2015. Superposed deformation in the Helanshan Structural
1178 Belt: Implications for Mesozoic intracontinental deformation of the North China Plate. *Journal of*
1179 *Asian Earth Sciences*, 114, 140–154. <https://doi.org/10.1016/j.jseaes.2015.05.027>

1180 Ji, W.B., Faure, M., Lin, W., Chen, Y., Chu Y., Xue Z.H., 2018. Multiple emplacement and
1181 exhumation history of the Late Mesozoic Dayunshan–Mufushan batholith in southeast China and
1182 its tectonic significance: 1. Structural analysis and geochronological constraints. *Journal of*
1183 *Geophysical Research: Solid Earth* 123, 689–710. <https://doi.org/10.1002/2017JB014597>

1184 Jian, P., Liu, D., Kröner, A., Windley, B. F., Shi, Y., Zhang, F., Shi, G., et al., 2008. Time scale of
1185 an Early to Mid-Paleozoic orogenic cycle of the long-lived Central Asian Orogenic Belt, Inner
1186 Mongolia of China: implications for continental growth. *Lithos* 101, 233–259. <https://doi.org/10.1016/j.lithos.2007.07.005>

1187

1188 Jiao, R.C., He, J.R., Wang, R.R., W, Q.Q., Hui, G.J., 2016. LA–ICP–MS U–Pb dating of zircons
1189 from Tuchengzi Formation in Qianjiadian of North Beijing and its significance (in Chinese with
1190 English abstract). *Geology in China* 43 (5), 1750–1760.

1191 Kapp, P., DeCelles, P.G., Gehrels, G.E., Heizler, M., Ding, L., 2007. Geological records of the
1192 Lhasa–Qiangtang and Indo–Asian collisions in the Nima area of central Tibet. *Geological Society
1193 of America Bulletin* 119, 917–933.

1194 Kim, S.W., Kwon, S., Ko, K., Yi, K., Cho, D.L., Kee, W.S., Kim, B.C., 2015. Geochronological
1195 and geochemical implications of Early to Middle Jurassic continental adakitic arc magmatism in
1196 the Korean Peninsula. *Lithos* 227, 225–240.

1197 Kravchinsky, V.A., Cogné, J.P., Harbert, W.P., Kuzmin, M.I., 2002. Evolution of the Mongol–
1198 Okhotsk Ocean as constrained by new palaeomagnetic data from the Mongol–Okhotsk suture
1199 zone, Siberia. *Geophysical Journal International* 148, 34–57.

1200 Lan, T.G., Fan, H.R., Santosh, M., Hu, F.F., Yang, K.F., Yang, Y.H., Liu, Y.S., 2012. Early
1201 Jurassic high–K calc–alkaline and shoshonitic rocks from the Tongshi intrusive complex, eastern
1202 North China Craton: implication for crust–mantle interaction and post–collisional magmatism.
1203 *Lithos* 140–141, 183–199.

1204 Lapiere, H., Jahn, B.M., Charvet, J., Yu, Y.W., 1997. Mesozoic felsic arc magmatism and
1205 continental olivine tholeiites in Zhejiang Province and their relationship with the tectonic activity
1206 in southeastern China. *Tectonophysics* 274, 321–338.

1207 Li, C., Wang, Z., Lü, Q., Tan, Y., Li, L., Tao, T., 2021. Mesozoic tectonic evolution of the eastern
1208 South China Block: A review on the synthesis of the regional deformation and magmatism. *Ore
1209 Geology Reviews* 131(4), 104028.

1210 Li, C., Zhang, C., Cope, T. D., Lin, Y., 2016a. Out-of-sequence thrusting in polycyclic thrust belts:
1211 an example from the Mesozoic Yanshan belt, North China Craton. *Tectonics* 35, 2082–2116.
1212 <https://doi.org/10.1002/2016TC004187>

1213 Li, H., Zhang, H., Qu, H., Cai, X., Wang, M., 2014a. Initiation, the First Stage of the Yanshan
1214 (Yenshan) in Western Hills. Constraints from Zircon U–Pb Movement Dating (in Chinese with
1215 English abstract). *Geological Review* 60(5), 1026–1042.

1216 Li, J., Dong, S., Zhang, Y., Zhao, G., Johnston, S. T., Cui, J., Xin, Y., 2016b. New insights into
1217 Phanerozoic tectonics of South China: part 1, polyphase deformation in the Jiuling and
1218 Lianyunshan domains of the central Jiangnan orogen. *Journal of Geophysical Research Solid Earth*
1219 121(4), 3048-3080. <https://doi.org/10.1002/2015JB012778>

1220 Li, J. Y., 2006. Permian geodynamic setting of Northeast China and adjacent regions: closure of
1221 the Paleo-Asian Ocean and subduction of the Paleo-Pacific Plate. *Journal of Asian Earth Sciences*
1222 26(3), 207–224. <https://doi.org/10.1016/j.jseaes.2005.09.001>

1223 Li, M.J., Zheng, M.L., Cao, C.C., 2004. Evolution of superposed Jurassic and Cretaceous basins
1224 in Beishan-Alxa area (in Chinese with English abstract). *Oil and Gas Geology* 25(1), 54-57.

1225 Li, S. Z., Kusky, T. M., Zhao, G., Wu, F., Liu, J. Z., Sun, M., Wang, L., 2007a. Mesozoic tectonics
1226 in the Eastern Block of the North China Craton: implications for subduction of the Pacific plate
1227 beneath the Eurasian plate. *Geological Society London Special Publications* 280(1), 171-188.

1228 Li, S.Z., Jahn, B.M., Zhao, S.J., Dai, L.M., Li, X.Y., Suo, Y.H., Guo, L.L., Wang, Y.M., Liu, X.C.,
1229 Lan, H.Y., Zhou, Z.Z., Zheng, Q.L., Wang, P.C., 2017. Triassic southeastward subduction of North
1230 China Craton to South China Block: insights from new geological, geophysical and geochemical
1231 data. *Earth-Science Reviews* 166, 270-285.

1232 Li, S.Z., Zhao, G.C., Santosh, M., Liu, X., Dai, L.M., Suo, Y.H., Tam, P.Y., Song, M.C., Wang,
1233 P.C., 2012. Paleoproterozoic structural evolution of the southern segment of the Jiao-Liao-Ji Belt,
1234 North China Craton. *Precambrian Research* 200-203, 59-73.
1235 <https://doi.org/10.1016/j.precamres.2012.01.007>

1236 Li, S.Z., Zhao, S.J., Liu, X., Cao, H.H., Yu, S., Li, X.Y., Somerville, I., Yu, S.Y., Suo, Y.H., 2018.
1237 Closure of the Proto-Tethys Ocean and Early Paleozoic amalgamation of microcontinental blocks
1238 in East Asia. *Earth-Science Reviews* 186, 37-75.

1239 Li, S.M., Zhu, D.C., Wang, Q., Zhao, Z.D., Zhang, L.L., Liu, S.A., Chang, Q.S., Lu, Y.H., Dai,
1240 J.G., Zheng, Y.C., 2016d. Slab-derived adakites and slab asthenosphere-derived OIB-type
1241 rocks at 156 ± 2 Ma from the north of Gerze, central Tibet: records of the Bangong-Nujiang
1242 oceanic ridge subduction during the Late Jurassic. *Lithos* 262, 456–469

1243 Li, W., Jiang, D., Dong, Y., Zheng, Z., Zhao, J., Kang, W., Zhang, L., 2022. Mesozoic
1244 contractional deformation in central East Asia: Constraints from deformation and sedimentary

1245 record of the Helanshan fold and thrust belt, North China Craton. *Gondwana Research* 107, 235-
1246 255. <https://doi.org/10.1016/j.gr.2022.03.011>

1247 Li, W.P., Lu, F.X., Li, X.H., Zhou, Y.Q., Sun, S.P., Li, J.Z., Zhang, D.G., 2001. Geochemical
1248 features and origin of volcanic rocks of Tiaojishan Formation in Western Hills of Beijing (in
1249 Chinese with English abstract). *Acta Petrologica Et Mineralogica* 20 (2), 123–133.

1250 Li, X.H., Li, W.X., Li, Z.X., 2007b. On the genetic classification and tectonic implications of the
1251 Early Yanshanian granitoids in the Nanling Range, South China. *Chinese Science Bulletin* 52 (14),
1252 1873–1885.

1253 Li, Y., Xu, W. L., Zhu, R. X., Wang, F., Ge, W. C., Sorokin, A. A., 2019. Late Jurassic to early
1254 Early Cretaceous tectonic nature on the NE Asian continental margin: Constraints from Mesozoic
1255 accretionary complexes. *Earth-Science Reviews* 103042.
1256 <https://doi.org/10.1016/j.earscirev.2019.103042>

1257 Li, Z. H., Dong, S. W., Qu, H. J., 2014b. Timing of the initiation of the Jurassic Yanshan movement
1258 on the North China Craton: evidence from sedimentary cycles, heavy minerals, geochemistry, and
1259 zircon U–Pb geochronology. *International Geology Review* 56(3), 288-312.
1260 <https://doi.org/10.1080/00206814.2013.855013>

1261 Li, Z.H., Feng, S.B., Yuan, X.Q., Qu, H.J., 2014c. Chronology and its significance of the Lower
1262 Jurassic tuff in Ordos Basin and its periphery (in Chinese with English abstract). *Oil and gas*
1263 *geology* 35, 729-741.

1264 Li, Z. H., Qu, H. J., Gong, W. B., 2015. Late Mesozoic basin development and tectonic setting of
1265 the northern North China Craton. *Journal of Asian Earth Sciences* 114, 115-139.
1266 <https://doi.org/10.1016/j.jseaes.2015.05.029>

1267 Li, Z.H., Qu, H.J., Yang, Y.H., Gong, W.B., 2016c. Late Mesozoic sedimentary-volcanic filling
1268 record in Yungang basin and its tectonic implications (in Chinese with English abstract). *Geology*
1269 *in China* 43, 1481-1494.

1270 Liang, C., Liu, Y., Neubauer, F., Jin, W., Zeng, Z., Genser, J., et al., 2015. Structural characteristics
1271 and LA–ICP–MS U–Pb zircon geochronology of the deformed granitic rocks from the Mesozoic
1272 Xingcheng–Taili ductile shear zone in the North China Craton. *Tectonophysics* 650, 80–103.
1273 <https://doi.org/10.1016/j.tecto.2014.05.010>

1274 Liang, C., Neubauer, F., Liu, Y., Heberer, B., Genser, J., Dunkl, I., et al., 2022. Diachronous onset
1275 and polyphase cooling of the Taili-Yiwulüshan metamorphic core complex corridor, NE China,
1276 and its relationships to the formation of adjacent extensional basins. *Gondwana Research*
1277 <https://doi.org/10.1016/j.gr.2020.09.004>

1278 Lin, C.F., Liu, S.F., Zhuang, Q.T., Steel, R.J., 2018. Sedimentation of Jurassic fan-delta wedges
1279 in the Xiahuayuan Basin reflecting thrust-fault movements of the western Yanshan fold-and-thrust
1280 belt, China. *Sedimentary Geology* 368, 24–43. <https://doi.org/10.1016/j.sedgeo.2018.03.005>.

1281 Lin, C., Liu, S., Shi, X., Zhuang, Q., 2019. Late Jurassic-Early Cretaceous deformation in the
1282 western Yanshan fold-thrust belt: Insights from syn-tectonic sedimentation in the Chicheng basin,
1283 North China. *Tectonics* 38. <https://doi.org/10.1029/2018TC005402>

1284 Lin, S. Z., Zhu, G., Zhao, T., Song, L., Liu, B., 2014. Structural characteristics and formation
1285 mechanism of the Kalaqin metamorphic core complex in the Yanshan area, China. *Chinese*
1286 *Science Bulletin* 59, 3174–3189, <https://doi.org/10.1360/N972014-00100>

1287 Lin, W., Charles, N., Chen, K., Chen, Y., Faure, M., Wu, L., Wang, F., 2013a. Late Mesozoic
1288 compressional to extensional tectonics in the Yiwulüshan massif, NE China and its bearing on the
1289 evolution of the Yinshan–Yanshan orogenic belt part II: Anisotropy of magnetic susceptibility and
1290 gravity modeling. *Gondwana Research* 23(1), 78–94. <https://doi.org/10.1016/j.gr.2012.02.012>

1291 Lin, W., Faure, M., Chen, Y., Ji, W.B., Wang, F., Wu, L., Charles, N., Wang, J., Wang, Q.C.,
1292 2013b. Late Mesozoic compressional to extensional tectonics in the Yiwulüshan massif, NE China
1293 and its bearing on the evolution of the Yinshan-Yanshan orogenic belt. Part I: Structural analyses
1294 and geochronological constraints. *Gondwana Research* 23, 54–77.
1295 <https://doi.org/10.1016/j.gr.2012.02.013>.

1296 Lin, W., Faure M., Monie´, P. Schäerer, U. Zhang L., Sun Y., 2000. Tectonics of SE China: New
1297 insights from the Lushan massif (Jiangxi Province). *Tectonics* 19, 852–871.
1298 <https://doi.org/10.1029/2000TC900009>.

1299 Lin, W., Faure, M., Nomade, S., Shang, Q., Renne, P. R., 2008. Permian–Triassic amalgamation
1300 of Asia: insights from Northeast China sutures and their place in the final collision of North China
1301 and Siberia. *Comptes Rendus Geoscience* 340(2-3), 190-201.

1302 Lin, W., Shi, Y. H., Wang, Q. C., 2009. Exhumation tectonics of the HP-UHP orogenic belt in
1303 Eastern China: new structural–petrological insights from the Tongcheng massif, Eastern
1304 Dabieshan. *Lithos* 109, 285–303.

1305 Lin, W., Wang, Q. C., Faure, M., Arnaud, N., 2005. Tectonic evolution of Dabie orogen: in the
1306 view from polyphase deformation of the Beihuaiyang metamorphic zone. *Science China Series D*
1307 48(7), 886-899.

1308 Lin, W., Wang, Q. C., Chen, K., 2008. Phanerozoic tectonic of South China block: New insights
1309 from the polyphase deformation in the Yunkai massif. *Tectonics* 27, TC6004,
1310 <https://doi.org/10.1029/2007TC002207>.

1311 Lin, W., Wei, W., 2020. Late Mesozoic extensional tectonics in the North China Craton and its
1312 adjacent regions: a review and synthesis. *International Geology Review* 1–29.
1313 <https://doi.org/10.1080/00206814.2018.1477073>

1314 Lin, W., Zeng, J., Meng, L., Qiu, H., Wei, W., Ren, Z., Chu, Y., et al. Extensional tectonics and
1315 North China Craton destruction: Insights from the magnetic susceptibility anisotropy (AMS) of
1316 granite and metamorphic core complex. *Science China Earth Science*. 64, 1557–1589 (2021).
1317 <https://doi.org/10.1007/s11430-020-9754-1>

1318 Lin, Y., Zhang, C., Li, C., Deng, H., 2020. From dextral contraction to sinistral extension of
1319 intracontinental transform structures in the Yanshan and northern Taihang Mountain belts during
1320 Early Cretaceous: Implications to the destruction of the North China Craton. *Journal of Asian*
1321 *Earth Sciences* 189, 104139. <https://doi.org/10.1016/j.jseaes.2019.104139>

1322 Liu, B., Neubauer, F., Liang, C., Liu, J., Li, W., 2020. Geological control of the eastern Great
1323 Wall: Mountain-basin relationships in the eastern North China Craton. *Gondwana Research*
1324 102(1–2), 60–76. <https://doi.org/10.1016/j.gr.2020.06.023>

1325 Liu, D.L., Shi, R.D., Ding, L., Zou, H.B., 2018a. Late cretaceous transition from subduction to
1326 collision along the Bangong-Nujiang Tethys: New volcanic constraints from central Tibet. *Lithos*
1327 296, 452–470

1328 Liu, L., Xu, X., Xia, Y., 2016. Asynchronizing paleo-Pacific slab rollback beneath SE China:
1329 Insights from the episodic Late Mesozoic volcanism. *Gondwana Research* 37, 397-407,
1330 <https://doi.org/10.1016/j.gr.2015.09.009>.

1331 Liu, J., Zhao, Y., Liu, X.M., 2006. Age of the Tiaojishan Formation volcanics in the Chengde
1332 Basin, northern Hebei province (in Chinese with English abstract). *Acta Petrologica Sinica* 22,
1333 2617–2630.

1334 Liu, J., Zhao, Y., Liu, X., Wang, Y., Liu, X., 2012. Rapid exhumation of basement rocks along the
1335 northern margin of the North China craton in the early Jurassic: Evidence from the Xiabancheng
1336 Basin, Yanshan Tectonic Belt. *Basin Research* 24(5), 544-558. <https://doi.org/10.1111/j.1365-2117.2011.00538.x>

1338 Liu, S.F., Li, Z., Zhang, J.F., 2004. Mesozoic basin evolution and tectonic mechanism in Yanshan,
1339 China. *Science China Earth Sciences* 47, 24–38

1340 Liu, S. F., Lin, C. F., Liu, X. B., Zhuang, Q. T., 2018b. Syn-tectonic sedimentation and its linkage
1341 to fold-thrusting in the region of Zhangjiakou, North Hebei, China. *Science China Earth Sciences*
1342 61(6), 681-710. <https://doi.org/10.1007/s11430-017-9175-3>

1343 Liu, S.F., Zhang, J.F., Hong, S.Y., Ritts, B.D., 2007. Early Mesozoic basin development and its
1344 response to thrusting in the Yanshan fold and thrust belt, China. *International Geology Review* 49
1345 (11), 1025–1049.

1346 Liu, Y.J., Li, W.M., Feng, Z.Q., Wen, Q.B., Neubauer, F., Liang, C.Y., 2017. A review of the
1347 Paleozoic tectonics in the eastern part of Central Asian Orogenic Belt. *Gondwana Research* 43,
1348 123–148. <https://doi.org/10.1016/j.gr.2016.03.013>

1349 Lu, F.X., Wang, C.Y., Zheng, J.P., Zhang, R.S., 2004. Lithospheric composition and structure
1350 beneath the northern margin of the Qinling orogenic belt. *Science China Series D* 47, 13–22.

1351 Mattauer, M., Matte, P., Malavieille, J., Tapponnier, P., Maluski, H., Qin, X.Z., Lu, Y.L., Tang,
1352 Y.Q., 1985. Tectonics of the Qinling belt: build-up and evolution of eastern Asia. *Nature* 317
1353 (6037), 496–500. <https://doi.org/10.1038/317496a0>

1354 Meng, L., Lin, W., 2021. Episodic Crustal Extension and Contraction Characterizing the Late
1355 Mesozoic Tectonics of East China: Evidence From the Jiaodong Peninsula, East China. *Tectonics*
1356 40, e2020TC006318. <https://doi.org/10.1029/2020TC006318>

1357 Meng, Q.R., Wei, H.H., Wu, G.L., Duan, L., 2014. Early Mesozoic tectonic settings of the northern
1358 North China Craton. *Tectonophysics* 611 (1), 155–166.
1359 <https://doi.org/10.1016/j.tecto.2013.11.015>

1360 Meng, Q. R., Wu, G. L., Fan, L. G., Wei, H. H., 2019. Tectonic evolution of early Mesozoic
1361 sedimentary basins in the North China Craton. *Earth-Science Reviews* 190, 416–438.
1362 <https://doi.org/10.1016/j.earscirev.2018.12.003>

1363 Meng, Q. R., Zhang, G. W., 1999. Timing of collision of the North and South China blocks:
1364 controversy and reconciliation. *Geology* 27 (2), 123–126. [https://doi.org/10.1130/0091-](https://doi.org/10.1130/0091-7613(1999)027<0123:TOCOTN>2.3.CO;2)
1365 [7613\(1999\)027<0123:TOCOTN>2.3.CO;2](https://doi.org/10.1130/0091-7613(1999)027<0123:TOCOTN>2.3.CO;2)

1366 Metelkin, D.V., Vernikovskiy, V.A., Kazansky, A.Y., Wingate, M.T.D., 2010. Late Mesozoic
1367 tectonics of Central Asia based on paleomagnetic evidence. *Gondwana Research* 18, 400–419.

1368 Niu, B.G., He, Z.J., Song, B., Ren, J., 2003. SHRIMP dating of volcanic rocks of the Zhangjiakou
1369 Formation and its significance (in Chinese with English abstract). *Geological Bulletin China* 22
1370 (2), 140–141.

1371 Niu, B.G., He, Z.J., Song, B., Ren, J., Xiao, L., 2004. SHRIMP geochronology of volcanics of the
1372 Zhangjiakou and Yixian Formation, northern Hebei Province, with a discussion on the age of the
1373 Xing'anling Group of the Great Hinggan Mountain and volcanic strata of the southeastern coastal
1374 area of China. *Acta Geological Sinica (English Edition)* 78 (6), 1214–1228.

1375 Paterson, S.R., Vernon, R.H., Tobisch, O.T., 1989. A review of criteria for the identification of
1376 magmatic and tectonic foliations in granitoids. *Journal of Structural Geology* 11 (3), 349–363.

1377 Qi, G. W., Zhang, J. J., Wang, M., 2015. Mesozoic tectonic setting of rift basins in eastern North
1378 China and implications for destruction of the North China Craton. *Journal of Asian Earth Sciences*
1379 111, 414–427. <https://doi.org/10.1016/j.jseaes.2015.06.022>

1380 Qiu, H., Lin, W., Chen, Y., Faure, M., Meng, L., Ren, Z., Zeng, J., Hou, Q., 2021. Magma
1381 chamber-related transition from magmatic to solid-state fabrics within the Late Triassic granitic
1382 Dushan pluton (North China). *Geophysical Journal International* 227, 759–775.
1383 <https://doi.org/10.1093/gji/ggab252>

1384 Qiu, H., Lin, W., Faure, M., Chen, Y., Meng, L., Zeng, J., Ren, Z., Li, Q., 2020. Late Triassic
1385 extensional tectonics in the northern North China Craton, insights from a multidisciplinary study
1386 of the Wangtufang pluton. *Journal of Asian Earth Sciences* 200, 104462.
1387 [10.1016/j.jseaes.2020.104462](https://doi.org/10.1016/j.jseaes.2020.104462)

1388 Ratschbacher, L., Hacker, B. R., Calvert, A., Webb, L. E., Hu, J., 2003. Tectonics of the Qinling
1389 (Central China): tectonostratigraphy, geochronology, and deformation history. *Tectonophysics* 1-
1390 53.

1391 Ritts, B. D., Darby, B. J., Cope, T., 2001. Early Jurassic extensional basin formation in the Daqing
1392 Shan segment of the Yinshan belt, northern North China Craton, Inner Mongolia. *Tectonophysics*
1393 339(3-4), 239-258. [https://doi.org/10.1016/S0040-1951\(01\)00115-9](https://doi.org/10.1016/S0040-1951(01)00115-9)

1394 Sagong, H., Kwon, S.T., Ree, J.H., 2005. Mesozoic episodic magmatism in South Korea and its
1395 tectonic implication. *Tectonics*, 24(5), TC5002.1-TC5002.18.

1396 Shao, J.A., Zhang, J.H., 2014. The early mesozoic continental crust reformation in Yanshan area-
1397 giving discussion to Indosinian movement. *Earth Science Frontiers* 21, 302–309 (in Chinese with
1398 English abstract)

1399 Shao, J.A., Meng, Q.R., Wei, H.Q., Zhang, L.Q., Wang, P.Y., 2003. Nature and tectonic
1400 environment of Late Jurassic volcanic-sedimentary basins in northern Hebei Province (in Chinese
1401 with English abstract). *Geological Bulletin of China* 22(10), 751–761.

1402 Shi, X., Liu, S., Lin, C., 2019. Growth structures and growth strata of the Qianjiadian Basin in the
1403 western Yanshan fold and thrust belt, North China. *Science China Earth Sciences* 62, 1092–1109,
1404 <https://doi.org/10.1007/s11430-018-9345-6>

1405 Shu, L.S., Zhou, X.M., Deng, P., Zhu, W.B., 2007. Mesozoic-Cenozoic basin features and
1406 evolution of South China. *Acta Geologica Sinica*. 81 (4), 573–586.

1407 Silva, D., Piazzolo, S., Daczko, N. R., Houseman, G., Raimondo, T., Evans, L., 2018.
1408 Intracontinental orogeny enhanced by far-field extension and local weak crust. *Tectonics* 37,
1409 4421–4443. <https://doi.org/10.1029/2018TC005106>

1410 Su, N., Zhu, G., Liu, C., Zhang, S., Li, Y., Yin, H., Wu, X., 2020. Alternation of back-arc extension
1411 and compression in an overriding plate: evidence from Cretaceous structures in the western
1412 Liaoning region, eastern China. *International Journal of Earth Sciences* 109(2), 707-727.

1413 Su, N., Zhu, G., Wu, X., Yin, H., Lu, Y., Zhang, S., 2021. Back-arc tectonic tempos: Records from
1414 Jurassic–Cretaceous basins in the eastern North China Craton. *Gondwana Research* 90, 241-257.

1415 Swisher, C.C., Wang, X.L., Zhou, Z.H., Wang, Y.Q., Jin, F., Zhang, J.Y., Xu, X., Zhang, F.C.,
1416 2002. Further support for a Cretaceous age for the feathered dinosaur beds of Liaoning, China:
1417 new $^{40}\text{Ar}/^{39}\text{Ar}$ dating of the Yixian and Tuchengzi formations. Chinese Science Bulletin
1418 47(2),135–138.

1419 Tang, J., Xu, W., Wang, F., Ge, W., 2018. Subduction history of the Paleo-Pacific slab beneath
1420 Eurasian continent: Mesozoic-Paleogene magmatic records in Northeast Asia. Science China
1421 Earth Sciences 61(5), 527–559. <https://doi.org/10.1016/10.1007/s11430-017-9174-1>

1422 Tomurtogoo, O., Windley, B.F., Kröner, A., Badarch, G., Liu, D.Y., 2005. Zircon age and
1423 occurrence of the Adaatsag ophiolite and Muron shear zone, central Mongolia: constraints on the
1424 evolution of the Mongol–Okhotsk Ocean, suture and orogen. Journal of the Geological Society
1425 162, 125–134.

1426 Trap, P., Faure, M., Lin, W., Le Breton, N., Monié, P., 2012. Paleoproterozoic tectonic evolution
1427 of the Trans-North China Orogen: toward a comprehensive model. Precambrian Research 222,
1428 191–211. <https://doi.org/10.1016/j.precamres.2011.09.008>

1429 Tarling, D. H., Hrouda, F., 1993. Magnetic Anisotropy of Rocks. London, U. K.: Chapman and
1430 Hall.

1431 Wang, F., Xu, W.L., Xing, K.C., Wang, Y.N., Zhang, H.H., Wu, W., Sun, C.Y., Ge, W.C., 2019.
1432 Final closure of the Paleo–Asian Ocean and Onset of Subduction of Paleo–Pacific Ocean:
1433 Constraints from Early Mesozoic magmatism in Central southern Jilin Province, NE China.
1434 Journal of Geophysical Research: Solid Earth 124, 2601–2622.

1435 Wang, L.L., Hu, D.Y., Zhang, L.J., Zheng, S.L., He, H.Y., Deng, C.L., Wang, X.L., Zhou, Z.H.,
1436 Zhu, R.X., 2013b. SIMS U-Pb zircon age of Jurassic sediments in Linglongta, Jianchang, western
1437 Liaoning: constraint on the age of the oldest feathered dinosaurs (in Chinese with English abstract)
1438 Chinese Science Bulletin, 58, 1346–1353.

1439 Wang, J., 2013. Late Mesozoic extensional structure in the northern North China Craton and its
1440 geodynamic implications (in Chinese with English abstract). Dissertation for Doctoral Degree.
1441 Beijing: Institute of Geology and Geophysics, Chinese Academy of Sciences, 1–181.

- 1442 Wang, S.E., Gao, L.Z., Wan, X.Q., Song, B., 2013c. Ages of the Tuchengzi Formation in western
1443 Liaoning-northern Hebei area in correlation with those of international strata. *Geological Bulletin*
1444 of China 32(11), 1673–1690.
- 1445 Wang, Y., Dong, S., Shi, W., Chen, X., Jia, L., 2017. The Jurassic structural evolution of the
1446 western Daqingshan area, eastern Yinshan belt, North China. *International Geology Review* 1-23.
1447 <https://doi.org/10.1080/00206814.2017.1300784>
- 1448 Wang, Y., Zhou, L., Zhao, L., 2013a. Cratonic reactivation and orogeny: an example from the
1449 northern margin of the North China Craton. *Gondwana Research* 24 (3–4), 1203–1222.
1450 <https://doi.org/10.1016/j.gr.2013.02.011>.
- 1451 Wang, T., Zheng, Y., Zhang, J., Zeng, L., Donskaya, T., Guo, L., Li, J., 2011. Pattern and
1452 kinematic polarity of late Mesozoic extension in continental NE Asia: Perspectives from
1453 metamorphic core complexes. *Tectonics* 30(6), TC6007, <https://doi.org/10.1029/2011TC002896>.
- 1454 Wang, Z., Zhao, Y., Zou, H., Li, W., Liu, X., Wu, H., Xu, G., Zhang, S., 2007. The early Jurassic
1455 Nandaling flood basalts in the Yanshan belt, North China craton: the origin and geodynamic
1456 implications. *Lithos* 96, 543–566.
- 1457 Windley, B.F., Alexeiev, D., Xiao, W., Kröner, A., Badarch, G., 2007. Tectonic models for
1458 accretion of the Central Asian Orogenic Belt. *Journal of the Geological Society* 164 (1), 31–47.
1459 <https://doi.org/10.1144/0016-76492006-022>
- 1460 Wong W. H., 1927. Crustal movements and igneous activities in Eastern China since Mesozoic
1461 time. *Bulletin of Geological Society of China* 6, 9-37.
- 1462 Wong, W. H., 1929. The Mesozoic orogenic movement in eastern China. *Bulletin of Geological*
1463 *Society of China* 8, 33–44.
- 1464 Wu, G.L., Meng, Q.R., Zhu, R.X., Fan, L.G., Zhu, J.C., 2021. Middle Jurassic orogeny in the
1465 northern North China Block. *Tectonophysics* 801, 228713.
- 1466 Wu, F.Y., Yang, J.H., Wilde, S.A., Zhang, X.O., 2005. Geochronology, petrogenesis and tectonic
1467 implications of Jurassic granites in the Liaodong Peninsula, NE China. *Chemical Geology* 221,
1468 127–156.

- 1469 Wu, F. Y., Xu, Y. G., Gao, S., Zheng, J. P., 2008. Lithospheric thinning and destruction of the North
1470 China Craton (in Chinese with English abstract). *Acta Petrologica Sinica* 24, 1145–1174.
- 1471 Wu, F. Y., Yang, J. H., Lo, C. H., Wilde, S. A., Sun, D. Y., Jahn, B. M., 2007. The Heilongjiang
1472 Group: A Jurassic accretionary complex in the Jiamusi Massif at the western Pacific margin of
1473 northeastern China. *Island Arc* 16(1), 156–172. <https://doi.org/10.1111/j.1440-1738.2007.00564.x>
- 1474 Wu, F. Y., Yang, J. H., Xu, Y. G., Wilde, S. A., Walker, R. J., 2019. Destruction of the North
1475 China Craton in the Mesozoic. *Annual Review of Earth and Planetary Sciences* 47(1), 73–95.
1476 <https://doi.org/10.1146/annurev-earth-053018-060342>
- 1477 Wu, F. Y., Yang, J. H., Zhang, Y. B., Liu, X. M., 2006. Emplacement ages of the Mesozoic granites
1478 in southeastern part of the Western Liaoning Province. *Acta Petrologica Sinica* 22(2), 315–325.
- 1479 Wu, F. Y., Zhao, G. C., Sun, D. Y., Wilde, S. A., Zhang, J. H., 2007. The Hulan Group: its role in the
1480 evolution of the Central Asian Orogenic Belt of NE China. *Journal of Asian Earth Sciences* 30,
1481 542–556.
- 1482 Xiao, W. J., Windley, B., Hao, J., Zhai, M. G., 2003. Accretion leading to collision and the Permian
1483 Solonker suture, Inner Mongolia, China: termination of the Central Asian Orogenic Belt. *Tectonics*
1484 22, 1069–1089. <http://doi.org/10.1029/2002TC001484>
- 1485 Xiao, W., Windley, B. F., Sun, S., Li, J., Huang, B., Han, C., Yuan, C., Sun, M., Chen, H., 2015.
1486 A tale of amalgamation of three Permo-Triassic collage systems in Central Asia: oroclinal sutures,
1487 and terminal accretion. *Annual Review of Earth and Planetary Sciences* 43 (1), 477–501.
1488 <https://doi.org/10.1146/annurev-earth-060614-105254>
- 1489 Xu, B., Charvet, J., Chen, Y., Zhao, P., Shi, G., 2013. Middle Paleozoic convergent orogenic belts
1490 in western Inner Mongolia (China): framework, kinematics, geochronology and implications for
1491 tectonic evolution of the Central Asian Orogenic Belt. *Gondwana Research* 23 (4), 1342–1364.
1492 <https://doi.org/10.1016/j.gr.2012.05.015>
- 1493 Xu, Z., Lu, Y., Tang, Y., Mattauer, M., Matte, P., Malavieille, J., Tapponnier, P., Maluski, H.,
1494 1986. Deformation characteristics and Tectonic evolution of the eastern Qinling orogenic belt.
1495 *Acta Geologica Sinica* 60(3), 23–35. <https://doi.org/10.1111/j.1755-6724.1986.mp60003003.x>

1496 Xu, H., Liu, Y.Q., Kuang, H.W., Jiang, X.J., Nan, P., 2012. U-Pb SHRIMP age for the Tuchengzi
1497 Formation, northern China, and its implications for biotic evolution during the Jurassic-Cretaceous
1498 transition. *Paleoworld* 21, 222–234.

1499 Yan, M., Zhang, D., Fang, X., Ren, H., Zhang, W., Zan, J., Song, C., Zhang, T., 2016.
1500 Paleomagnetic data bearing on the Mesozoic deformation of the Qiangtang Block: implications
1501 for the evolution of the Paleo-and Meso-Tethys. *Gondwana Research* 39, 292–316

1502 Yang, Q., Shi, W., Hou, G., Zhang, Y., Zhao, Y., 2021. Late Mesozoic Intracontinental
1503 Deformation in the Northern Margin of the North China Craton: A Case Study From the Shangyi
1504 Basin, Northwestern Hebei Province, China. *Frontiers in Earth Science* 9, 1-26.

1505 Yang, J.H., Wu, F.Y., Shao, J.A., Wilde, S.A., Xie, L.W., Liu, X.M., 2006. Constraints on the
1506 timing of uplift of the Yanshan Fold and Thrust Belt, North China. *Earth and Planetary Science*
1507 *Letters* 246, 336–352

1508 Yang, J. H., Wu, F. Y., Chung, S. L., Wilde, S. A., Chu, M. F., 2004. Multiple sources for the
1509 origin of granites: geochemical and Nd/Sr isotopic evidence from the Gudaoling granite and its
1510 mafic enclaves, Northeast China. *Geochimica Et Cosmochimica Acta* 68(21), 4469-4483.

1511 Yang, M., Liang, L., Jin, Z., Qu, X., Zhou, D., 2013. Segmentation and inversion of the Hangjinqi
1512 fault zone, the northern Ordos basin (North China). *Journal of Asian Earth Sciences* 70–71, 64–
1513 78.

1514 Yang, W., Li, S.G., 2008. Geochronology and geochemistry of the Mesozoic volcanic rocks in
1515 western Liaoning: implications for lithospheric thinning of the North China craton. *Lithos* 102,
1516 88–117.

1517 Yang, X., Dong, Y., 2018. Mesozoic and Cenozoic multiple deformations in the Helanshan
1518 Tectonic Belt, Northern China. *Gondwana Research* 60, 34–53.
1519 <https://doi.org/10.1016/j.gr.2018.03.020>

1520 Yang, X., Dong, Y., 2020. Multiple phases of deformation in the Southern Helanshan Tectonic
1521 Belt, Northern China. *Journal of Asian Earth Sciences* 104497.
1522 <https://doi.org/10.1016/j.jseaes.2020.104497>

1523 Yang, Y., Li, W., Ma, L., 2005. Tectonic and stratigraphic controls of hydrocarbon systems in the
1524 Ordos Basin: a multicycle cratonic basin in central China. *AAPG Bulletin* 89(2), 255-269.

- 1525 Yin, A., Nie, S., 1996. A Phanerozoic palinspastic reconstruction of China and its neighboring
1526 regions. In: Yin, A., & Harrison, T.A. (Eds.), *The Tectonic Evolution of Asia*. Cambridge
1527 University Press, New York, pp. 442–485.
- 1528 Yu, H.F., Zhang, Z.C., Shuai, G.W., Chen, Y., Tang, W.H., 2016. SHRIMP and LA–ICP–MS U-
1529 Pb ages and geological significance of the volcanic rocks in the Tiaojishan Formation in Ming
1530 Tombs area–Western Hills, Beijing (in Chinese with English abstract). *Geological Review* 4, 807–
1531 826.
- 1532 Yu, X.Q., Wu, G.G., Zhao, X., Gao, J.F., Di, Y.J., Zheng, Y., Dai, Y.P., Li, C.L., Qiu, J.T., 2010.
1533 The Early Jurassic tectono-magmatic events in southern Jiangxi and northern Guangdong
1534 provinces, SE China: constraints from the SHRIMP zircon U-Pb dating. *Journal of Asian Earth*
1535 *Sciences* 39, 408–422.
- 1536 Yuan, H.L., Liu, X.M., Liu, Y.S., Gao, S., Ling, W.L., 2005. U-Pb zircon geochronology and
1537 geochemistry of Late Mesozoic volcanic rocks in Western Hills, Beijing. *Science China* 35(9),
1538 821–836.
- 1539 Zeng, J., Wei, W., Lin, W., Meng, L., Qiu, H., Chu, Y., Ren, Z., Wang, Y., Feng, Z., Li, Q., Ling,
1540 X., 2021. The Late Jurassic extensional event in the Yanshan fold and thrust belt (North China):
1541 New insights from an integrated study of structural geology, geophysics, and geochemistry of the
1542 Siganding granitic pluton. *Journal of Asian Earth Sciences* 211, 104708.
1543 <https://doi.org/10.1016/j.jseaes.2021.104708>
- 1544 Zhang, A., Liu, S., Lin, C., Zhang, B., 2019. Timing of deposition in the Dengzhangzi and
1545 Guojiadian Basins of the Yanshan fold-thrust belt, North China. *International Geology Review* 9,
1546 1-22.
- 1547 Zhang, C., Wang, G., Wu, Z., Zhang, L., Sun, W., 2002. Thrust tectonics in the eastern segment
1548 of the intraplate Yanshan orogenic belt, western Liaoning province, North China (in Chinese with
1549 English abstract). *Acta Geologica Sinica* 76(1), 64-76.
- 1550 Zhang, C. H., Wu, G. G., Xu, D. B., Wang, G. H., Sun, W. H., 2004a. Mesozoic tectonic
1551 framework of the intraplate and evolution in the central segment Yanshan orogenic belt (in Chinese
1552 with English abstract). *Geological Bulletin of China* 23(9–10), 864-875.

1553 Zhang, C.H., Zhang, Y., Li, H.L., Wu, G.G., Wang, G.H., Xu, D.B., Xiao, W.F., Dai, L., 2006.
1554 Late Mesozoic thrust tectonics framework in the western part of the Yanshan orogenic belt and
1555 the Western Hills of Beijing: characteristics and significance (in Chinese with English abstract).
1556 Earth Science Frontiers 13(2), 165-183.

1557 Zhang, H., Yuan, H.L., Hu, Z.C., Liu, X.M., Diwu, C.R., 2005. U-Pb zircon dating of the Mesozoic
1558 volcanic strata in Luanping of north Hebei and its significance (in Chinese with English abstract):
1559 Earth Science-Journal of China University of Geoscience, 30, 6, 07-720.

1560 Zhang, H., Wang, M.X., Liu, X.M., 2008a. Constraints on the upper boundary age of the
1561 Tiaojishan Formation volcanic rocks in West Liaoning-North Hebei by LA-ICP-MS dating.
1562 Science Bulletin 53(22), 3574-3584

1563 Zhang, H., Wei, Z.L., Liu, X.M., Li, D., 2009. Constraints on the age of the Tuchengzi Formation
1564 by LA-ICP-MS dating in northern Hebei-western Liaoning, China. Science China Earth Sciences
1565 52 (4), 461-470.

1566 Zhang, H.-F., 2007. Temporal and spatial distribution of Mesozoic mafic magmatism in the North
1567 China Craton and implications for secular lithospheric evolution. Geological Society, London,
1568 Special Publications 280(1), 35-54. <https://doi.org/10.1144/sp280.2>

1569 Zhang, H.F., Sun, M., Zhou, M.F., Fan, W.M., Zhou, X.H., Zhai, M.G., 2004b. Highly
1570 heterogeneous late Mesozoic lithospheric mantle beneath the North China Craton: evidence from
1571 Sr-Nd-Pb isotopic systematics of mafic igneous rocks. Geological Magazine 141, 55-62.

1572 Zhang, K.J., Zhang, Y.X., Tang, X.C., Xia, B., 2012. Late Mesozoic tectonic evolution and growth
1573 of the Tibetan plateau prior to the Indo-Asian collision. Earth-Sciences Reviews 114, 236-249.

1574 Zhang, S. H., Zhao, Y., Davis, G. A., Ye, H., Wu, F., 2014. Temporal and spatial variations of
1575 Mesozoic magmatism and deformation in the North China Craton: implications for lithospheric
1576 thinning and decratonization. Earth-Science Reviews 131(4), 49-87.
1577 <https://doi.org/10.1016/j.earscirev.2013.12.004>

1578 Zhang, X., Zhang, H., Jiang, N., Wilde, S. A., 2010. Contrasting Middle Jurassic and Early
1579 Cretaceous mafic intrusive rocks from western Liaoning, North China craton: petrogenesis and
1580 tectonic implications. Geological Magazine 147(06), 844-859.
1581 <https://doi.org/10.1017/s0016756810000373>

1582 Zhang, Y., Dong, S., Zhao, Y., Zhang, T., 2008b. Jurassic tectonics of North China: a synthetic
1583 view. *Acta Geologica Sinica-English Edition* 82(2), 310-326.

1584 Zhang, Y., Shi, W., Dong, S., 2011. Changes of Late Mesozoic tectonic regimes around the Ordos
1585 Basin (North China) and their geodynamic implications. *Acta Geologica Sinica* 85(6), 1254-1276.

1586 Zhang, Y., Qiu, E., Dong, S., Li, J., Shi, W., 2022. Late Mesozoic intracontinental deformation
1587 and magmatism in North and NE China in response to multi-plate convergence in NE Asia: An
1588 overview and new view. *Tectonophysics* 835, 229377,
1589 <https://doi.org/10.1016/j.tecto.2022.229377>

1590 Zhang, Y., Shi, W., Dong, S., Wang, T., Yang, Q., 2020. Jurassic intracontinental deformation of
1591 the central North China Plate: Insights from syn-tectonic sedimentation, structural geology, and
1592 U-Pb geochronology of the Yungang Basin, North China. *Tectonophysics* 778, 228371.

1593 Zhao, G., Wilde, S. A., Cawood, P. A., Sun, M., 2001. Archean blocks and their boundaries in the
1594 North China Craton: lithological, geochemical, structural and P-T, path constraints and tectonic
1595 evolution. *Precambrian Research* 107(1), 45–73. [https://doi.org/10.1016/S0301-9268\(00\)00154-6](https://doi.org/10.1016/S0301-9268(00)00154-6)

1596 Zhao, P., Chen, Y., Xu, B., Faure, M., Shi, G., Choulet, F., 2013. Did the Paleo-Asian Ocean
1597 between NCC and Mongolia Block exist during the late Paleozoic? first paleomagnetic evidence
1598 from central-eastern Inner Mongolia, China. *Journal of Geophysical Research: Solid Earth* 118
1599 (5), 1873–1894. <https://doi.org/10.1002/jgrb.50198>

1600 Zhao, Y., 1990. The Mesozoic orogenesis and tectonic evolution of the Yanshan area (in Chinese
1601 with English abstract). *Geology Review* 36 (1), 1–13.

1602 Zhao, Y., Cui, S.Q., Guo, T., Xu, G., 2002. Evolution of a Jurassic basin of the Western Hills,
1603 Beijing, North China and its tectonic implications (in Chinese with English abstract). *Geological*
1604 *Bulletin of China* 21, 211–217.

1605 Zhao, Y., Zhang, S.H., Xu, G., Yang, Z.Y., Hu, J.M., 2004. The Jurassic major tectonic events of
1606 the Yanshanian intraplate deformation belt (in Chinese with English abstract). *Geological Bulletin*
1607 *of China* 23 (9–10), 854–863.

1608 Zhao, Y., Song, B., Zhang, S.H., Liu, J., 2006. Geochronology of the inherited zircons from
1609 Jurassic Nandaling basalt of the Western Hills of Beijing, North China: Its implications (in Chinese
1610 with English abstract). *Earth Science Frontiers* 2006, 13(2), 184-190.

1611 Zhou, J.B., Wilde, S.A., Zhao, G.C., Han, J., 2018. Nature and assembly of microcontinental
1612 blocks within the Paleo-Asian Ocean. *Earth-Science Reviews* 186, 76–93.
1613 <https://doi.org/10.1016/j.earscirev.2017.01.012>

1614 Zhu, D.C., Zhao, Z.D., Niu, Y.L., Mo, X.X., Chung, S.L., Hou, Z.Q., Wang, L.Q., Wu, F.Y.,
1615 2011a. The Lhasa Terrane: Record of a microcontinent and its histories of drift and growth. *Earth*
1616 *and Planetary Science Letters* 301, 241–255

1617 Zhu, D.C., Li, S.M., Cawood, P.A., Wang, Q., Zhao, Z.D., Liu, S.A., Wang, L.Q., 2016. Assembly
1618 of the Lhasa and Qiangtang terranes in central Tibet by divergent double subduction. *Lithos* 245,
1619 7–17.

1620 Zhu, G., Chen, Y., Jiang, D., Lin, S., 2015. Rapid change from compression to extension in the
1621 North China Craton during the Early Cretaceous: Evidence from the Yunmengshan metamorphic
1622 core complex. *Tectonophysics* 656, 91–110. <https://doi.org/10.1016/j.tecto.2015.06.009>

1623 Zhu, G., Jiang, D., Zhang, B., Chen, Y., 2011b. Destruction of the eastern North China Craton in
1624 a back-arc setting: evidence from crustal deformation kinematics. *Gondwana Research* 22(1), 86-
1625 103. <https://doi.org/10.1016/j.gr.2011.08.005>

1626 Zhu, G., Liu, C., Gu, C., Zhang, S., Li, Y., Su, N., Xiao, S., 2018. Oceanic plate subduction history
1627 in the western Pacific Ocean: Constraint from late Mesozoic evolution of the Tan-Lu Fault Zone.
1628 *Science China Earth Sciences* 61(4), 386–405. <https://doi.org/10.1007/s11430-017-9136-4>

1629 Zorin, Yu.A., 1999. Geodynamics of the western part of the Mongolia–Okhotsk collisional belt,
1630 Trans-Baikal region (Russia) and Mongolia. *Tectonophysics* 306, 33–56.

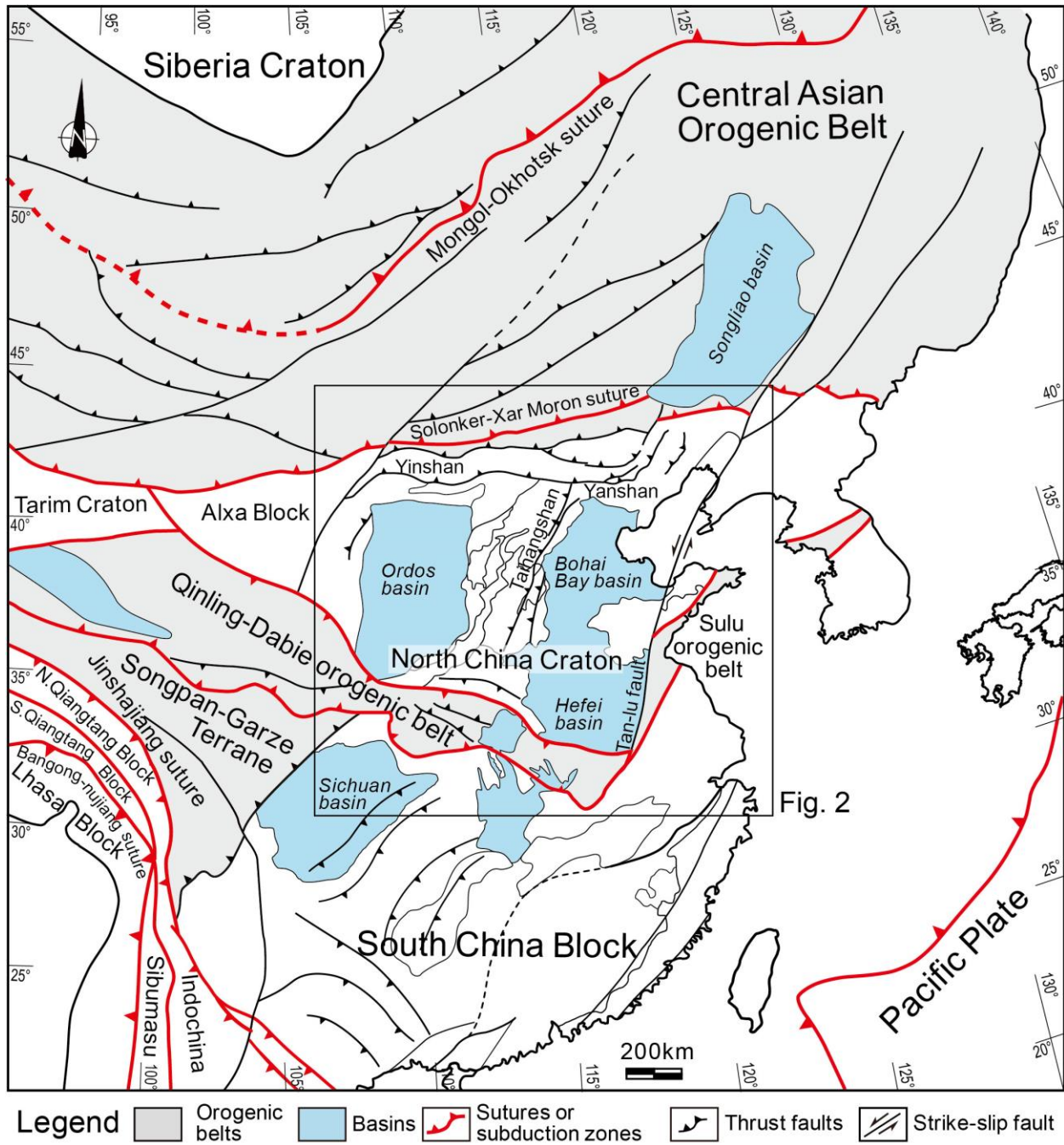
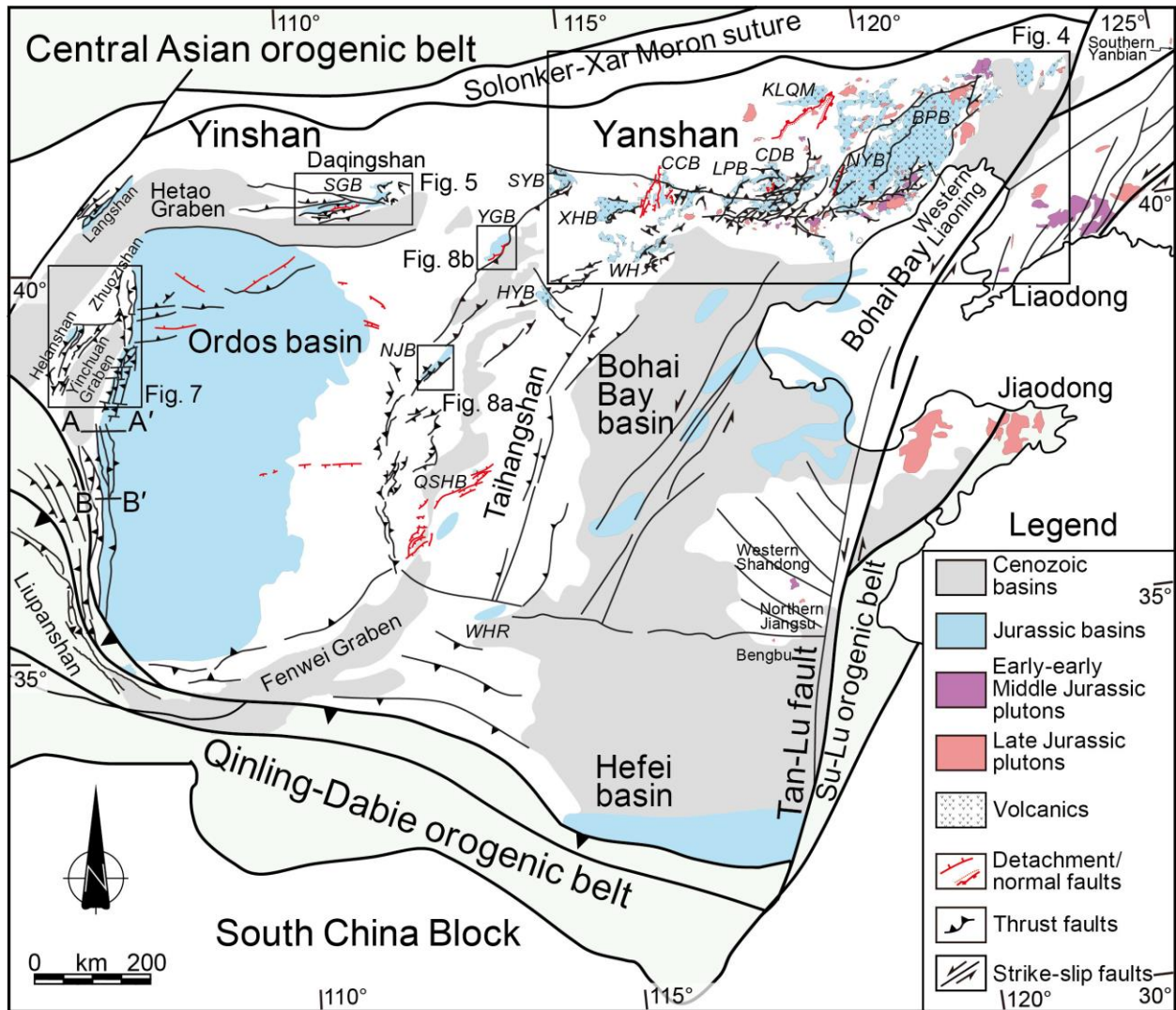


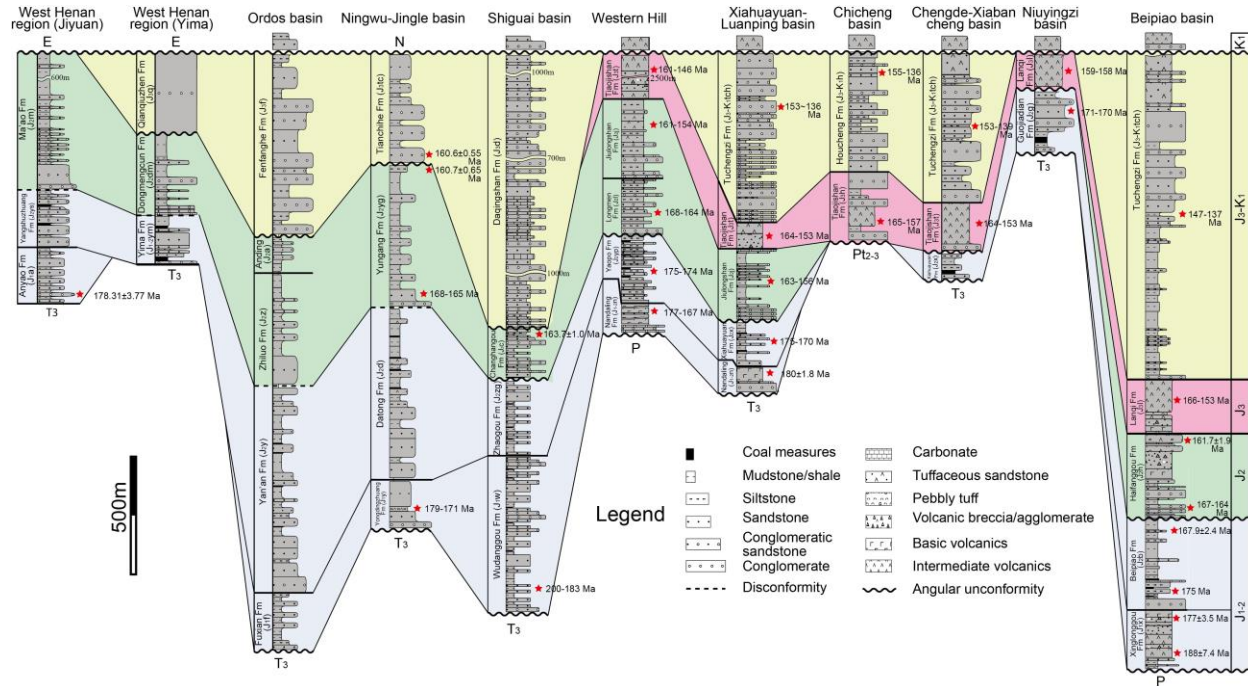
Fig. 2

1632

1633 **Fig. 1.** Simplified geological sketch map of the East Asian continent.

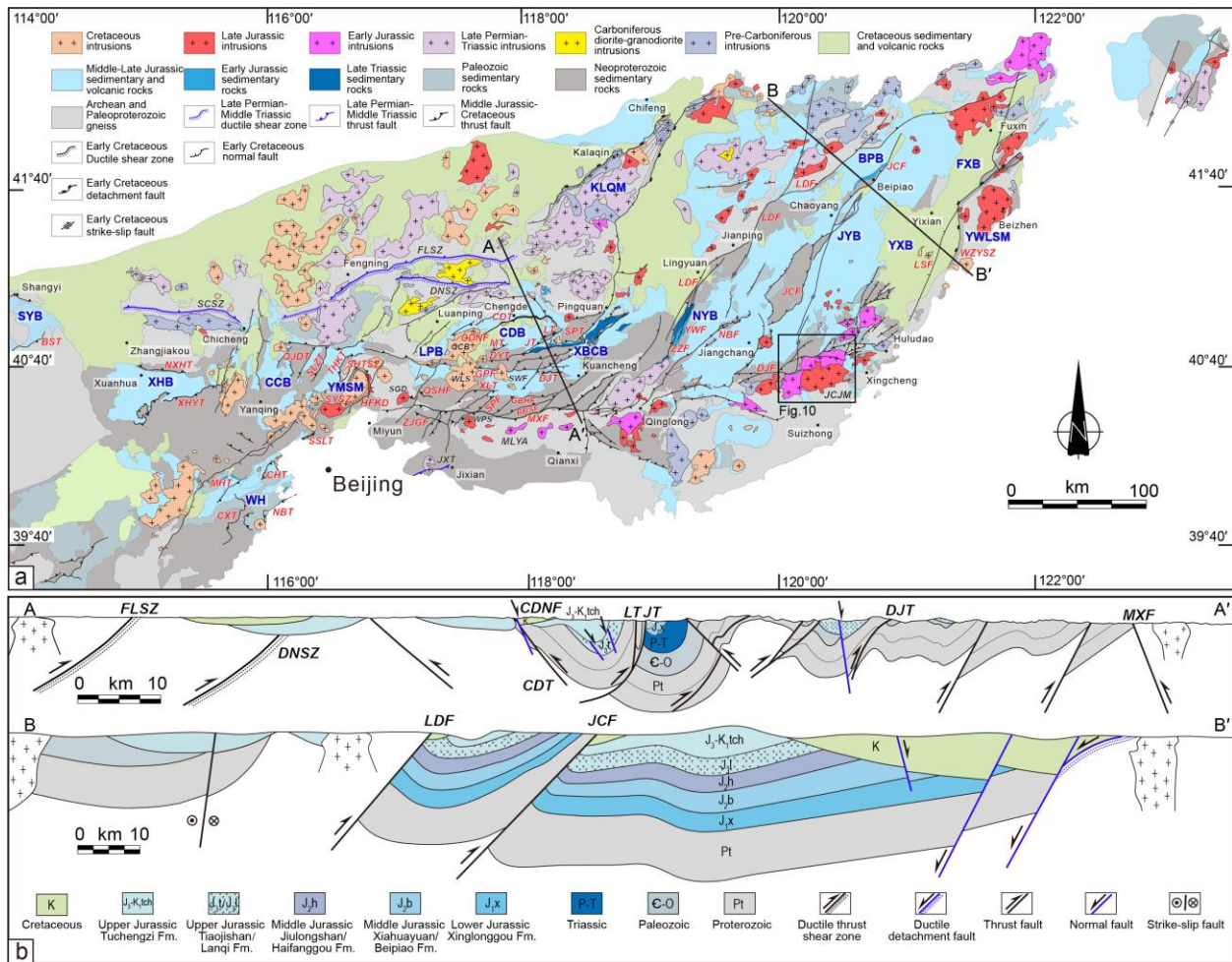


1634
 1635 **Fig. 2.** Simplified geological map showing the Jurassic–earliest Cretaceous structures and
 1636 magmatic rocks in the NCC (Modified from Zhang et al., 2011). SGB: Shiguai basin; YGB:
 1637 Yungang basin; HYB: Hunyuan basin; NJB: Ningwu-Jingle basin; QSHB: Qinshuihe basin;
 1638 WHR: West Henan region; SYB: Shangyi basin; XHB: Xuanhua basin; WH: Western Hill; CCB:
 1639 Chicheng basin; CDB: Chengde basin; NYB: Niuyingzi basin; LPB: Luanping basin; BPB:
 1640 Beipiao basin; KLQM: Kalaqin metamorphic core complex (MCC). See Fig. 1 for locations.



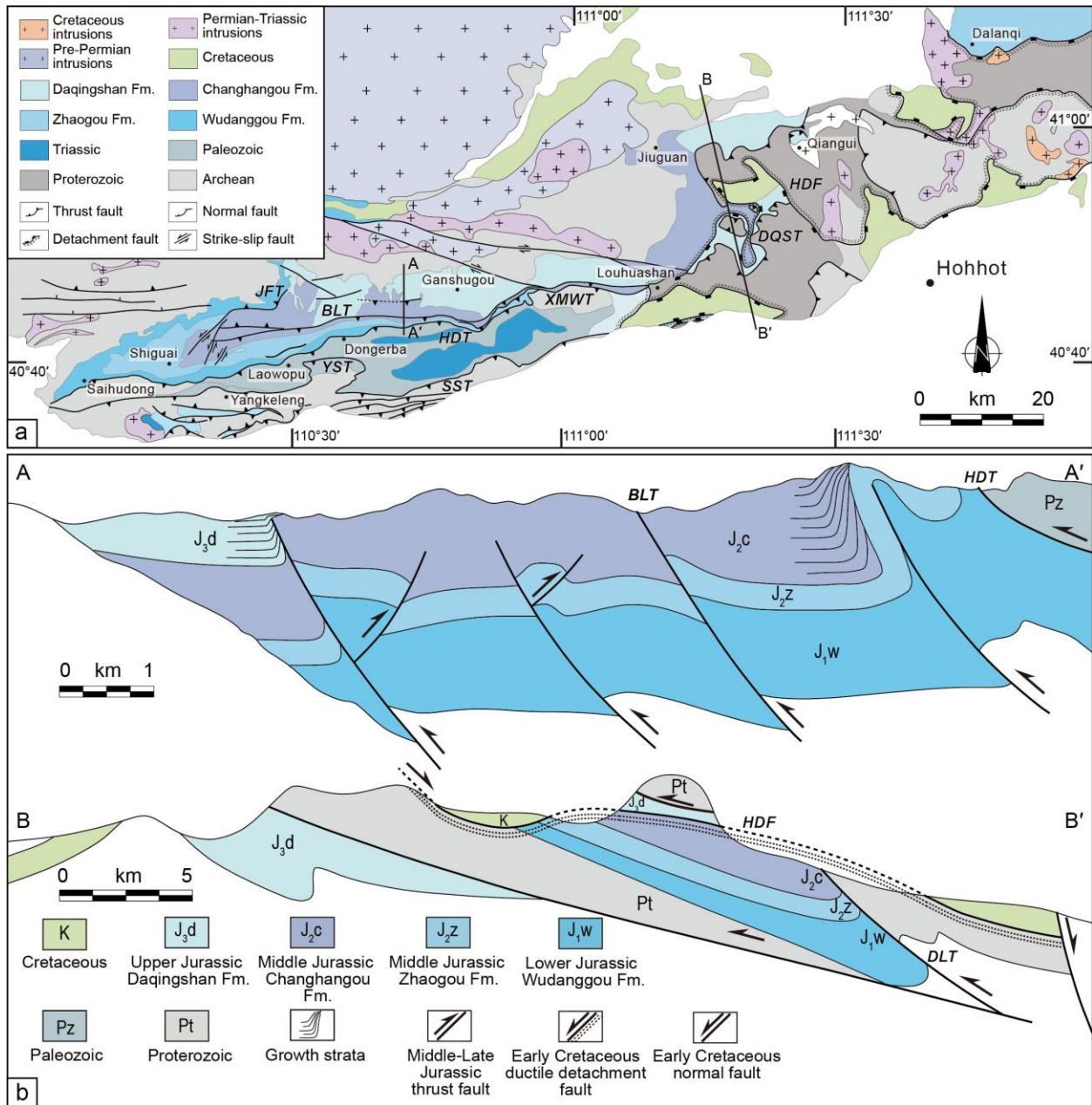
1641

1642 **Fig. 3.** Stratigraphic correlation and chronostratigraphic framework of the Jurassic–lowest
 1643 Cretaceous strata (Data from [BGMNM, 1983](#); [BGMH, 1989](#); [BGML, 1989](#)). The red stars indicate
 1644 the sampling sites of the zircon U-Pb and ^{40}Ar - ^{39}Ar data, which are summarized in [Table S1](#). See
 1645 [Fig. 2](#) for locations of the basins.



1646

1647 **Fig. 4.** Overview map of the Yanshan belt. (a) Simplified tectonic map of the Yanshan belt
 1648 (modified from BGMH, 1989; BGML, 1989; Qiu et al. 2020, 2021; See Fig. 2 for location). (b)
 1649 Geological cross-sections across the Yanshan belt (modified from Davis et al., 2001; Li et al.,
 1650 2016a; Su et al. 2021). SYB: Shangyi basin; XHB: Xuanhua basin; WH: Western Hill; CCB:
 1651 Chicheng basin; LPB: Luanping basin; CDB: Chengde basin; XBCB: Xiabancheng basin; NYB:
 1652 Niuyingzi basin; JYB: Jinyang basin; YXB: Yixian basin; BPB: Beipiao basin; FXB: Fuxian basin;
 1653 KLQM: Kalaqin MCC; YMSM: Yunmengshan MCC; YWLSM: Yiwulüshan MCC. See Table 2
 1654 for the abbreviations of the structures.

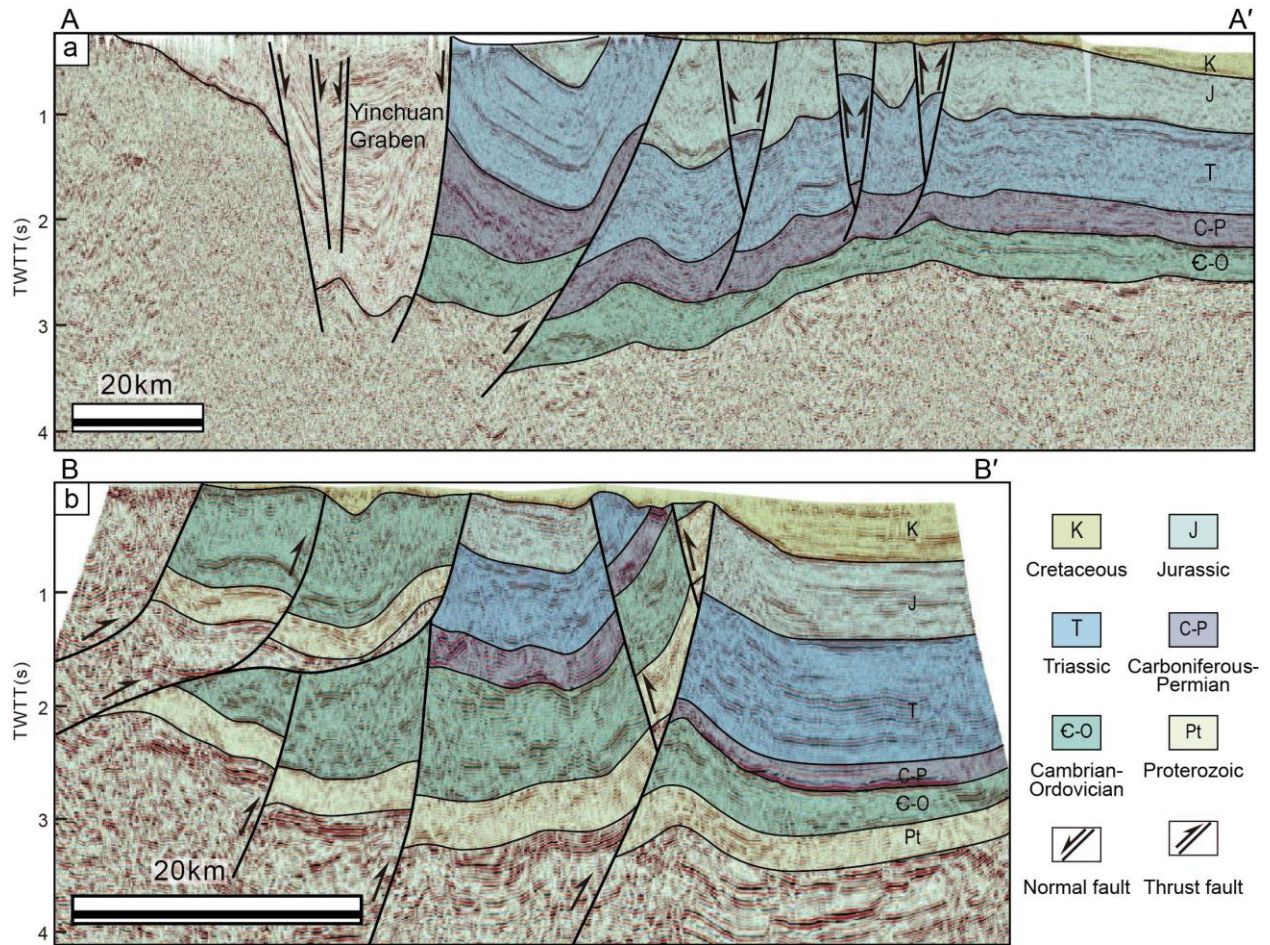


1655

1656 **Fig. 5.** Overview map of Daqingshan in the Yinshan belt (modified from BGMNM, 1983; Gong

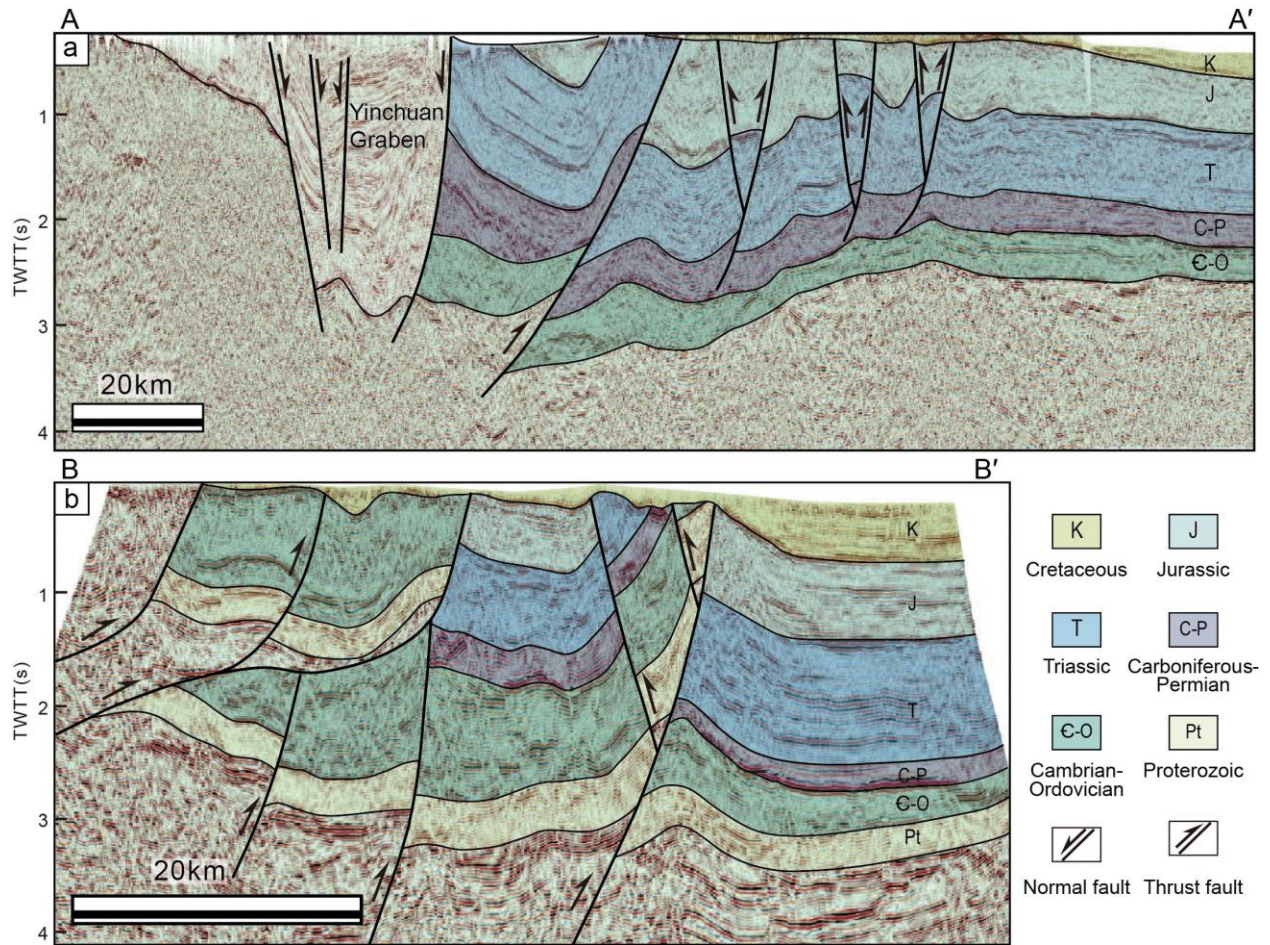
1657 et al., 2017; Wang et al., 2017). (a) Simplified tectonic map of Daqingshan. See Fig. 2 for location.

1658 (b) Geological cross-sections across Daqingshan. See Table 2 for the abbreviations of structures.



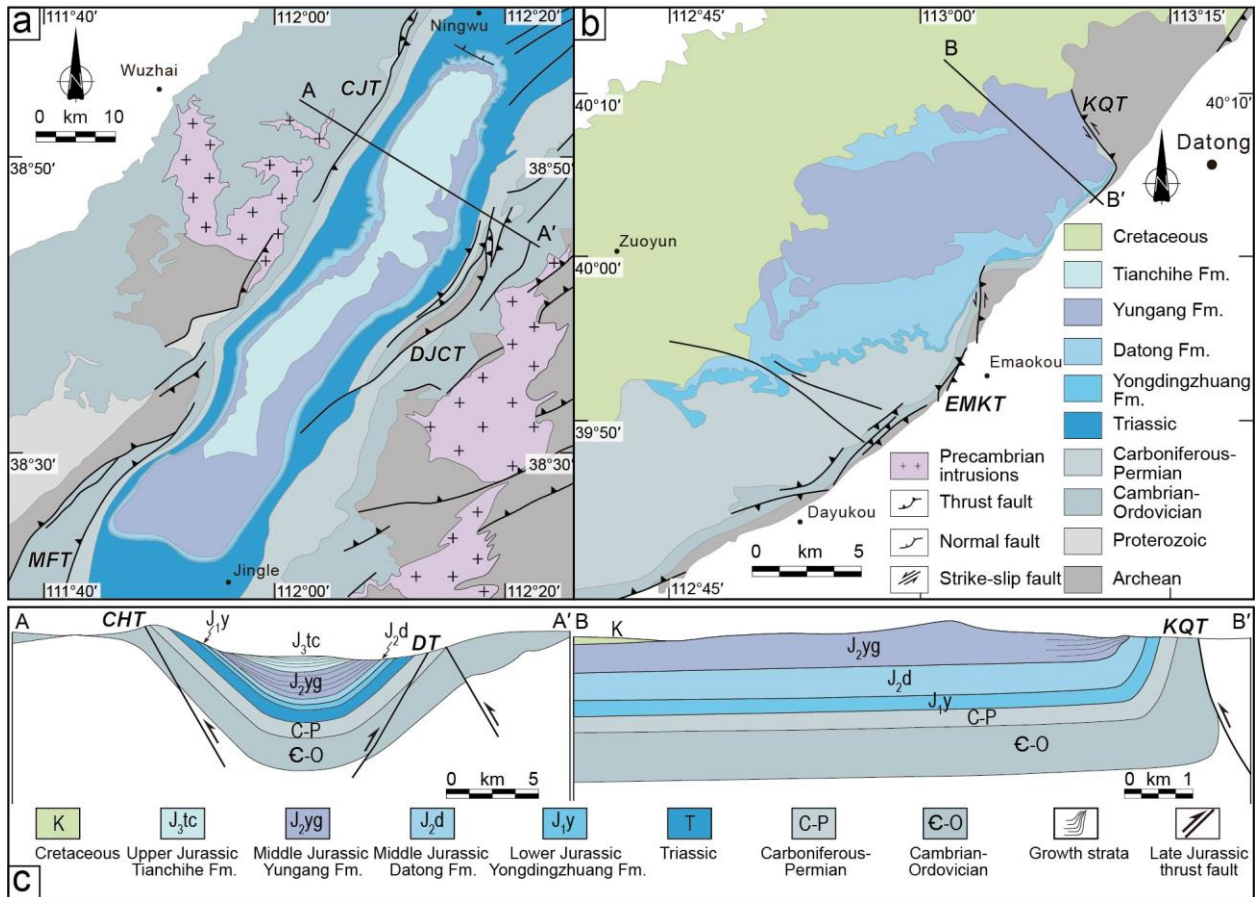
1659

1660 **Fig. 6.** Seismic reflection profiles across the Western Ordos fold-thrust belt (modified from Feng,
 1661 Feng, 2021; See Fig. 2 for locations).



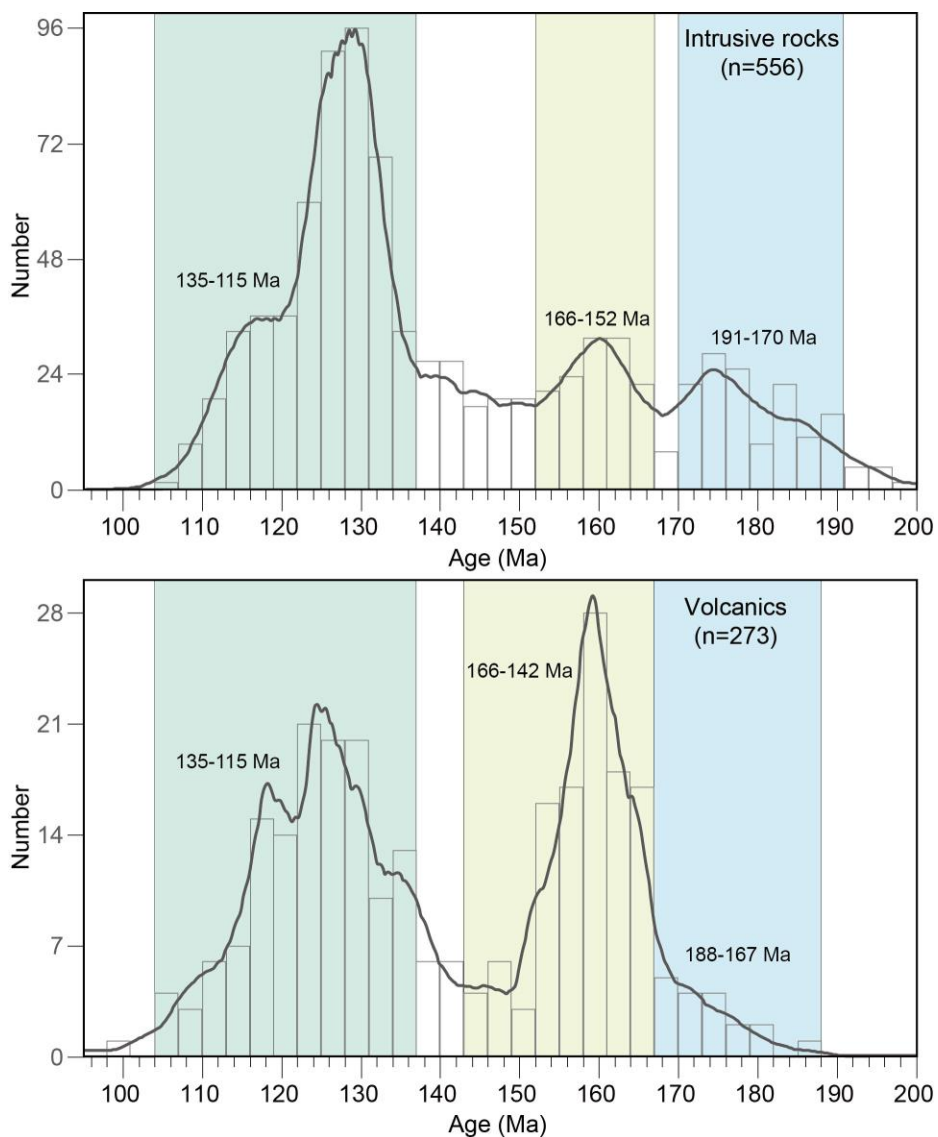
1662

1663 **Fig. 7.** Overview map of Helanshan-Zhuozishan in the west of the Ordos basin (modified from
 1664 [Darby and Ritts, 2002](#); [Yang and Dong, 2018](#); [Li et al., 2022](#); [Cheng et al., 2022](#)). (a) Simplified
 1665 tectonic map of Helanshan-Zhuozishan. See [Fig. 2](#) for locations. (b)–(e) Geological cross-sections
 1666 across Helanshan-Zhuozishan. See [Table 2](#) for the abbreviations of the structures.



1667

1668 **Fig. 8.** Overview map of the Ningwu-Jingle and Yungang basins in the east of the Ordos basin
 1669 (modified from [Chen et al., 2019](#); [Zhang et al., 2020](#)). (a) Simplified tectonic map of the Ningwu-
 1670 Jingle basin. See [Fig. 2](#) for location. (b) Simplified tectonic map of the Yungang basin. See [Fig. 2](#)
 1671 for location. (c) Geological cross-sections across the Ningwu-Jingle and Yungang basins. See
 1672 [Table 2](#) for the abbreviations of the structures.



1673

1674 **Fig. 9.** The U-Pb or ^{39}Ar - ^{40}Ar age probability of Jurassic–Early Cretaceous magmatism in NCC.

1675 Data are from [Chen et al. \(1997, 2014\)](#), [Davis et al. \(2001\)](#), [Li et al. \(2001, 2014b, 2014c, 2015,](#)

1676 [2016a\)](#), [Ritts et al. \(2001\)](#), [Swisher et al. \(2002\)](#), [Zhao et al. \(2002, 2004, 2006b\)](#), [Cope \(2003,](#)

1677 [2017\)](#), [Niu et al. \(2003, 2004\)](#), [Shao et al. \(2003\)](#), [Lu et al. \(2004\)](#), [Yuan et al. \(2005\)](#), [Zhang et al.](#)

1678 [\(2005\)](#), [Yang et al. \(2006\)](#), [Liu et al. \(2006, 2018b\)](#), [Cope, et al. \(2007\)](#), [Yang and Li \(2008\)](#), [Zhang](#)

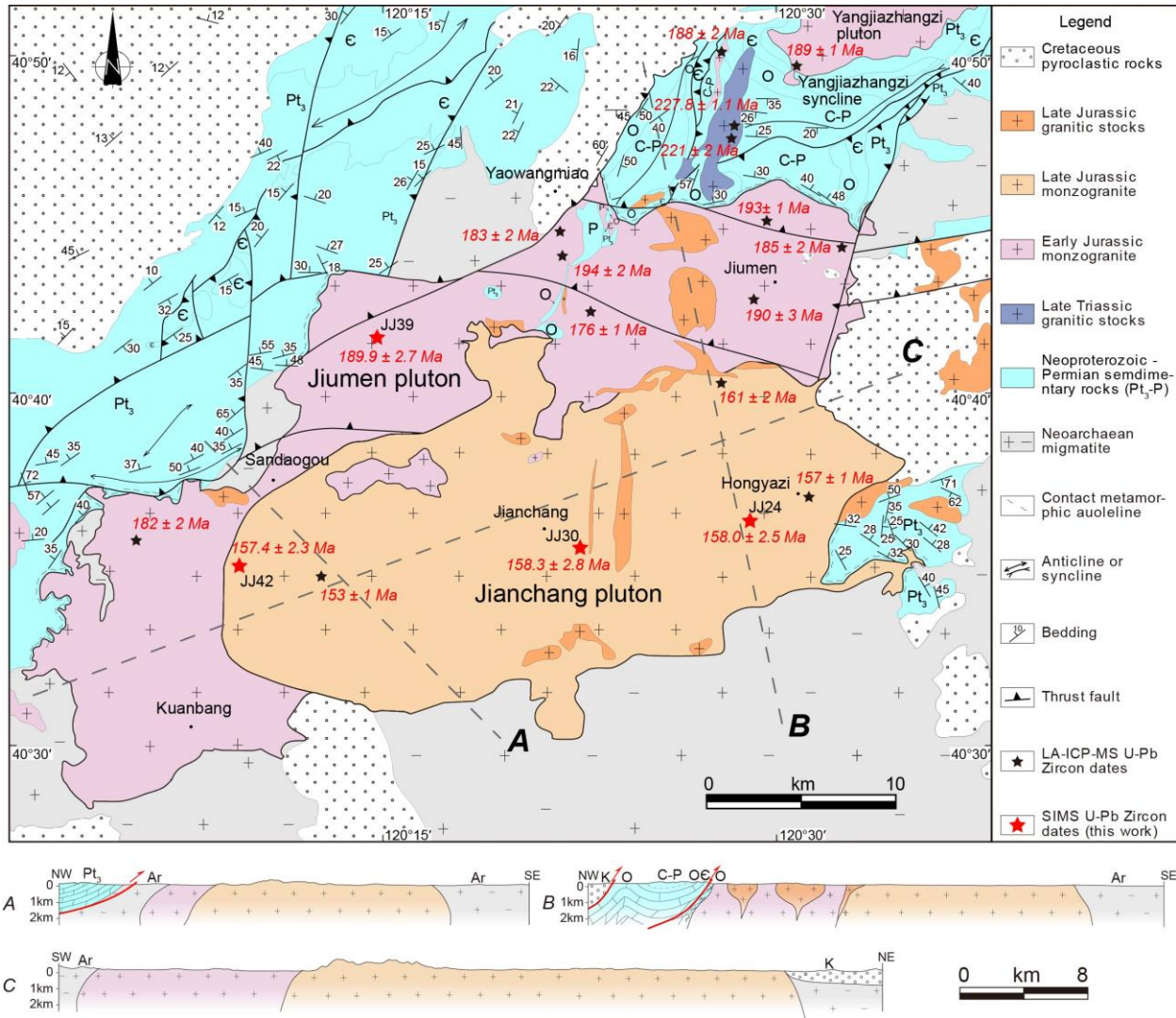
1679 [et al. \(2008a, 2009\)](#), [Davis and Darby \(2010\)](#), [Liu et al. \(2012\)](#), [Xu et al. \(2012\)](#), [Wang et al. \(2013b,](#)

1680 [2017\)](#), [Chang et al. \(2014\)](#), [Zhang et al. \(2014, 2019, 2020\)](#), [Qi et al. \(2015\)](#), [Jiao et al. \(2016\)](#), [Yu](#)

1681 [et al. \(2016\)](#), [He et al. \(2017\)](#), [Fu et al. \(2018\)](#), [Gao et al. \(2018\)](#), [Lin et al. \(2018, 2019\)](#), [Chen et](#)

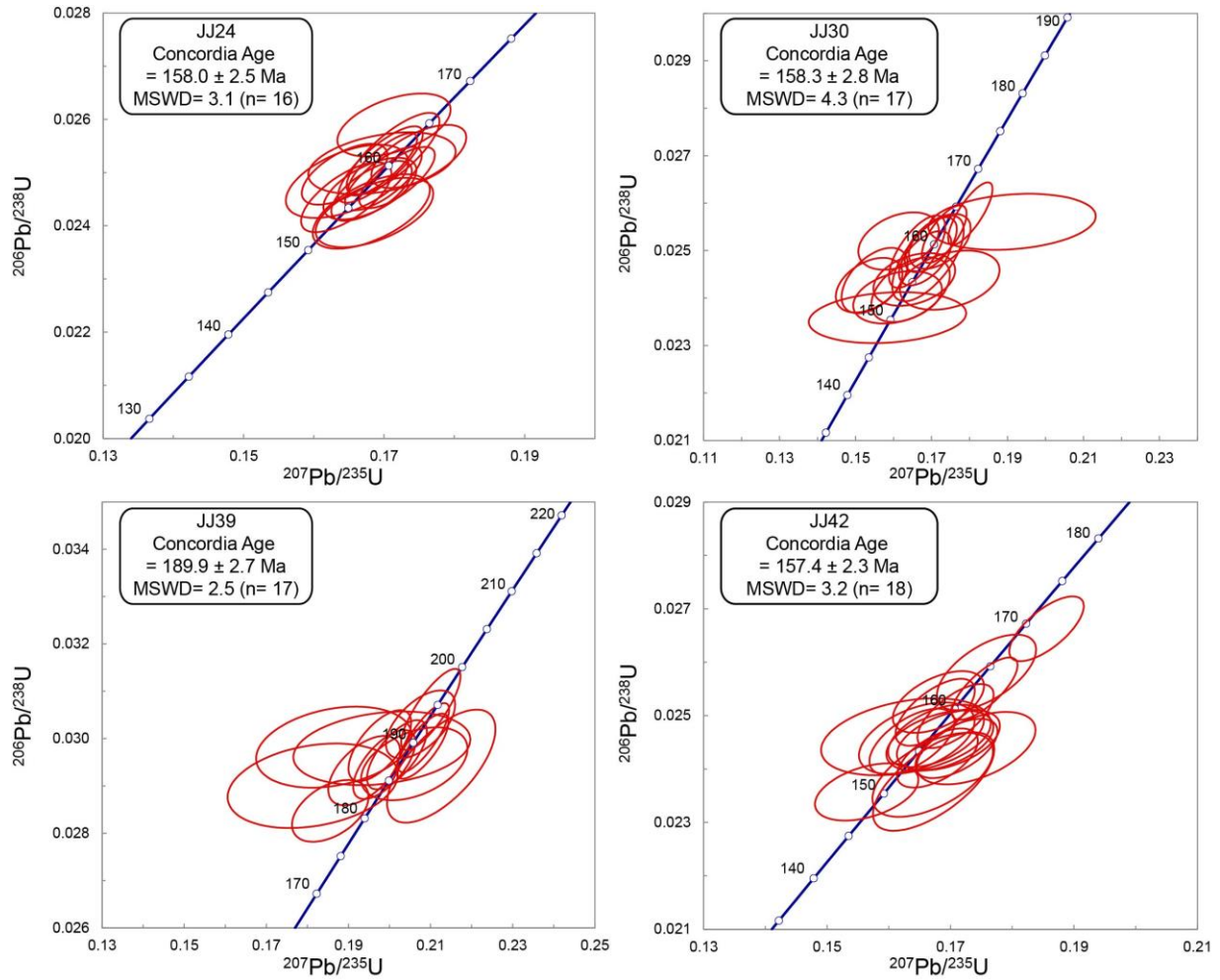
1682 [al. \(2019\)](#), [Hao et al. \(2019, 2020\)](#), [Huang \(2019\)](#), [Meng et al. \(2019\)](#), [Su et al. \(2021\)](#), [Wu et al.](#)

1683 [\(2021\)](#), [Guo et al. \(2022\)](#), and references therein.



1684

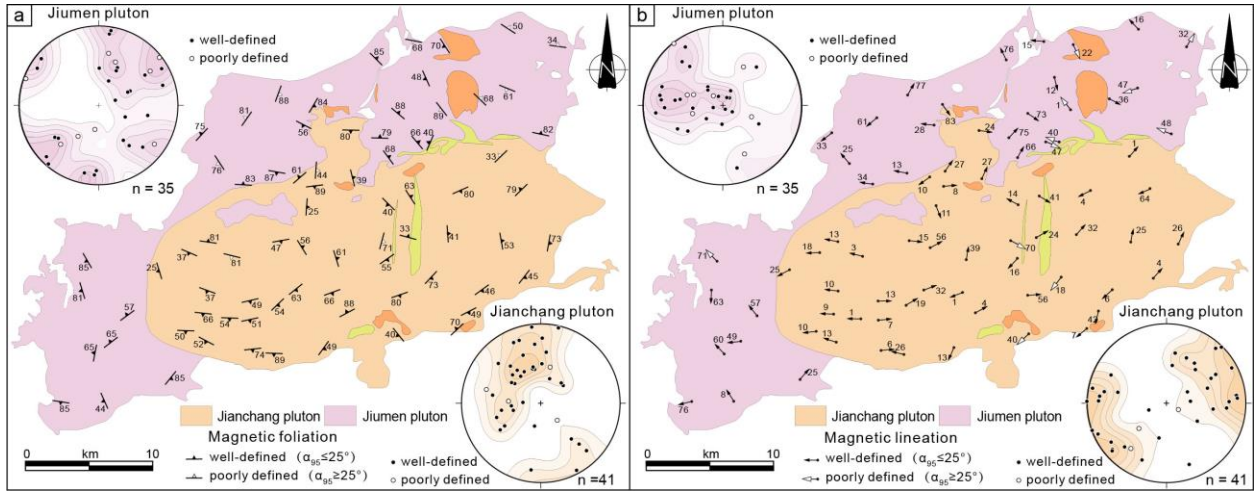
1685 **Fig. 10.** Structural geological map of the Jianchang-Jiumen plutons and adjacent areas. U–Pb
 1686 zircon data are from Wu et al. (2006) and Cui (2015). See Fig. 4 for location.



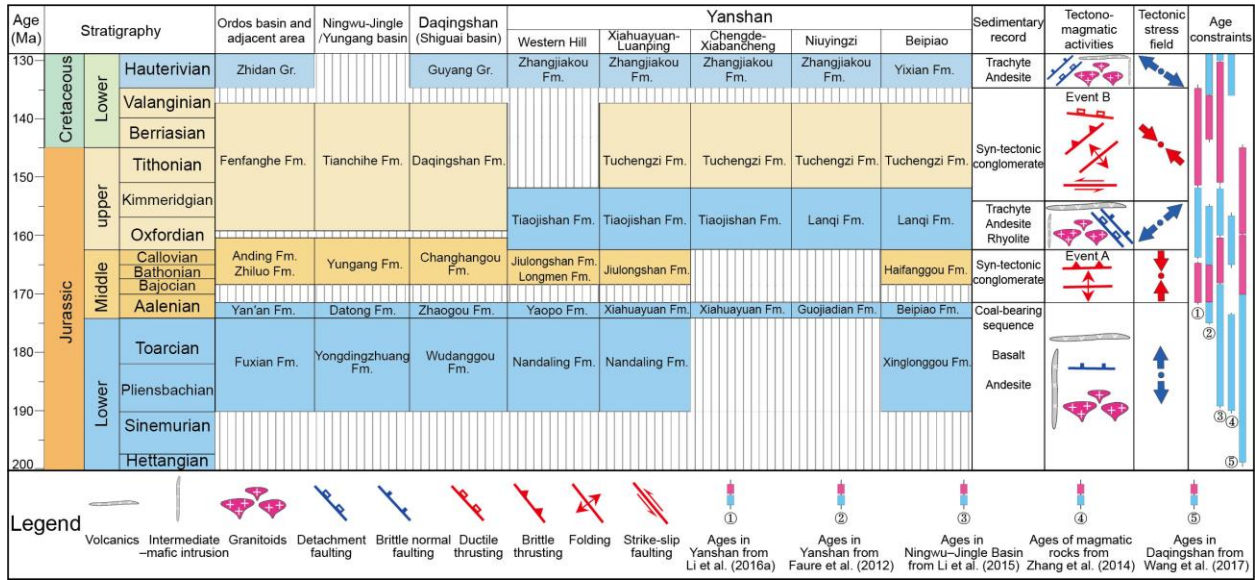
1687

1688 **Fig. 11.** U-Pb diagrams of Concordia age of representative zircons from collected samples in the
 1689 Jianchang-Jiumen plutons. MSWD: mean square of weighted deviates.

1690



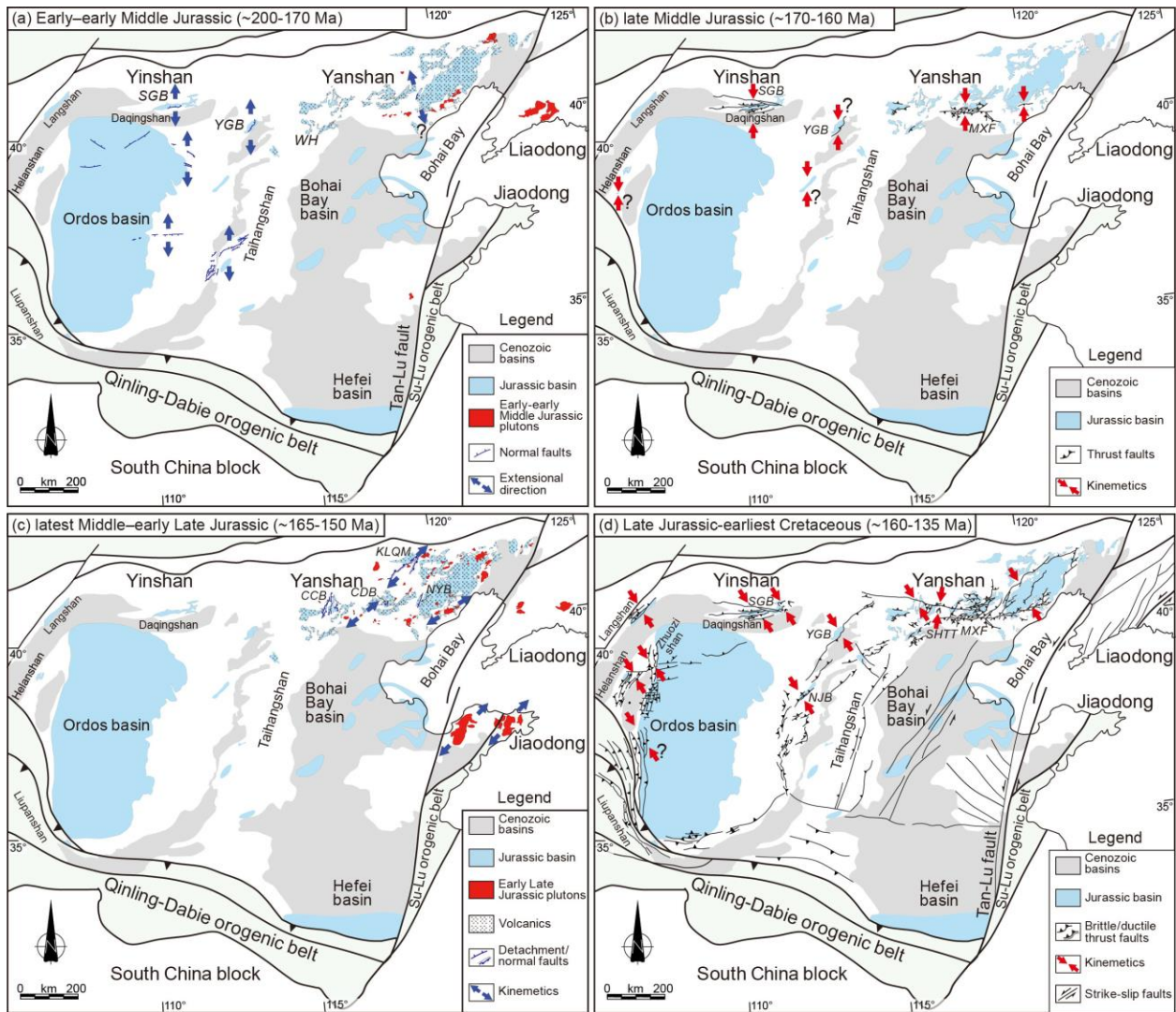
1691 **Fig. 12.** Magnetic fabric patterns and orientation diagrams of K_3 and K_1 in the Jianchang-Jiumen
1692 plutons. (a) Foliations. (b) Lineations.



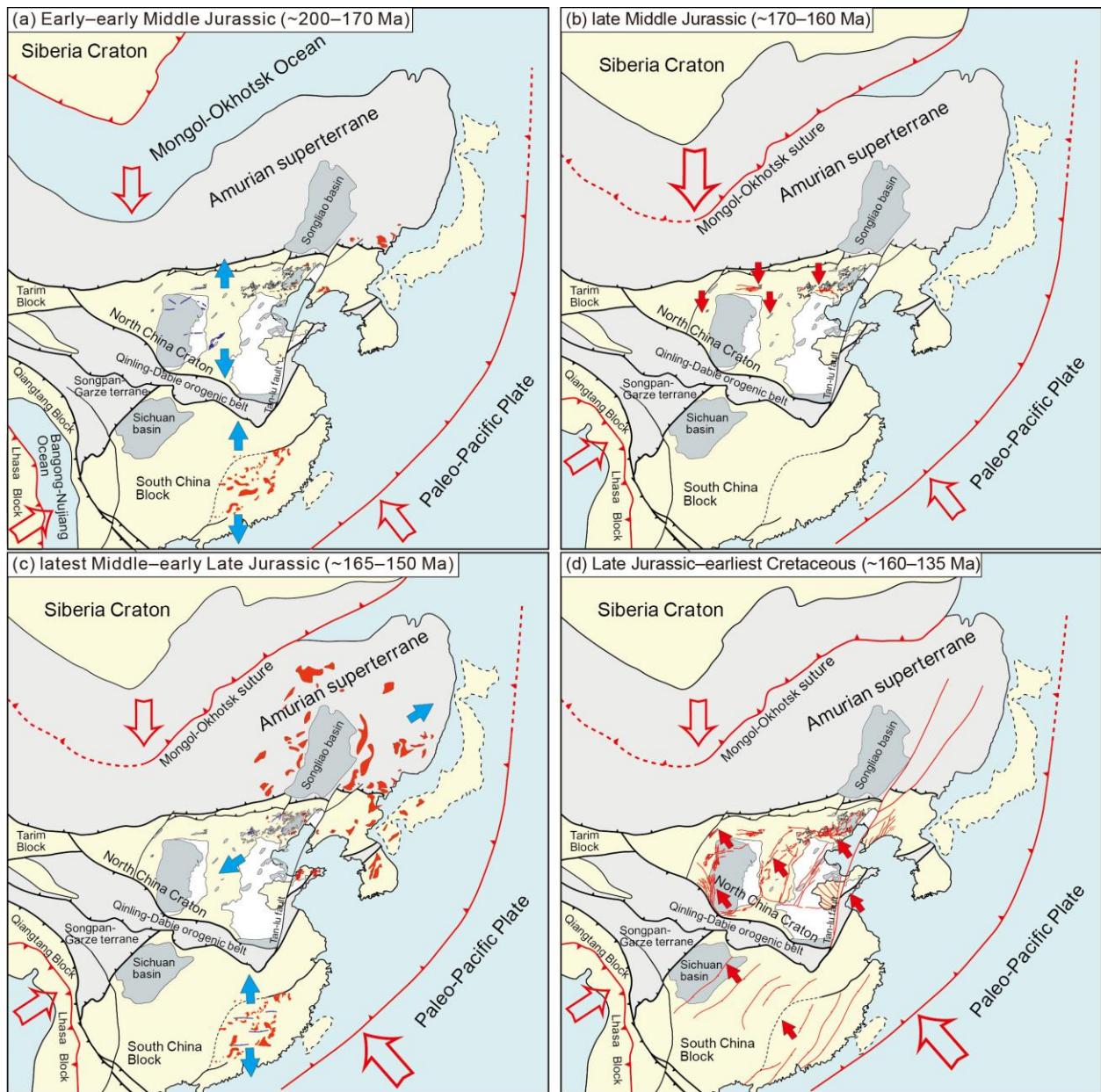
1693

1694

Fig. 13. Synthetic Jurassic–Early Cretaceous tectonostratigraphic framework of the NCC.

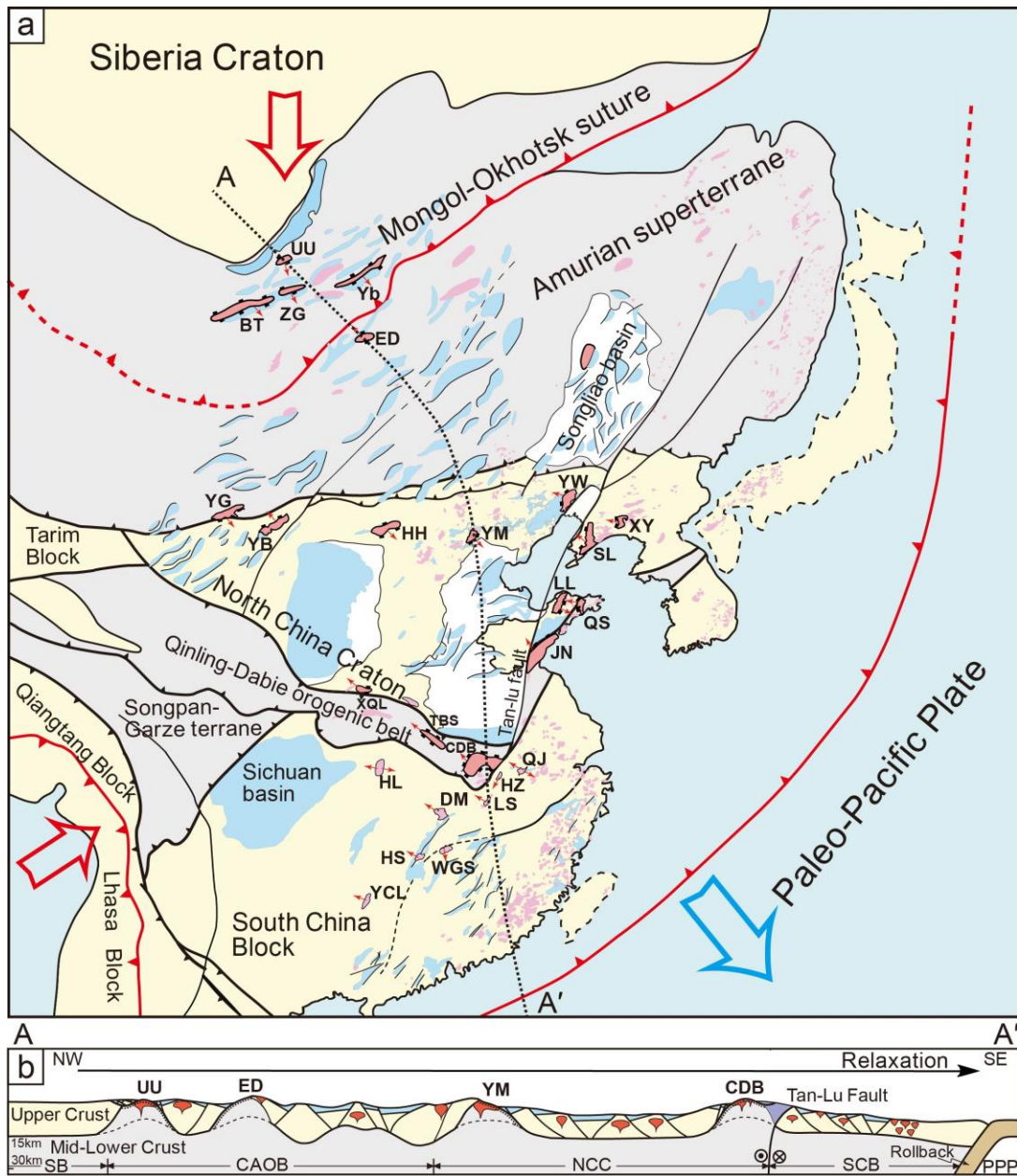


1695
 1696 **Fig. 14.** Jurassic–earliest Cretaceous regional tectonics of the NCC. (a) Early–early Middle
 1697 Jurassic (~200–170 Ma) extensional structures and magmatism in the NCC. (b) late Middle
 1698 Jurassic (~170–160 Ma) compressional structures in the NCC. (c) latest Middle–early Late Jurassic
 1699 (~165–150 Ma) local extensional structures and magmatism in the NCC. (d) Late Jurassic–earliest
 1700 Cretaceous (~160–135 Ma) compressional structures in the NCC. See Fig. 2 for the abbreviations
 1701 of the basins and structures.



1702

1703 **Fig. 15.** Simplified geological maps showing Jurassic–earliest Cretaceous tectonic evolution in
 1704 North China, and geodynamics. (a) Early–early Middle Jurassic (~200–170 Ma). (b) late Middle
 1705 Jurassic (~170–160 Ma). (c) latest Middle–early Late Jurassic (~165–150 Ma). (d) Late Jurassic–
 1706 earliest Cretaceous (~160–135 Ma).



1707

1708 **Fig. 16.** Early Cretaceous regional tectonics of the NCC, showing the Early Cretaceous (~135–
 1709 115 Ma) extensional structures and magmatism, and dynamics. The MCCs and syn-tectonic
 1710 magmatic domes in East Asia (Wang et al., 2011; Ji et al., 2018; Lin and Wei, 2018 and references
 1711 therein): UU: Ulan Ude, BT: Buteel, ZG: Zagan, Yb: Yablonovy, ED: Ereendavaa, YG: Yagan,
 1712 YB: Yingba, HH: Hohhot, YM: Yunmengshan, YW: Yiwulüshan, SL: South Liaoning, XY:
 1713 Xiuyan, LL: Linglong, QS: Queshan, JN: Jiaonan, XQL: Xiaoqinling, TBS: Tongbaishan; CDB:
 1714 Central Dabieshan; HL: Huangling; QJ: Qingyang-Jiuhua; HZ: Hongzhen; LS: Lushan; WGS:
 1715 Wugongshan; DM: Dayunshan-Mufushan; HS: Hengshan; and YCL: Yuechengling.

1716 **Table 1.** Summary of distribution and characteristics of the Jurassic–Early Cretaceous strata in
 1717 the NCC (Dating data for age constraints were detailedly compiled in [Table S1](#)).

Sequence	Tectonic unit	Formation	Basin	lithology	Sedimentary facies	Age constraints (Ma)	Thickness (m)	
Lower Jurassic sequence	Yanshan belt	Nandaling Fm.	Western Hill	Conglomerates, sandstones, volcanics, and lahar	Fuvial facies	177–167	0–676	
		Nandaling Fm.	Xiahuayuan and Luanping	Basalt interlayered with andesite and pyroclastic rocks	/	180 ± 1.8	0–330	
	Yinshan belt	Xinglonggou Fm.	Beipiao	Andesite, dacites, pyroclastic rocks, and tuff	Fuvial facies	188–176	0–400	
		Wudanggou Fm.	Shiguai	Cobble–boulder conglomerates, shales and lenticular sandstones	Alluvial, shallow lacustrine and deltaic facies	200–183	0–500	
	Ordos basin and adjacent areas	Fuxian Fm.	Ordos	Conglomerates and sandstones	Alluvial and braided fluvial facies	/	0–195	
		Yongdingzhuang Fm.	Ningwu–Jingle and Yungang	Conglomerates and sandstones	Alluvial and fluvial facies	188–171	0–220	
	lower Middle Jurassic sequence	Yanshan belt	Lower Yima Fm.	Yima district	Conglomerates and coarse-grained sandstones	Alluvial and braided fluvial facies	/	/
			Anyao Fm.	Jiyuan region	Sandstones, mudstones and turbidites	Fan deltaic facies	178.31 ± 3.77	/
		Yaopo Fm.	Western Hill	Sandstones and mudstones intercalated with thick coal measures	Meandering fluvial, swamp, and shallow-lacustrine facies	175–174	0–676	
		Xiahuayuan Fm.	Xiahuayuan and Luanping	Basal conglomerates, sandstones, siltstones, mudstones, and coal measures	Lacustrine and swamp facies	175–170	0–430	
Beipiao Fm.			Beipiao	Sandstones and mudstones intercalated with thick swamp coal measures	Lacustrine and swamp facies	175–168	0–820	
Xiahuayuan Fm.		Xiabancheng	Coal-bearing conglomerates and sandstones	Lacustrine and swamp facies	/	0–279		
		Guojadian Fm.	Niuyingzi	Coal-bearing conglomerates, sandstones, and mudstones	Fuvial and swamp facies	171–163	/	
Yinshan belt		Zhaogou Fm.	Shiguai basin	Pebby conglomerates, sandstones, siltstones, black shales, and coal measures	Fluvial, lacustrine, and swamp facies	The early Middle Jurassic palynoflora	0–750	
Ordos basin and adjacent areas		Yan'an Fm.	Ordos basin	Lag gravels, sandstones, coal-bearing deposits	Meandering fluvial, shallow-lacustrine and swamp facies	/	0–326	
		Datong Fm.	Ningwu–Jingle and Yungang	Fine-grained sandstones, mudstones, and coal beds	Lacustrine facies	/	0–400	
Upper Yima Fm.	Yima district	Sandstones, mudstones, coal beds	Meandering fluvial, shallow-lacustrine and swamp facies	/	/			
Yangshuzhuang Fm.	Jiyuan region	Sandstones, mudstones, coal beds	Meandering fluvial, shallow-lacustrine and swamp facies	/	/			
upper Middle Jurassic sequence	Yanshan belt	Longmen Fm.	Western Hill	Conglomerates intercalated with thin-bedded sandstones	Fuvial to alluvial facies	168–164	0–395	
		Jiulongshan Fm.	Western Hill	Conglomerates, pebbly sandstones, and tuffaceous sandstones and siltstones	Deltaic to lacustrine facies	161–154	0–1536	
	Jiulongshan Fm.	Xiahuayuan and Luanping	Conglomerates, sandstones, and mudstones	Fuvial, alluvial, lacustrine, and deltaic facies	163–156	0–1670		
		Haifanggou Fm.	Beipiao	Conglomerates, sandstones, siltstones, mudstones, and pyroclastic interlayers	Alluvial to lacustrine facies	167–161	0–400	
	Yinshan belt	Changhangou Fm.	Shiguai	Conglomerates, sandstones, and mudstones, tuff and gypsum	Fluvial and lacustrine facies	163.7 ± 1.0	0–420	
	Ordos basin and adjacent areas	Zhiluo Fm.	Ordos	Sandstones, siltstones, marlstone, mudstones, and shales	Fluvial and lacustrine facies	/	0–268	
		Anding Fm.	Ordos	Sandstones, siltstones, marlstone, mudstones, and shales	Fluvial and lacustrine facies	/	0–148	
	Yungang Fm.	Ningwu–Jingle and Yungang	Basal conglomerates, sandstones and sandy shales	Fluvial and lacustrine facies	168–161	0–462		
		Dongmengcun Fm.	Yima district	Basal conglomerates, sandstones, mudstones and shales	Fluvial and lacustrine facies	/	/	
	Ma'ao Fm.	Jiyuan region	Basal conglomerates, sandstones, mudstones and shales	Fluvial and lacustrine facies	/	/		
lower Upper Jurassic sequence	Yanshan belt	Tiaojiashan Fm.	Western Hill	Intermediate andesitic lavas, volcanic breccia, andesitic tuff, pyroclastics, and interbedded clastic rocks	/	161–146	0–2952	
		Tiaojiashan Fm.	Xiahuayuan and Luanping	Andesitic lavas, basalt lavas, volcanic breccia, tuffaceous clastic rocks	/	164–153		
	Tiaojiashan Fm.	Xiabancheng	Andesite, pyroclastics, tuffaceous sandstones, with mudstone interbeds	/	164–153			
	Tiaojiashan Fm.	Chicheng	Breccia, andesitic tuff, pyroclastic rocks, and interbedded sedimentary rocks	/	165–157			
	Tiaojiashan Fm.	Hunyuan	Andesite interlayers and conglomerates interbedded sandstones, or mudstones	/	152.77 ± 0.6			
	Lanqi Fm.	Niuyingzi	Andesite, basaltic andesite, and pyroclastic rocks	/	159–158	0–1360		
	Lanqi Fm.	Beipiao	Andesite, basaltic andesite, and pyroclastic rocks	/	166–153			
Upper Jurassic sequence	Yanshan belt	Tuchengzi/Houcheng Fm.	/	Conglomerates, sandstones, and mudstones	Fuvial, alluvial to lacustrine facies	155–135	0–2760	
	Yinshan belt	Daqingshan Fm.	Shiguai	Cobble-pebble conglomerates, sandstones, and siltstones	Alluvial and fluvial facies	/	0–3900	
	Ordos basin and adjacent areas	Fengfanghe Fm.	Ordos	Conglomerates and sandstones	Alluvial and braided fluvial facies	/	0–1174	
Tianchihe Fm.		Ningwu–Jingle and Yungang	Conglomerates, sandstones, and mudstones	Alluvial, fan delta facies	160.6 ± 0.55	0–900		
Lower Cretaceous sequence	Yanshan belt	Zhangjiakou Fm.	Beipiao	Andesite and pyroclastics with a basal conglomerate	Fluvial facies	136–127	0–3867	
		Donglingtai Zhangjiakou Fm.	Western Hill	Rhyolite and volcanic breccias	/			
	Yinshan belt	The rest of yanshan belt	Rhyolitic tuff, rhyolite, andesite and quartz trachyte with sedimentary rocks	Fluvial facies				
		Guyang Gr.	Daqingshan	Conglomerates and sandstones with volcanic rocks	Fluvial and lacustrine facies	/	/	
	Ordos basin and adjacent areas	Zhidan Gr.	Ordos	Conglomerates, sandstones	Fluvial facies	/	0–213	
Zuoyun Fm.	Ningwu–Jingle and Yungang	Conglomerates, sandstones, and mudstones	Fluvial and lacustrine facies	130.1 ± 0.8	/			

1719 **Table 2.** Summary of geometry and kinematics of the Jurassic–Early Cretaceous contractional
 1720 structures in the NCC.

Tectonic units	Thrusts	Strikes	Fault-slip data	Involved strata	Time constraints		References	
					Event A of the Yanshanian orogeny	Event B of the Yanshanian orogeny		
Central Yanshan belt	Mengjiazhuang thrust (MT)	ENE	/	Ar-Pt, J _{1-2n} : tight fold; J _{3t} : open fold	Pre-J _{1-2n}	Post-J _{1-2n} , pre-J _{3t}	Li et al., 2016a	
	Jiyuqing thrust (JT)	ENE	/	Ar-Pt, C-O, T, J _{2x} : tight fold; J _{3t} -J ₃ -K _{1tch} : open fold	Pre-J _{1-2n}	Post-J _{2x} , pre-J _{3t}	Li et al., 2016a	
	Liadaohe thrust (LT)	ENE	/	Ar-Pt, C-O, T, J _{2x} : tight fold; J _{3t} -J ₃ -K _{1tch} : open fold	Pre-J _{1-2n}	Post-J _{2x} , pre-J _{3t}	Li et al., 2016a	
	Duanhuwa-Jianbaoshan thrust (DJT)	E	/	Ar-Pt, C, J _{2x}		Post-J _{2x} , pre-J _{3t}	Li et al., 2016a	
	Qingshuifu fault (QSHF)	E	/	Ar-Pt		Pre-Siganding pluton (160–157 Ma)	Chen, 1998; Zeng et al., 2021	
	Zhujiagou fault (ZJGF)	E	/	Ar-Pt		Pre-Wangping-shi pluton (162.3±1.3 Ma)	Chen, 1998	
	Xinglong thrust (XLT)	E	/	Ar-Pt, C-O		Pre-J _{3t}	Chen, 1998; Davis et al., 2001	
	Miyun-Xifengkou fault (MXF)	E	/	Ar-Pt		Pre-mafic dyke (160 Ma)	Chen, 1998	
	Gaobanhe/Sampo/Banbishaan faults (GBHF/SPF/BBSF)	NE	/	Ar-Pt		Pre-J _{3t}	Chen, 1998	
	Gubeikou-Pingquan thrust (GPT)	E	NW-SE direction	Ar-Pt, C-O, J _{1x} /J _{3t} -J ₃ -K _{1tch}			Post-J _{3t} , pre-Wulingshan and Shouwangfen plutons (132–130Ma)	Li et al., 2016a
	Dayingzi thrust (DYT)	ENE	/	Ar-Pt, C-O, J _{3t} -J ₃ -K _{1tch}			Post-J _{3t} , pre-K _{1z}	Li et al., 2016a
	Shetang ductile shear zone (SHTSZ)	E	/	Ar			Coeval with Yumengshan pluton (145 Ma)	Davis et al., 2001
	Chengde thrust (CDT)	ENE	/	Ar-Pt, J _{3t} -J ₃ -K _{1tch}			Post-J _{3t} , pre-K _{1z}	Davis et al., 2001
	Shanggu-Pingquan thrust (SPT)	NE	/	Ar-Pt, C-O, T, J _{2x} , J _{3t} -J ₃ -K _{1tch}			Post-J _{3t} , pre-Guozhangzi and Jishan plutons (113–111 Ma)	Li et al., 2016a
Western Yanshan belt	Nandazhai-Babaoshan thrust (NBT)	NE	/	Ar-Pt, C-O, C-P, J _{1-2n} -J _{3t}			Post-J _{3t} , pre-K _{1d}	Zhang et al., 2006
	Changcao-Xiayunling thrust (CXT)	NE	/	Ar-Pt, C-O, C-P, J _{1-2n} -J _{3t}			Post-J _{3t} , pre-K _{1d}	Zhang et al., 2006
	Caojiapu-Huangtuliang thrust (CHT)	NE	/	Ar-Pt, C-O, C-P, J _{1-2n} -J _{3t}			Post-J _{3t} , pre-K _{1d}	Zhang et al., 2006
	Malan-Hulin thrust (MHT)	NE	/	Ar-Pt, C-O, C-P, J _{1-2n} -J _{3t}			Post-J _{3t} , pre-K _{1d}	Zhang et al., 2006
	Shisanling thrust (SSL)	NE	/	Ar-Pt, C-O, J _{1-2n} -J _{3t}			Post-J _{3t} , pre-127.0±1.5 Ma pluton	Davis et al., 2001
	Xihuayuan thrust (XHYT)	NE	/	Ar-Pt, C-O, J _{1-2n} -J ₃ -K _{1tch}			Post-J _{3t} , pre-K _{1z}	Zhang et al., 2006; Lin et al., 2019
	Qianjiadian thrust (QJDT)	NE	NW-SE direction	Ar-Pt, J _{3t} -J ₃ -K _{1h}			Post-J _{3t} , pre-K _{1z}	Zhang et al., 2006; Lin et al., 2019
	Shalanzhi thrust (SLZT)	NE	NW-SE direction	Ar-Pt, J _{3t} -J ₃ -K _{1h}			Post-J _{3t} , pre-K _{1z}	Zhang et al., 2006; Lin et al., 2019
	Tanghekou thrust (THKT)	NE	NW-SE direction	Ar-Pt, J _{3t} -J ₃ -K _{1h}			Post-J _{3t} , pre-K _{1z}	Zhang et al., 2006; Lin et al., 2019
	Banshen-Shuiquanguo thrust (BST)	NE	NW-SE direction	Ar-Pt, J _{1x} -J ₃ -K _{1tch}			Post-J _{3t} , pre-K _{1z}	Yang et al., 2021
	Eastern Yanshan belt	Yangzhangzi-Wafangdian fault (YWF)	NE	/	Ar-Pt, C-O, C-P, J _{2g} , J _{3l}		Post-J _{2g} , pre-160.2 Ma rhyolitic porphyry	
Nangongyingzi-Beipiao fault (NBF)		NE	/	Ar-Pt, C-O, C-P, J _{3l} -J ₃ -K _{1tch}		Pre-J _{3l}	Post-J _{3l} , pre-K _{1y}	Zhang et al., 2002
Jianchang-Chaoyang fault (JCF)		NE	/	Ar-Pt, C-O, C-P, J _{1x} -J ₃ -K _{1tch}			Post-J _{3l} , pre-K _{1y} and post-K _{1y}	Zhang et al., 2002
Yinshan belt	Datun-Jinzhou fault (NEF)	NE	/	Ar-Pt, C-O, C-P, J _{3l} -J ₃ -K _{1tch}			Post-J _{3l} , pre-K _{1y}	Zhang et al., 2002
	Lingyuan-Dongguanyingzi fault (LDF)	NE	/	Ar-Pt, C-O, C-P, J _{3l} -J ₃ -K _{1tch}			Post-J _{3l} , pre-K _{1y}	Zhang et al., 2002
Ordos basin and adjacent areas	Hetangou-Dongerba thrust (HDT)	E	N-S direction/ NW-SE direction	Ar, C-O, C-P, J _{1w} -J _{3d}		Post-J _{2g} , pre-J _{3d}	Post-J _{2c} , pre-K _{1g}	Wang et al., 2017
	Beilrishan thrust (BLT)	E	NW-SE direction	Ar, C-O, C-P, J _{1w} -J _{3d}			Post-J _{2c} , pre-K _{1g}	Wang et al., 2017
	Daqingshan thrust (DQST)	/	NW-SE direction	Ar-Pt, J _{1w} -J _{3d}			Post-J _{2c} , pre-K _{1g}	Gong et al., 2015
	Thrusts in Langshan	NE	/	Ar, J			J ₃ to K ₁	Darby and Ritts, 2007
	Chunjing thrust (CJT)	NE	/	Ar-Pt, C-O, C-P, J _{1y} -J _{3t}			Post-J _{2y} , pre-K _{1zy}	Zhang et al., 2020
	Mafangzhen thrust (MFT)	NE	/	Ar-Pt, C-O, C-P, J _{1y} -J _{3t}			Post-J _{2y} , pre-K _{1zy}	Zhang et al., 2020
	Dujiacun thrust (DJCT)	NE	/	Ar-Pt, C-O, C-P, J _{1y} -J _{3t}			Post-J _{2y} , pre-K _{1zy}	Zhang et al., 2020
	Kouquan thrust (KQT)	NE-NNW	NW-SE direction	Ar-Pt, C-O, C-P, J _{1y} -J _{2yg}			Post-J _{2y} , pre-K _{1zy}	Chen et al., 2019
	Ernaokou fault (EMKF)	NNE	NW-SE direction	Ar-Pt, C-O, C-P, J _{1y} -J _{2yg}			Post-J _{2y} , pre-K _{1zy}	Chen et al., 2019
	Thrusts in western Ordos basin	N	/	Ar-Pt, C-O, C-P, T, J			post-J, pre-K	Feng et al., 2021
Thrusts in Zhuozishan	N	NW-SE direction	Ar-Pt, C-O, C-P, T, J _{1f} -J _{2jf}			Post-J _{2a} , pre-K _{1z}	Li et al., 2022	
Xiaosongshan thrust (XST)	NE	NW-SE direction	Ar-Pt, C-O, C-P, T, J _{1f} -J _{2a}			Post-J _{2a} , pre-K _{1z}	Huang, et al., 2015; Yang and Dong, 2018, 2020; Li et al., 2022	
Chaiqigou-Tatagou fault (CTF)	NE	NW-SE direction	Ar-Pt, C-O, C-P, T			Post-J _{2a} , pre-K _{1z}	Huang, et al., 2015; Yang and Dong, 2018, 2020; Li et al., 2022	
Dashuigoumen-Dawukou fault (DDF)	NE	NW-SE direction	Ar-Pt, C-O, C-P, T			Post-J _{2a} , pre-K _{1z}	Huang, et al., 2015; Yang and Dong, 2018, 2020; Li et al., 2022	
Dazhanchang fault (DZF)	NNE	NW-SE direction	Ar-Pt, C-O, D-P, T, J _{2z} , J _{3f}			Post-J _{2a} , pre-K _{1z}	Yang and Dong, 2020	

1722 **Table 3.** Summary of syn-emplacement fabrics of the Jurassic–Early Cretaceous granitic plutons
 1723 in the NCC (compiled from Lin et al., 2021 and references therein).

Period	No.	Pluton	Location	Lithology	Age	Syn-emplacement foliation	Syn-emplacement lineation
Early Jurassic	1	Jiumen	Eastern Yanshan	Monzogranite	189.9±2.7 Ma	Highly scattered with variable dips	Highly scattered with variable dips
Late Jurassic	1	Yiwulüshan	Eastern Yanshan	Biotite granodiorite	162–153 Ma	Overprint by the Wangziyu detachment fault	Overprint by the Wangziyu detachment fault
	2	Jianchang	Eastern Yanshan	Monzogranite	158–157 Ma	Margin-parallel with moderate to high dips	Gentle to moderate NE-SW plunging
	3	Siganding	Central Yanshan	Monzogranite and diorite	160–159 Ma	Margin-parallel with moderate to high dips	Gentle to moderate NE-SW plunging
	4	Kunyushan	Jiaodong peninsula	Biotite monzogranite	160–153 Ma	Concentric patterns with moderate to low dips	Predominately (E)NE-(W)SW plunging
	5	Qeshan	Jiaodong peninsula	Biotite monzogranite	162–156 Ma	NW–SE striking with variable dips	Highly scattered with variable dips
	6	Linglong	Jiaodong peninsula	Biotite monzogranite	163–152 Ma	Concentric patterns	Dominantly (E)NE-(W)SW plunging
	7	Luanjiahe	Jiaodong peninsula	Biotite monzogranite	157–152 Ma	SE- or NW-dipping with high angles	NE-SW plunging with gentle dips
	8	Wendeng	Jiaodong peninsula	Biotite monzogranite	160–151 Ma	Margin-parallel with moderate to high dips	Highly scattered with gentle dips
Early Cretaceous	1	Yunmengshan	Western Yanshan	Granodiorite	145–141 Ma	Overprint by the Shuiyu detachment fault	Overprint by the Shuiyu detachment fault
	2	Gudaoling	Liaodong peninsula	Biotite monzogranite	127–118 Ma	W- or WSW- dipping with moderate to low angles	Sub-horizontal NW-SE plunging
	3	Yinmawanshan	Liaodong peninsula	Porphyritic granite	129–120 Ma	Margin-parallel with moderate to gentle dips	Various plunges and dips in the west and E-W plunging in the
	4	Guojialing	Jiaodong peninsula	Porphyritic granodiorite	130–128 Ma	NW-dipping with moderate-low angles in the west and NNW- or NE- dipping with low angles in the east	NW-SE plunging with moderate to low dips
	5	Congjia	Jiaodong peninsula	Porphyritic granodiorite	130–128 Ma	NE- or SE- dipping	Sub-horizontal NW-SE plunging
	6	Wang'anzen	Taihangshan	Granodiorite and monzogranite	130–128 Ma	Concentric pattern with a NE-SW long axis	Predominantly NW-SE or E-W trending with moderate to high dips
	7	Fengjiayu-Xibailianyu	Central Yanshan	Monzogranite and diorite	131–127 Ma	Concentric patterns with high and moderate to gentle dips, respectively	Scattered with moderate to gentle dips
	8	Gubeikou (Qiancengbei)	Central Yanshan	Granite	129–128 Ma	Roughly margin-parallel with moderate to low dips	Highly scattered with moderate to low dips
	9	Dahaituo	Western Yanshan	Quartz monzonite and monzogranite	119±2 Ma	Concentric pattern with a NE-SW long axis	Highly scattered with moderate to low dips
	10	Haiyang	Jiaodong peninsula	Porphyritic granodiorite	118–114 Ma	Concentric pattern with mainly sub-horizontal dips	Scattered with sub-horizontal dips
	11	Aishan	Jiaodong peninsula	Porphyritic granodiorite	118–115 Ma	Margin-parallel with moderate to low dips	Sub-horizontal NW-SE plunging

1724